Predicting and improving the behaviour of stepping motors

Vierbergen, R.G.

Award date:
2005

Eindhoven University of Technology
Department of Electrical Engineering
Control Systems

TU/e technische universiteit eindhoven

Predicting and Improving the Behaviour of Stepping Motors

by

R.G. Vierbergen

Master of Science thesis

Project period: december 2005
Report Number: 05A/07
Commissioned by: Prof.dr.ir. P.P.J. van den Bosch

Supervisor: Lars Idema, Océ Technologies B.V.

Additional Commission members:
Dr.ir. A. Veltman

Graduation project at Océ Technologies B.V.

Predicting and Improving the Behaviour of Stepping Motors

Faculty of electrical engineering
Department of Control System
University of technology Eindhoven

Student: R.G.Vierbergen
Student number: 447280

Table of contents

1 Abbreviations / technical terms

BLDC	Brushless DC (Indication for a DC motor without brushes)
Cogging	A small torque produced by the permanent magnet in the stepper motor, even without any power applied to the stator windings
Eddy currents	Circular currents induced in the motor housing by the changing magnetic field in the motor
EMF voltage	Voltage induced by the changes of the electro magnetic field in the stator poles, produced by movement of the rotor.
Hysteresis	The power loss during demagnetisation of ferromagnetic materials
Iron losses	Hysteresis and Eddy currents
PMDC	Permanent Magnetic DC (Indication for a DC motor with brushes)
PWM	Pulse Width Modulation
Rated current	Motor parameter supplied by manufacturer, the winding current for which the manufacturer has designed the stepping motor
Skin effect	The tendency of the current flow to establish close to the outer layer of the conductor. At higher frequencies this effect increases

2 Introduction

At the beginning of the investigation, the available knowledge about stepper motor behaviour was limited. At the present the implementation of stepping motors in Océ devices is still a time consuming procedure. It is true that for most applications the same performance (or maybe even better) may be acquired when using a closed loop controlled DC motor. So why use a stepper motor?

The two main reasons to choose stepper motors instead of DC motors, is lower costs and higher durability. The stepper motor has a high number of fixed rotor angle positions resulting to a feed-forward knowledge of the rotor position. Because of the build in rotor angle positions, the position error is small and non cumulative. This makes the use of encoders and complex control devices obsolete.

Besides the cost reduction by using feed forward control, the stepper motor also is cheaper to maintain. The stepper motor does not have brushes, making the motor more durable then the PMDC motor.

Besides the advantages of the stepping motor, there are some disadvantages:
- High power consumption at low angular speeds, even during low mechanical power demand, resulting in a larger heat production
- Discrete rotor preference positions make the angular speed of the rotor oscillatory, and at some speeds even unstable
- The stepping motor produces a high pitched noise because of the high stepping frequencies (up to 10 kHz)
- The rotor speed stalls, when being pulled out of its step position during high speed operation
- No feedback result in high demands on the a priori knowledge of application and motor behaviour

To get a better understanding of the stepper motor, and eventually improve motor behaviour, this investigation has two aims:
- Improving the predictability of stepping motor behaviour
  - Construct a simulation model of the stepper motor dynamics
  - Validate model with relevant measurements
  - Extend model to accept complex mechanical dynamics
- Improving the stepper motor behaviour
  - Analyse the stepper motor oscillation problems
  - Analyse the mechanical dampers theory
  - Analyse the mechanical dampers performance
  - Compare simulation model results with measurement results

It is obvious that only a good understanding of the stepping motor behaviour will help overcome the disadvantages stated before. Within Océ are several documents concerning stepping motors, and their general behaviour ([7], [8], [9] and [10]), chapter 3 consist of a small introduction about stepping motors.

To give a more physical interpretation to stepping motor behaviour, a basic simulation model is designed in chapter 4. If the simulation model behaves close to reality, the simulation result will give access to variables which by measurements are difficult or even impossible to acquire. To validate this simulation model, a series of experiments have been performed. These are described in chapter 5. The results of chapter 5 will be used for improving the model, if the simulation model performs poorly.

The model of chapter 4 mainly concentrates on the dynamics of the stepper motor. This way of constructing a model is fine for investigating the motor behaviour, but eventually the model has to be used to simulate the use of a stepper motor as part of a mechanical system. Chapter 6 shows how the model will be adapted to accept different types of mechanical loads.

During the investigation two types of mechanical dampers have been encountered, which seemed to result to a surprising improvement of the motor behaviour. Chapter 7 will analyse these dampers, and show the improvement of the motor behaviour, when such dampers are used. Also the performance restraints of such dampers will be discussed.

Chapter 8 will deal with a test set-up, to investigate the stepper motor behaviour, when driving a known mechanical system. The measurement results will be cross examined with simulation results. The test set-up will also be used to analyse one mechanical damper.

Finally chapter 9 will give a summary of the results obtained during the research, and discuss the conclusions and recommendations for further investigations. All relevant measurement results are available in the appendices. A user friendly stepper motor design tool for Matlab has been programmed, to make the simulation model more accessible to users with very basic Matlab knowledge. A discussion about this program is written in appendix D.

3 Theory about stepping motors

A stepping motor is an electrical motor, which converts electrical energy into mechanical movements. The stator contains the electrical windings, and the rotor is a permanent magnet, or a magnetic material (like soft iron). Because of this construction, the commutation of the stepping motor windings is done completely electronically, and the motor has no need for brushes. Depending on the electrical control the rotor may be kept on a fixed position, or be turned both ways, without the use of feedback.

These properties make a stepper motor a cheap and reliable motion control device, when used wisely. The next parts of this chapter will give a short description of the basic stepper motor properties.

3.1 Types of stepping motors and their basic principle of operation

Stepping motors come in two basic types, the permanent magnet (PM) and the variable reluctance (VR) motor. The idea behind each motor is the same, but as the names suggest, a PM motor has a permanent magnet rotor, while the VR motor has a toothed rotor made from a soft iron material. A special variation of the PM motor is the hybrid stepper motor. Actually the hybrid stepper motor incorporates physical properties of both the PM and the VR motor, hence the name hybrid. A small subpart has been devoted to the hybrid motor, because of its popularity.

3.1.1 The Variable Reluctance (VR) motor

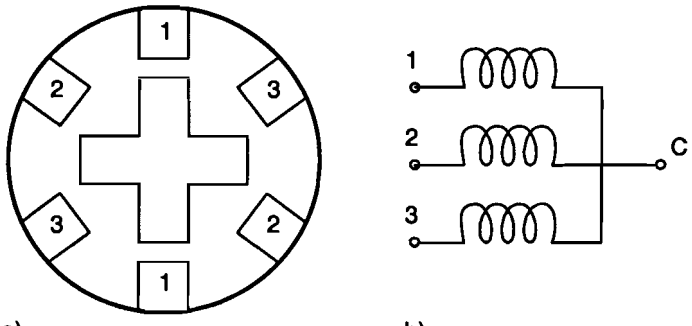

Figure 3-1: a) cross section of a VR motor, b) electrical winding schematic

Figure 3.1a shows a cross section of a three phase 30º VR motor. The rotor has four teeth, the stator has six poles and each phase winding is wrapped around opposing poles, as the numbers in figure 3.1a show. When excited, the two poles driven by one phase have opposite polarities (because of the winding direction of each pole).

Figure 3.1b shows the schematic of the motor windings, the three numbered wires are for each phase of the motor, and a common line to complete the circuit. Phase excitation is generally done by attaching the common line to the positive voltage, and placing switches between the phase windings and the ground. Energising a phase can be done by enabling the winding switch.

The rotor can move in steps of 30 degrees in clock or counter clock wise direction by exciting the phases. When a phase is excited, the rotor will move to minimise the airgap between the excited poles. In figure 3.1a the rotor position coincides with an excitation of phase one. In order to move the rotor 30 degrees clock wise, the phase excitation should be changed to phase two. For 30 degrees counter clock wise movement phase three should be excited.

Table 3.1 shows the order of switching for a one revolution clock wise rotor movement (12 steps). If the winding is switched on, the value in the table is one (current can flow from the common line through the winding to earth), and when the winding is switched off the value is

zero (no current can flow through the winding). Notice that for a clock wise rotor movement the magnetic field in the poles move in a counter clock wise direction.

Table 3-1: Clock wise rotor movement excitation scheme for VR motor

step:	0	1	2	3	4	5	6	7	8	9	10	11
Winding 1	1	0	0	1	0	0	1	0	0	1	0	0
Winding 2	0	1	0	0	1	0	0	1	0	0	1	0
Winding 3	0	0	1	0	0	1	0	0	1	0	0	1

The cross section from figure 3.1a is a simplified example, in practise the VR motors have more pole windings and or more rotor teeth, resulting in smaller step sizes. By using this method, VR motors with step angles of nearly one degree can be made.

3.1.2 The permanent magnet (PM) motor

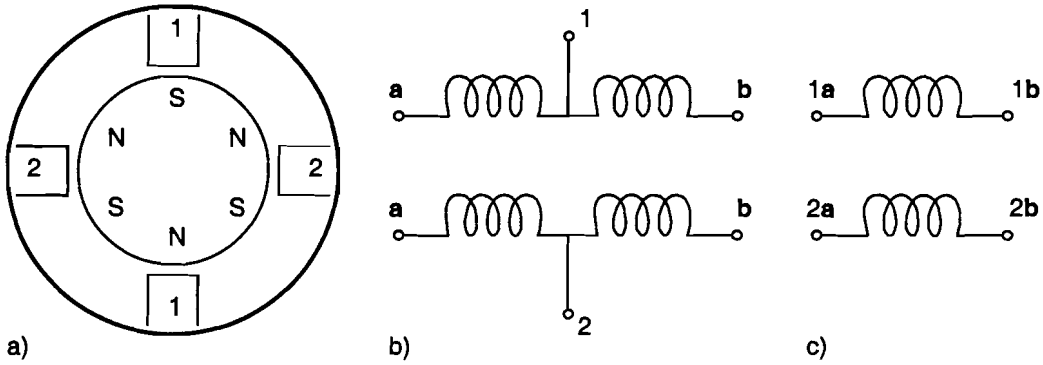

Figure 3-2: a) cross section of a PM motor, b) Unipolar winding schematic, c) bipolar winding schematic

A cross section of a two phase 30º PM motor is displayed in figure 3.2a. Now the rotor is a magnet with three north and three south poles, and the stator has four poles. As with the VR motor, each phase winding is wrapped around opposing pole pairs. And again the opposing poles have opposite magnetic polarities when being excited.

The phase excitation of the PM motor depends on the winding configuration of the motor. Figure 3.2b and 3.2c show the two possible winding configurations: unipolar and bipolar.

Unipolar PM stepper motors:
The phases of an unipolar motor are excited by connecting the common wire of each phase to the positive voltage, and connecting the **a** and **b** wires to the ground via switches. Phase excitation can be done by switching the **a** and **b** windings of each phase. Take for example phase 1. When enabling the switch of the **a** wire, a current path is established between the common wire and the ground, creating a positive magnetic polarity in the upper pole, and a negative magnetic polarity in the lower pole (by definition). The polarity of each pole can be inverted by disabling the **a** switch and enabling the **b** switch.

The rotor of the motor displayed by figure 3.2 is aligned with the situation that phase 1 is excited via wire **a**. To let the rotor turn for 30 degrees clock wise, phase 1 should be disabled, and phase 2 should be enabled via wire **a** (by definition, creating a positive magnetic polarity in the left stator pole, and a negative magnetic polarity in the right stator pole). For the counter clockwise 30 degree movement, phase 2 should be excited via wire **b**.

Table 3.2 shows the excitation scheme for one revolution clock wise rotation of an unipolar stepping motor. Again a winding is enabled when the value in the table is a one, and disabled when the value is a zero

Table 3-2: Clock wise rotor movement excitation scheme for unipolar PM motor

step:	0	1	2	3	4	5	6	7	8	9	10	11
winding 1**a**	1	0	0	0	1	0	0	0	1	0	0	0
winding 1**b**	0	0	1	0	0	0	1	0	0	0	1	0
winding 2**a**	0	1	0	0	0	1	0	0	0	1	0	0
winding 2**b**	0	0	0	1	0	0	0	1	0	0	0	1

Bipolar PM stepper motors:
The excitation scheme of the unipolar PM motor resembles the excitation scheme of the VR motor, by the fact that (half) a winding is only excited by a positive current, changing the magnetic polarity is either made obsolete by increasing the number of phases (VR), or by dividing the windings in two parts (unipolar PM). With the bipolar PM motor the magnetic polarity of the poles is changed by altering the voltage polarity over the windings.

As shown in figure 3.2c the two phases of a bipolar motor no longer have a common wire. Rotor movement can only be established if the voltage over a phase can change its polarity. The way this is done, is by using a H bridge per phase of the motor. Chapter 4 will deal with the voltage/current control of bipolar stepper motors, when creating a simulation model.

By definition, a positive magnetic polarity can be induced in the upper stator pole when a positive voltage is applied over winding **1a** - **1b** (resulting into a negative magnetic polarity in the lower pole). A positive magnetic polarity in the left stator pole is induced by putting a positive voltage over winding **2a** – **2b** (again resulting into a negative magnetic polarity in the right pole). The magnetic polarity of a pole is inverted by changing the voltage polarity over the winding.

Table 3.3 shows the excitation scheme for one revolution clock wise rotation of an bipolar stepping motor. The voltage of a phase are symbolically displayed by a plus, a minus and a zero.

Table 3-3: Clock wise rotor movement excitation scheme for bipolar PM motor

step:	0	1	2	3	4	5	6	7	8	9	10	11
Terminal **1a**	+	0	-	0	+	0	-	0	+	0	-	0
Terminal **1b**	-	0	+	0	-	0	+	0	-	0	+	0
Terminal **2a**	0	+	0	-	0	+	0	-	0	+	0	-
Terminal **2b**	0	-	0	+	0	-	0	+	0	-	0	+

The motor shown by figure 3.2a is a simple example, and also the drive methods are the basic way a stepper motor can be driven. In practise the permanent magnet of the rotor has more poles (up to 100), resulting in PM motors with smaller step sizes. Also using different drive modes gives the stepper motor better performance in both torque producing capacity and step accuracy.

3.1.3 The hybrid PM motor

The hybrid PM stepper motor has a permanent magnet rotor, but like the VR motor, the rotor is toothed. By placing the magnet along the rotor axle, a mix of an standard PM motor and a VR motor is created. Figure 3.3 shows a cross section of a two phase 9º Hybrid PM stepper motor, and a side view of the rotor. The stator has eight poles, and the rotor has ten teeth. The phase winding arrangement of the stator poles is shown by the numbers in figure 3.3. The plus and minus signs indicate the magnetic polarity of the phases, when being excited with a positive current.

The winding configuration for the hybrid PM motor is the same as for the basic PM motor, the choice is unipolar or bipolar. For explaining the functionality, lets assume that the motor from figure 3.3 has a bipolar winding configuration. In the situation of figure 3.3, the north pole of the rotor is aligned with phase 1+, and the south pole is aligned with phase 1-, meaning that the voltage polarity of phase one must be negative, and phase two is not excited.

In order to move the rotor one step in clockwise direction, phase one must be disabled, and phase two must be excited by a negative voltage. To move the rotor one counter clock wise step, phase two must be excited by a positive voltage, and phase one must be disabled again. The excitation scheme for hybrid motors is the same as for the standard PM motor.

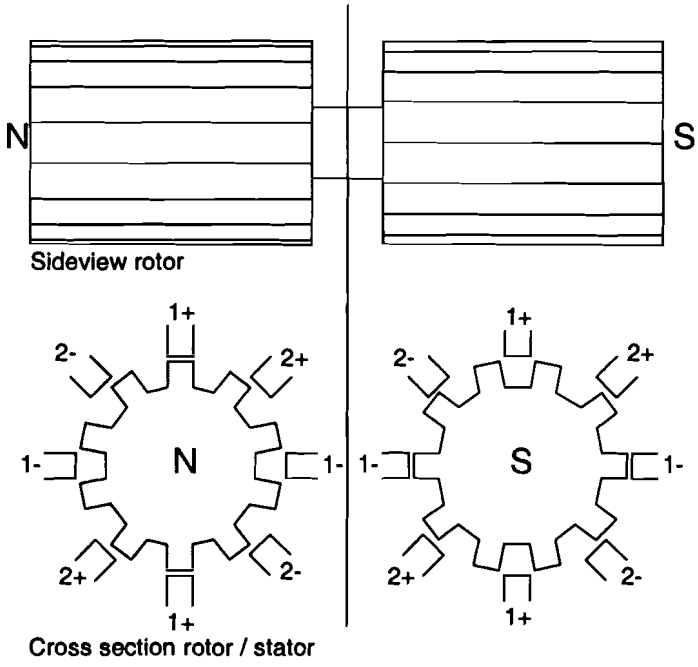

Figure 3-3: layout of the hybrid PM stepper motor

In practise the hybrid PM stepper motor has far more rotor teeth, and also the stator poles are toothed (to make sure the rotor teeth can be fully aligned or misaligned with the stator poles). Because of the high number of teeth, the hybrid motor comes with step angles of 1.8 degrees, or even smaller.

3.1.4 Choosing a stepper motor

VR motor:

Advantages

- No permanent magnet makes the motor robust
- Low drop in torque at high speeds (above 10kHz stepping rates)
- No cogging enables smoother movements

Disadvantages

- Noisy and vibrations
- In general, no microstepping
- Complex current control for high speeds

PM motor:

Advantages

- Very low cost
- Different drive methods for improving motor behaviour

Disadvantages

- Big step sizes
- Low stepping rates (around 1kHz)

Hybrid PM motor:

Advantages

- Very small step sizes
- High torque / price ratio
- High speeds (up to 5 kHz stepping rates)
- Different drive methods for improving motor behaviour

Disadvantages

- Some vibration problems
- Virtually no useful torque at very high speeds (around 5 kHz stepping rate)

Unipolar vs Bipolar:
An unipolar motor has less torque for the same volume as bipolar motor (around 30% less). But the driver complexity for an unipolar motor is much lower, and in general the unipolar motor has a slightly better performance at high speeds. Bipolar motors have a complex driver, but this results in a higher application flexibility. Nowadays, the bipolar drivers are not more expensive as the unipolar drivers.

3.2 Basic motor behaviour

In spite of the physical differences between the different types of motors, their behaviour is very similar. This part will deal with some basic properties. At times some additional information about the hybrid PM stepper motor is supplied, because this motor will be used for further investigation..

3.2.1 Static Torque

When searching for a stepping motor, the manufacturers generally supply information about its torque producing capability in the form of a graph known as the static torque / rotor position characteristics. A typical torque curve is shown in figure 3.4.

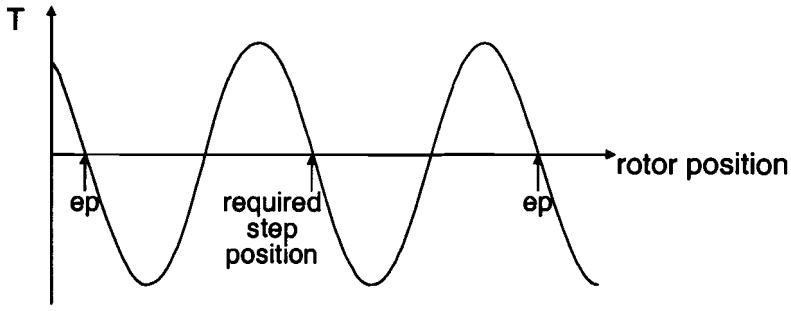

Figure 3-4: Torque/rotor position at rated phase current (ep = equilibrium points)

As can be seen from figure 3.4, when the rotor is at one of its step positions, the motor is not capable of producing any torque. Only when slightly displacing the rotor from its step position, the motor will produce a torque, in such a way that it forces the rotor to return to its step position. When trying to force the rotor to rotate by more then 2 steps, the rotor will turn to the next or previous equilibrium position (see the ep points in figure 3.4).

The static torque of a PM or hybrid PM motor is linearly related to the phase current, as long as the motor is not magnetically saturated. For the VR motor this relation ship is quadratic [2]. The maximum amount of static torque a motor can produce is known as the "peak static torque". This value should be a function of the phase current, but often the manufacturers only publish the peak static torque at the rated current (also called the holding torque).

For the Hybrid PM motor:
The torque as function of the displacement angle is often simplified as:

$$T = -T_{pk} \sin(p\theta) \qquad \textbf{Equation 3-1}$$

With T_{pk} the peak static torque [Nm], θ the rotor angle [rad], and p then number of rotor teeth. Notice from equation 3.1 that within $0 \leq \theta < 2\pi$ (one rotor revolution), the torque function has p equilibrium positions. Because the four possible ways to energise the two phases separately, this results in 4p equilibrium positions per rotor revolution, and thus a step size (in degrees) of:

$$step\_size = \frac{360^\circ}{4p} = \frac{90^\circ}{p} \qquad \textbf{Equation 3-2}$$

Another characteristic that will be used for further calculations is the rotor stator stiffness. The stiffness T' [Nm / rad] is defined as:

$$T = T' \cdot \theta$$ **Equation 3-3**

So for calculating the stiffness, one makes a linear approximation of the static torque around its step position. Figure 3.5 shows an example of how to acquire the stiffness from the static torque / rotor position characteristic. The stiffness approximation can also be calculated with equation 3.1: $T' = -T_{pk} \cdot p$ when the rotor angle is close to an equilibrium position.

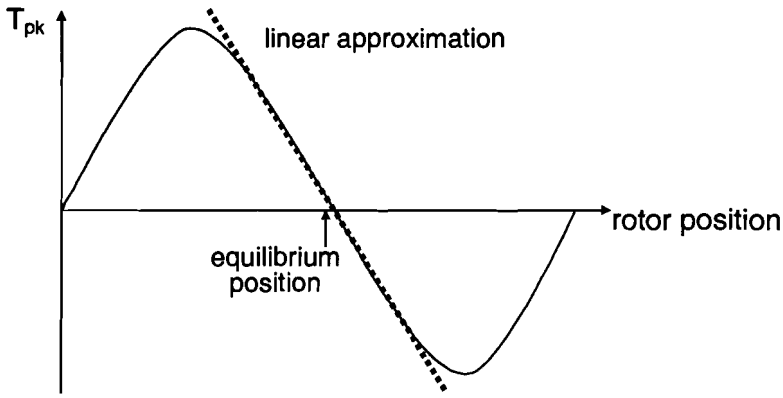

Figure 3-5: Derivation of stiffness from the static torque characteristic

3.2.2 Torque versus speed characteristics

When using a stepper motor, to change the position of a mechanical load by several steps, the designer must know the amount of torque the motor can produce while accelerating, decelerating or running at a constant speed. Part of the necessary information about these characteristics is supplied in the form of a pull-out speed / torque graph, showing the maximum amount of torque the stepper motor can produce at each stepping frequency (at the rated phase current). Figure 3.6 shows a typical speed / torque diagram.

The graph shown by figure 3.6 can be divided in four regions:

- Low stepping rates: At low stepping rates, the current is quickly established in the windings, when a phase is excited. The current also stays near to its rated value for a substantial time. This results in a fairly constant pull out torque
- High stepping rates: Now the current rise and decay time becomes a significant part of the total phase excitation time. The phase current cannot maintain its rated value, and therefore the torque produced by the motor is reduced.
- Mechanical resonance dips: These dips are caused by the oscillations produced by the mechanical resonance between the stator and the rotor / load combination.
- Electrical instability: Current through phase windings becomes unstable, causing an oscillatory rotor movement (consult appendix F and [13] for more information).

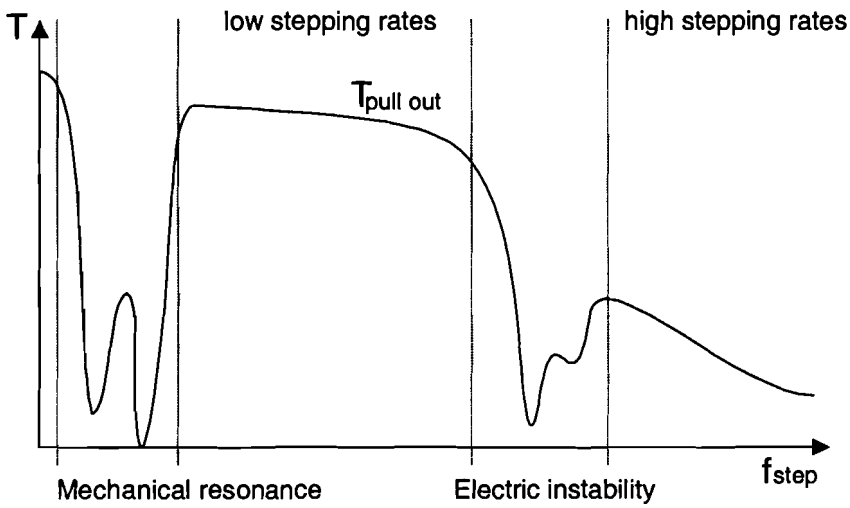

Figure 3-6: Pull-out torque speed characteristics

A lot of literature is available, trying to explain or predict the speed / torque behaviour of stepping motors ([1], [2], [13]). Most of the information was not satisfactory, and will not be reviewed in this chapter. The next chapters will cover a more in depth analysis of the hybrid stepping motor, showing that a simulation model can give more information about the pull-out torque curve. The only reliable prediction that can be made is the prediction of the mechanical resonances.

3.2.3 Mechanical resonance

At low stepping rates the motor comes to rest at each equilibrium position conforming with the position of the steps. The dynamical behaviour of each of these steps can be considered as a single step response. Figure 3.7 shows the typical single step response of a stepping motor. As can be seen from figure 3.7, the response is very oscillatory. The frequency of the oscillation can be predicted for any motor / load combination from the static torque / rotor position characteristics.

As defined by equation 3.3, the torque of the motor can be approximated with the stiffness: T = T' θ. If there is no load torque, then the motor torque is used to accelerate the motor/load inertia (J [kg m^2]). This results in the following equation:

$$-T'\theta = J(d\theta^2 / dt^2)$$
$$J(d\theta^2 / dt^2) + T'\theta = 0$$

Equation 3-4

This equation shows that the rotor motion is harmonic, with a natural frequency f_n [Hz] of:

$$f_n = \frac{1}{2\pi}\sqrt{\frac{T'}{J}}$$

Equation 3-5

Although the equations 3.6 and 3.7 suggest that the oscillation is undamped, in practice there is always a small amount of friction, making the oscillations slightly damped.

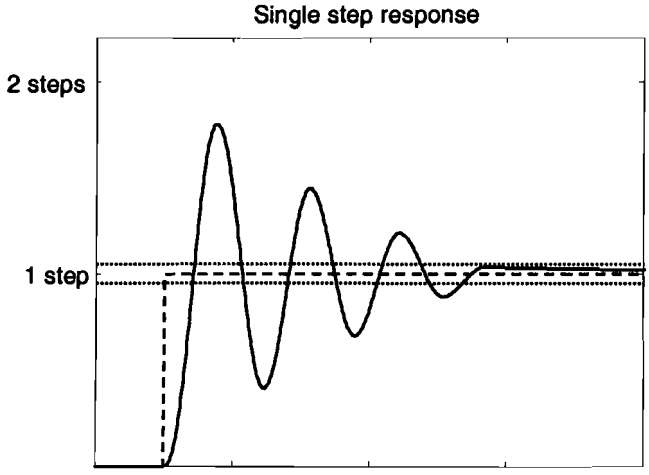

Figure 3-7: Typical single step response

As a result of the oscillatory single-step response, resonance effects occur for step rates up to the natural frequency of the rotor oscillation. Figure 3.8 shows two responses of a stepper motor, one with a step rate at 0.6 times the natural frequency, and one at a step rate near the natural frequency. The figure shows that for 0.6 f_n the rotor is always behind the equilibrium position when excited. This assures that the speed of the rotor is very slow, when changing its position. If the step rate is equal to f_n, then the rotor has a positive velocity, every time it has to change to next state. Because of the positive velocity the response to future steps will only be more oscillatory, and the rotor will be swinging out the equilibrium.

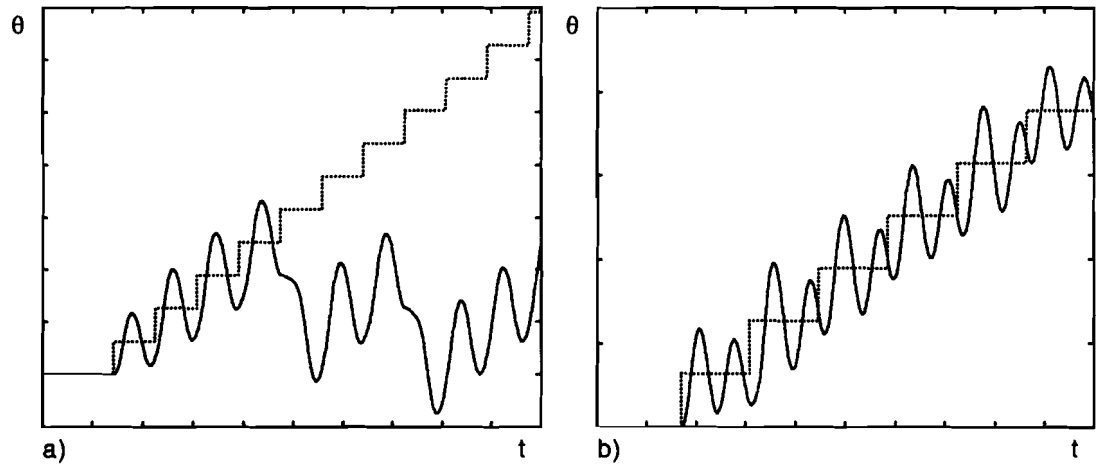

Figure 3-8: Responses to different stepping rates ($f_s = f_n$ in (a), $f_s = 0.6\ f_n$ in (b))

The resonant behaviour of the motor will lead to a loss of torque and synchronisation. This results in the torque dips shown figure 3.6. The location of these dips can be predicted if the natural frequency is known.

When a stepping motor is operating at a certain step rate, the rotation of the magnetic field in the stator is not continues, but has discrete positions. So besides the main rotating electronic field conforming with the stepping rate, also high frequency rotating fields have an effect on the rotor (higher harmonics of the winding currents). The high frequency rotating fields are an integer multiplication of the main frequency of the rotating field:

$$f_{HOD} = j \cdot f_{step} \qquad \textbf{Equation 3-6}$$

With f_{step} [Hz] the stepping rate, f_{HOD} [Hz] the higher order distortion frequencies and j = {2, 3, ... }. So any stepping rate higher then the natural frequency of the mechanical system cannot introduce the resonant frequency, but stepping rates which are lower then the natural frequency, can introduce the resonant frequency. Together with the natural frequency, the stepping rates that introduce oscillations, are the resonant stepping rates $f_{resonant}$[Hz]:

$$f_{resonant} = \frac{f_n}{j} = \frac{1}{2\pi j}\sqrt{\frac{T'}{J}} \qquad \textbf{Equation 3-7}$$

for j = {1, 2, 3, ...}.

3.3 *Known methods to improve motor behaviour*

The last section showed the problems when operating a stepper motor. Many of these problems can be avoided, when following some simple rules.

Load the motor properly:
The oscillatory behaviour of stepping motors is a result of the undamped behaviour of the rotor movement (as shown in figure 3.7). Choosing the right motor for the load to be driven will improve the motor behaviour. Recommendations for the choice of motor are:

- The motor must deliver between 30% and 70% of its torque, during operation
- The load inertia should be in between 1 to 10 times the rotor inertia of the motor
- For fast acceleration, a inertia ratio (motor:load) of 1:1 to 1:3 is to be preferred

By choosing a motor according to these three recommendations, the load will supply sufficient damping of the vibrations. But this is not enough to cancel the resonances and instabilities.

Fast acceleration through resonance and instability regions:
This is by far the easiest and most straight forward solution for improving the motor behaviour, when running the motors through unstable stepping rates. The mechanical resonances are always in the low region of step rates (up to 500Hz). Most motors can start at higher stepping rates with a single step, so this region can be avoided.

When stepping near the electrical instabilities, the rule still is true, but now the motor torque is already decaying, so the only thing to do is accelerate as fast as possible through the unstable region (remember the 30% - 70% torque rule).

Choosing a different step mode (not for VR motors):
Sometimes the motor has to operate at low speeds. Although it is preferred not to do so, a way to improve the motor behaviour, is to chose a different step mode. Chapter 4 deals with the exact way bipolar stepper motor drivers work. But the basic idea is to increase the amount of step positions by providing the motor with different winding currents.

Figure 3.9 shows two situations of a simplified PM motor. The winding currents of the left motor are as described in section 3.1.2. By changing the current of both phases to 70.7% of the current in the left motor, the rotor will turn exactly to the middle of both phases, as the right motor illustrates. This is the half step position, as it is half the rotation of a full step. Because the currents have been chosen at a level of 70.7%, the holding torque of right motor is equal to the holding torque of the left motor:

$$I_{eff} = \sqrt{70.7^2 + 70.7^2} = 100\%$$

With I_{eff}, the current that effectively is used to induce the magnetic field in the motor. So by changing the current settings, virtually any step position could be created, while the torque versus angle properties around the equilibrium position remain the same (for both the physical and the electronically new introduced equilibrium points).

When decreasing the step length, also the overshoot will be decreased. For example, at half stepping (stepping with I = {0, 70.7%, 100%} for an unipolar motor, and I = {-100% -70.7%, 0, 70.7%, 100%} for a bipolar motor) the overshoot of a single step response is also half the overshoot of a full step, while the torque / angle properties remain the same.

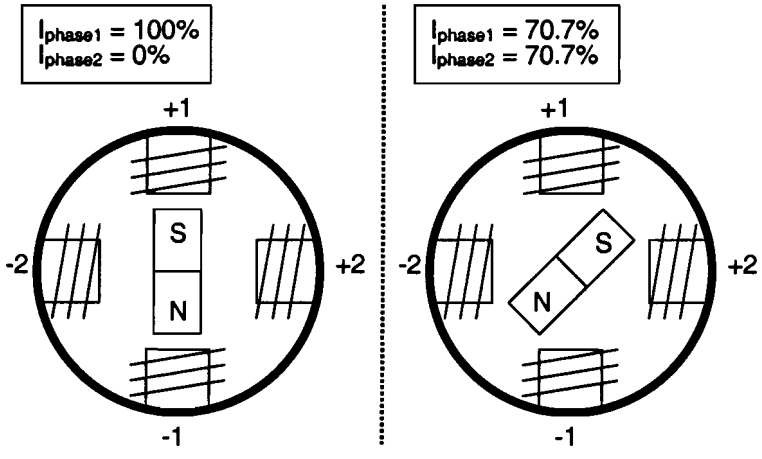

Figure 3-9: Creating alternative step positions with current control

Choosing higher step modes will make the motor less and less sensitive for natural resonances. Unfortunately this does not help for the electrical instabilities, just because the fact that at this region of step rates, the current control is failing, making it impossible to create alternative current levels.

Choose a different approach to control the motor (not for VR motors):
The standard way to control stepper motors, is to force a constant current through the windings, the constant current drivers. Although this works fine for most situations, the method is crude and inefficient. Even if the rotor is at rest, a current is maintained through

the winding(s). Also during movement the rotor continuously has to accelerate and decelerate, which results in a loss of energy. Beside the energy problem, the vibrations problems are also the result of the oscillatory rotor movement.

These problems can be avoided, if the exact rotor angle position would be known, and the voltages would be controlled using to the rotor angle as feedback. This can be achieved by using an encoder to register the location and speed of the rotor, and use this information for a carefully controlled movement. An other idea is to measure the winding currents of the motor, and use a stepper motor model to calculate the rotor position and speed. Again with this feedback the stepper motor movement is better controllable.

A downside to this approach is the increasing costs (actually one of the reasons why to use a stepper motor, is to reduce costs). The encoder needed for registering the angle must have a higher resolution than the motor step resolution, and high resolution encoders are expensive (maybe even more expensive then the motor itself). When using the winding currents as feedback, fast AD converters are necessary for registering these currents, again increasing the total costs.

Also the fact that a fast feedback controller is needed for making the right control actions, makes the solutions even more expensive. These alternatives are only interesting when the precision and stability of the system are critical.

Mechanical dampers:
Besides the package electrical options, a series of mechanical solutions are available to damp rotor vibrations. These methods seem promising, and chapter 7 is devoted to the mechanical principles behind the methods, and the resulting improvement on motor behaviour when using mechanical dampers.

4 Design of the simulation model for the bipolar (Hybrid) PM motor

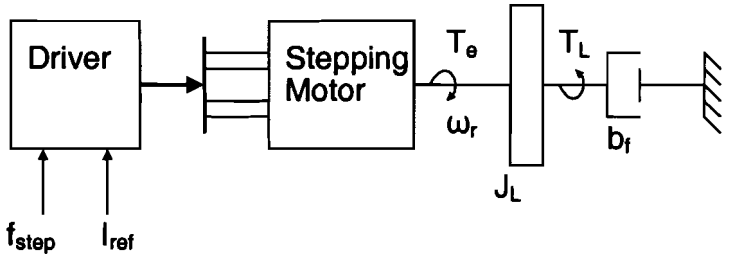

Figure 4-1: Schematic of a stepping motor connected to a load

At Océ the stepper motor of choice is the bipolar hybrid PM motor, so this motor will be modelled. Appendix E describes the design for unipolar hybrid PM motors, but no further investigation about unipolar motors have been performed. Because the ordinary PM and the Hybrid PM motor basically have the same motor behaviour, this model can also be used with the PM stepper motor.

Before a simulation model for the stepping motor can be designed, all relevant dynamics of the system must be known. Figure 4.1 shows a schematic representation of stepping motor connected to a simple mechanical load. The complete system can be divided into three parts:

- The electrical driver of the motor
- The electrical / mechanical interaction in the motor
- The mechanical load connected to the motor

Each of these parts has their own dynamical characteristics, and must be considered separately.

Motor manufacturers supply a limited amount of information about their stepper motors. Because the stepper motor must be simulated by using the manufacturer motor specifications, the stepper motor dynamics must be simplified. The following motor phenomena will not be modelled:

- Mutual inductance between stator and rotor
- Eddy currents
- Skin effect
- Hysteresis

The resulting simulation model will not be very accurate, but the aim is to predict the following aspects of motor behaviour:

- Winding currents to estimate electrical losses in the windings
- Location of problematic stepping rates (mechanical resonance's, electrical instability)
- Mechanical interaction between motor and load, mainly during acceleration and deceleration
- Torque production of the motor
- Mechanical interaction between stator and environment (chapter 6)

Because the motor data supplied by manufacturers is not very accurate (specification errors of up to 40%), high precision predictions can not be made by any simulation model. Rather then having a bulky model predicting very accurately with bad input parameters, the simulation model must give an impression of the behaviour of the stepper motor used to drive a known load, and still be easy to use.

The next sections will deal with the design of this simplified simulation model. Chapter 5 will show a series of measurements, to validate the simulation model. And chapter 6 will deal with extending the simulation model, to accept higher order load dynamics. The final model is implemented in a user friendly simulation environment (Appendix D).

4.1 *Derivation of the model dynamics*

When looking at the right part of figure 4.1, the mechanical dynamics of the load can be described by a friction torque T_f [Nm], a dynamic load torque T_L [Nm], and the inertia of the load J_L [kg m^2]. The relation between the torque T_e [Nm], produced by the stepping motor, and the mechanical dynamics of the load can be described by the following differential equations:

$$\dot{\omega}_r = \frac{1}{(J_L + J_r)}(T_e - T_f - T_L) \qquad \textbf{Equation 4-1}$$

$$\dot{\theta}_r = \omega_r \qquad \textbf{Equation 4-2}$$

With J_r [kg m^2] the rotor inertia of the stepping motor, ω_r [rad/s] the rotor angular speed, and θ_r [rad] the rotor angle. For the term T_f the following expression will be used:

$$T_f = b_f \cdot \omega_r + c_f \cdot sign(\omega_r) \qquad \textbf{Equation 4-3}$$

with b_f [Nm s rad^{-1}] the viscous friction and c_f [Nm] the coulomb friction.

The electrical part of the motor is shown in figure 4.2. The figure shows a schematic of one phase winding. The relation between the voltage and current in one phase winding can be described with the following differential equation:

$$\dot{I}_{phase} = \frac{1}{L_w}(V_{phase} - I_{phase}R_w - V_{phase,emf}) \qquad \textbf{Equation 4-4}$$

With I_{phase} [A] the phase current, R_w [Ω] the winding resistance, L_w [H] the winding inductance, and $V_{emf,phase}$ [V] the voltage induced by the motion of the rotor.

To complete the set of equations, the interaction between the mechanical and electrical parts made by the motor should be described. Figure 4.3 shows a simplified schematic of a stepping motor (for p = 1). The torque produced by the motor can defined as:

$$T_e = -\frac{T_{pk}}{I_0}\left(I_A \sin(p\theta_r) - I_B \cos(p\theta_r)\right) \qquad \textbf{Equation 4-5}$$

With T_{pk} the peak static torque and I_0 [A] the rated current of the stepping motor. The rotor angle θ_r [rad] is defined as in the arrow in the upper left corner of figure 4.3.

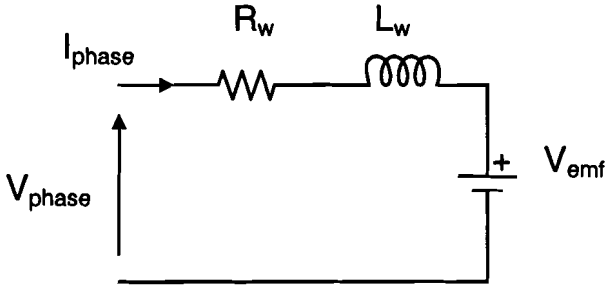

Figure 4-2: Electrical schematic of one winding

The voltage induced by the rotor motion ($V_{phase,emf}$ [V]) is equal to:

$$V_{phase,emf} = \frac{d\Phi}{dt} \qquad \textbf{Equation 4-6}$$

With Φ [Wb], the magnetic flux change for each stator pole. For each phase this results in:

$$\begin{cases} V_{A,emf} = -p\psi_M \sin(p\theta_r)\omega_r \\ V_{B,emf} = p\psi_M \cos(p\theta_r)\omega_r \end{cases}$$ **Equation 4-7**

Again the rotor angle is defined as in figure 4.3. The constant ψ_M [Vs^{-1}] describes the maximal flux linking each winding with the rotor poles.

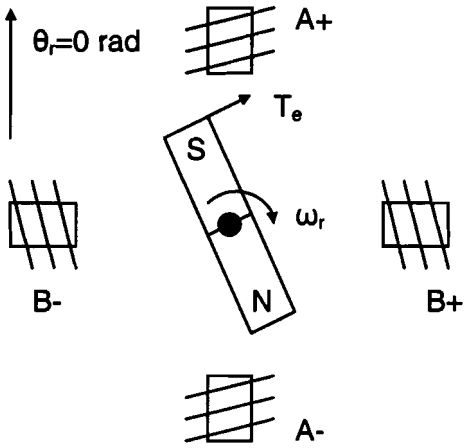

Figure 4-3: Schematic of a stepping motor with p = 1

The stepper motor has now been modelled as an ideal current/voltage to torque/angular speed converter together with a phase resistance and the viscous/coulomb frictions to account for the power losses (heat, iron losses ...). Figure 4.4 gives an impression of the power flow in the model. Because of this construction the maximum flux linkage must be equal to:

$$\psi_M = \frac{T_{pk}}{p \cdot I_0}$$ **Equation 4-8**

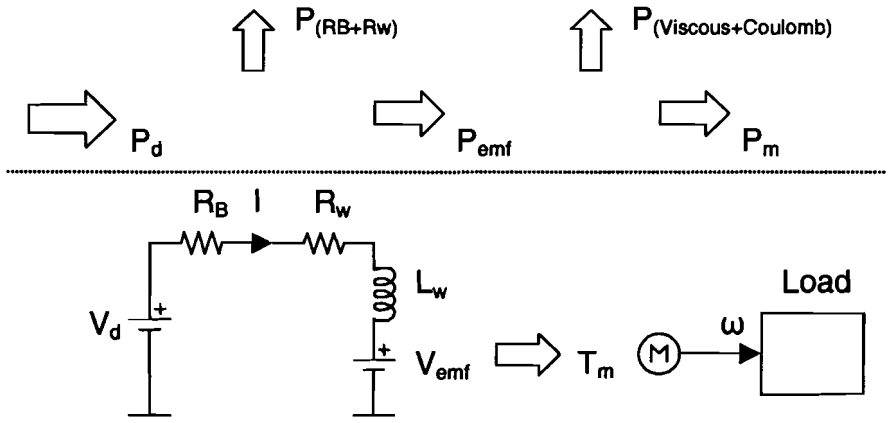

Figure 4-4: Power flow from motor driver to load

With equation 4.8, the equations 4.5 and 4.7 can be rewritten as:

$$\begin{cases} T_e = -k\left(I_A \sin(p\theta_r) - I_B \cos(p\theta_r)\right) \\ V_{A,emf} = -k \sin(p\theta_r)\omega_r \\ V_{B,emf} = k \cos(p\theta_r)\omega_r \end{cases}$$ **Equation 4-9**

With k [Nm A^{-1} or V s rad^{-1}] the motor constant:

$$k = \frac{T_{pk}}{I_0} = p\psi_M$$ **Equation 4-10**

Now the complete dynamics of the stepper motor connected to a mechanical load are described in mathematical form. To complete the whole system only the stepper motor driver has to be defined. The most common drivers used in stepper motor applications are choppers. Figure 4.5 shows a schematic of a chopper drive H-bridge, connected to one of the phases of the stepper motor.

The main purpose of a chopper is to force a pre-defined current through the winding of the stepper motor. By enabling the right combination of transistors the driver is able to force both positive and negative currents through the windings. But instead of just using a fixed voltage to create a current through the winding, the chopper uses a pulse width modulated voltage which is much higher then the actual voltage required for the current. This way the rise time of the current is smaller. Figure 4.6 shows a voltage / current diagram of a chopper.

As can be seen in figure 4.6, the current in the winding can be regulated by switching the voltage over the winding. This can be done for example by switching T_4 on, and switching T_1 with a PWM signal. The PWM signal is regulated with the voltage over R_s which is an indication of the current through the winding. If the voltage over R_s is too small T_1 must be switched off (situation 1 from figure 4.6), and if the voltage over R_s is too big T_1 must be switched on (situation 2). Because of the induction in the winding, the current will not decay rapidly to zero, and thus maintaining a current for a short time. When the H-bridge operates in situations 1 and 2, it is in the slow decay mode.

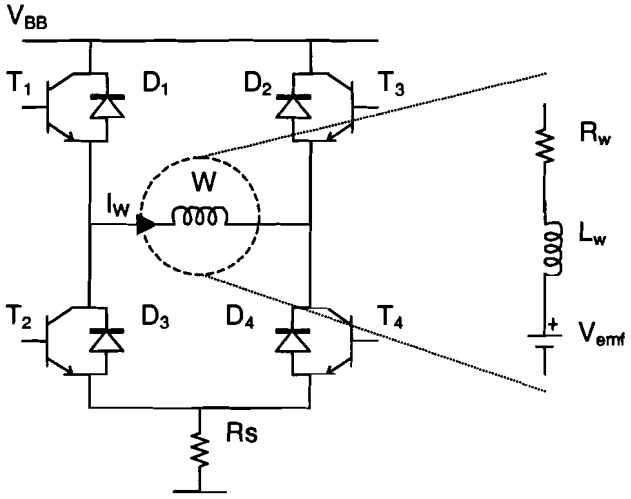

Figure 4-5: Voltage chopper H-bridge

But as figure 4.6 shows, in situation 3 when the voltage over the winding is turned off, the current decays much faster as when the circuit was in situation 2. This is done by also disabling T_4. Now the current in the winding can only flow through the diodes in the opposite direction of the voltage source V_{BB}. This ensures a high decay in the current, hence the name fast-decay mode. By exchanging T_1 with T_2, and T_4 with T_3 in the previous example, a negative current can be created trough the winding.

Modelling the voltage chopper is a bit more complicated then the other parts of the simulation model. The three situations described in the former part will be used as a guideline:

1. The current through the winding is lower then the reference current:
   The voltage is turned on, and an extra resistance is added to the voltage equation (4.4), R_{sd} the slow current decay rate resistance (the resistance of the H-bridge)
2. The current through the winding is higher then the reference current:

The voltage is turned off, still the slow current decay rate resistor is added to the voltage equation

3. The reference current is equal to zero:

The voltage is turned off, and now another resistance is added to the voltage equation, R_{fd} the fast decay resistor. This resistor simulates the fast current decay by forcing the current through a bigger resistor ($R_{fd} > R_{sd}$).

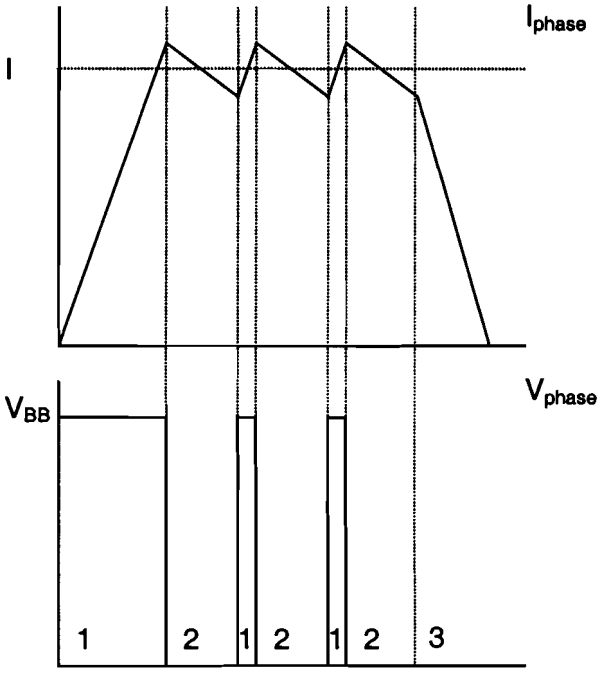

Figure 4-6: Voltage / current diagram of a chopper

4.2 *Implementing dynamics in a simulation model*

Instead of implementing the differential equations from part 4.1 directly in a model, the equations will be sampled, resulting in a set of difference equations. By doing so the performance of the simulation algorithm depends on the chosen sample-rate. This way of calculating is not the most efficient and reliable way to simulate, but it is simple to implement, and portable to different simulation environments and programming languages. The results are reliable as long as the sampling time is at most half the highest time constant of the simulation model. Even further shortening the sample time will improve the accuracy of the simulations.

First, consider the mechanical part of the system dynamics. The expression for the torque from equation 4.1 can be rewritten as:

$$N(\omega_r[k+1]-\omega_r[k]) = \frac{1}{J_L + J_R}(T_e[k]-T_f[k]-T_L[k]) \qquad \textbf{Equation 4-11}$$

With k the sample index, and N the amount of samples per second. The expression $N(\omega_r[k+1] - \omega_r[k])$ is the sampled derivative for the angular speed of the rotor (euler) . Equation 4.11 can be rewritten as:

$$\omega_r[k+1] = \frac{T_e[k]-T_f[k]-T_L[k]}{(J_L + J_R)N} + \omega_r[k] \qquad \textbf{Equation 4-12}$$

Because the torque T_e is produced by the stepping motor it must comply with (equation 4.9):

$$T_e[k] = -k\left(I_A[k]\sin(p\theta_r[k]) - I_B[k]\cos(p\theta_r[k])\right) \qquad \textbf{Equation 4-13}$$

And equation 4.11 has to comply with the rotor position derived from equation 4.2:

$$N(\theta_r[k+1]-\theta_r[k])=\omega_r[k]\Rightarrow\theta_r[k+1]=\frac{\omega_r[k]}{N}+\theta_r[k]$$ **Equation 4-14**

Already a part of the electrical - mechanical interaction between motor and environment is described by equation 4.11. The other part is the emf voltage produced by the rotation of the rotor (from equation 4.9):

$$\begin{cases}V_{A,emf}[k]=-k\sin(p\theta_r[k])\omega_r[k]\\V_{B,emf}[k]=k\cos(p\theta_r[k])\omega_r[k]\end{cases}$$ **Equation 4-15**

And finally to complete the set of equations, the electrical part of the model is described as (derived from equation 4.4):

Equation 4-16

$$N(I_{phase}[k+1]-I_{phase}[k])=\frac{1}{L_w}(V_{phase}[k]-I_{phase}[k]R_w-V_{phase,emf}[k])$$

Rewriting 4.14 to describe the current through the windings:

$$\begin{cases}I_A[k+1]=\frac{1}{N\cdot L_w}\left(V_A[k]-V_{A,emf}[k]\right)+\frac{N\cdot L_w-R_w}{N\cdot L_w}I_A[k]\\I_B[k+1]=\frac{1}{N\cdot L_w}\left(V_B[k]-V_{B,emf}[k]\right)+\frac{N\cdot L_w-R_w}{N\cdot L_w}I_B[k]\end{cases}$$ **Equation 4-17**

Equations 4.12, 4.13, 4.14, 4.15 and 4.17 describe the way the different states of the electrical - mechanical system interact. Figure 4.7 shows a schematic of the interaction between all states.

The only part that is not yet described, is the driving circuit for the stepping motor. Part 4.1 describes how a current can be forced through the windings of a stepping motor, and part 3.1 describes how the two phases of the stepping motor must be excited to make the rotor rotate clock or counter clockwise. But for the simulation model these principles must be formalised.

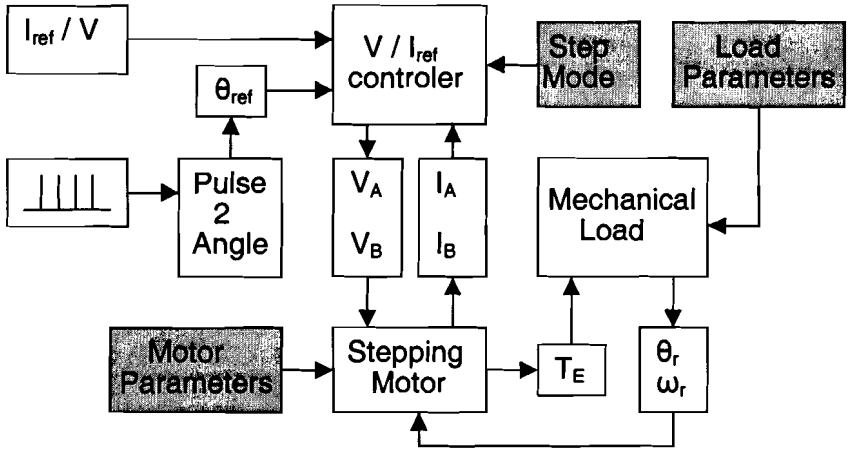

Figure 4-7: Interaction between different part of the simulation model

The input of the motor driver is a pulse train containing the step moments in time, and the driver converts this information to the current switching in the H-bridge. The chopper is set to a current I_{ref} the reference current for the windings, and the chopper has a voltage V_m to induce this reference current. First lets consider the basic way of driving the stepping motor,

with full stepping. Figure 4.8 shows the required current through both phases for full stepping.

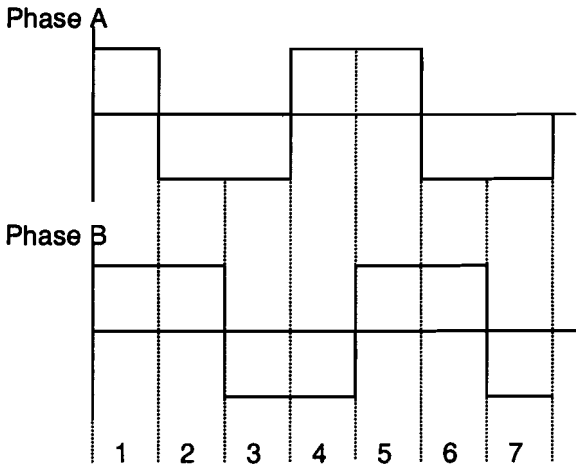

Figure 4-8: Required driver currents for full step mode

The required currents have the periodical form of a sinus. If every reference step angle is indexed by the integer i, then the reference currents for each phase can be described by:

$$\begin{cases} I_{A,ref}[k] = \sqrt{2} \cdot I_{ref} \cos\left(\frac{\pi}{2} i - \frac{\pi}{4}\right) \\ I_{B,ref}[k] = \sqrt{2} \cdot I_{ref} \sin\left(\frac{\pi}{2} i - \frac{\pi}{4}\right) \end{cases}$$ **Equation 4-18**

with the reference step angle θ_{ref} [rad] defined as:

$$\theta_{ref}[k] = i \frac{\pi}{2p}$$ **Equation 4-19**

So if at sample moment k a pulse is encountered in the input pulse train, the step index i will be increased or decreased with one, depending on the required direction of the rotor (clockwise / counter clockwise). So the chopper has to regulate the voltage in such way that the phase current equals its reference value. This is done by logical operations:

- **If** $I_{phase,ref} > 0$ **then**
  - **If** $I_{phase} < I_{phase,ref} - \gamma$ **then** $V_{phase} = V_m$
  - **If** $I_{phase} > I_{phase,ref} + \gamma$ **then** $V_{phase} = 0$

- **If** $I_{phase,ref} < 0$ **then**
  - **If** $I_{phase} > I_{phase,ref} + \gamma$ **then** $V_{phase} = -V_m$
  - **If** $I_{phase} < I_{phase,ref} - \gamma$ **then** $V_{phase} = 0$

With γ a constant to prevent the chopper from continuously chopping.

In the construction of the model some properties of the motor have been simplified:
- The torque is linearly dependent on the current through the winding
- The relation between the torque and the rotor angle is assumed to be sinusoidal
- The emf voltage is linearly dependent on the angular speed of the rotor
- The relation between the emf voltage and the rotor angle is sinusoidal
- The model does not take into account the magnetic saturation of the stator poles, eddy currents, skin effect and hysteresis
- The model only makes an estimation of the motor behaviour. The accuracy of the simulation depends on the chosen sample rate

Together with the unknown performance of the simulation model, these limitations give a good idea on the needed measurements to validate the model. Chapter 5 will analyse the performance of the algorithm against real measurements.

4.3 *Enhancing the current driver: implementation of different step modes*

Ideally the stepping motor would be driven by forcing sinusoidal currents through the windings. This would make sure that the rotor no longer has discrete angle positions, improving the damping of the rotor movement. Modern driver circuits deliver an approximation by using different step modes, varying from half stepping to micro stepping. Figure 4.9 shows some different driving modes.

The basic form of the reference currents remains to be sinusoidal, but they are divided into different fixed current levels. Equation 4.18 can still be used, with two little changes:

$$\begin{cases} I_{A,ref}[k] = \sqrt{2} \cdot I_{ref} \cos\left(\dfrac{\pi}{2 \cdot M} i - \dfrac{\pi}{4}\right) \\ I_{B,ref}[k] = \sqrt{2} \cdot I_{ref} \sin\left(\dfrac{\pi}{2 \cdot M} i - \dfrac{\pi}{4}\right) \end{cases}$$

Equation 4-20

The constant M is defined as the stepping mode. With M = 1 resulting in full step, M = 2 in half step, M = 4 in quarter step and so on. Now the reference step angle expression from equation 4.19 must also be changed to:

$$\theta_{ref}[k] = i \frac{\pi}{2p \cdot M}$$

Equation 4-21

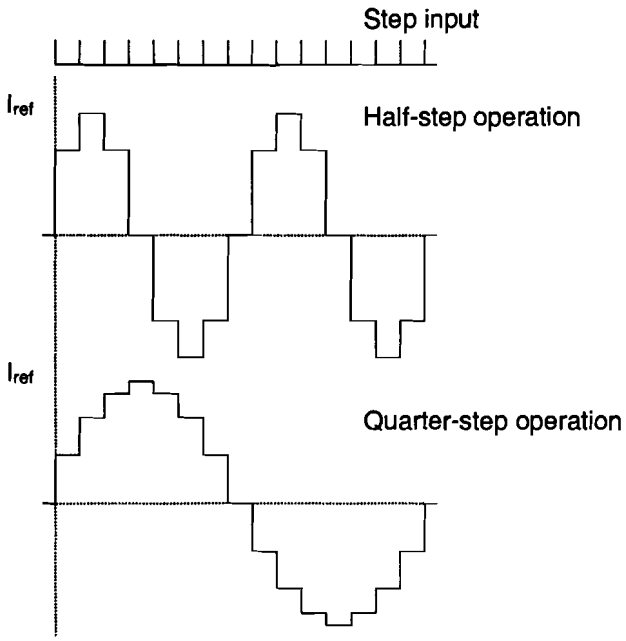

Figure 4-9: Different current driving modes

Notice that just like the real motor drivers, the simulation driver really makes steps according to the stepping mode. Unlike the real motor drivers, the proposed changes do not take into account the effect of choosing different decay modes, as explained in section 4.1. Motor driver manufacturers like Allegro implement mixed current decay modes to improve the performance of the driver chip. The precise reasons why to use mixed decay modes, and the resulting currents through the winding can be found at [3]. In the simulation model the mixed

decay mode is simulated with a variable resistor. Figure 4.10 shows how the mixed decay mode is implemented for quarter step operation.

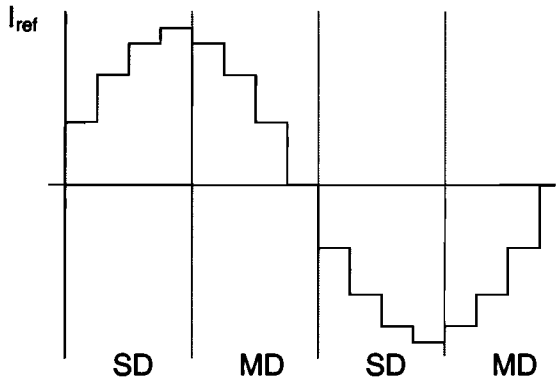

Figure 4-10: Current decay modes: SD = slow decay, MD = mixed decay

When the motor driver operates in the mixed decay mode, the bridge resistance is set to:

$$R_b[k] = \frac{R_{MD}}{|I_{ref}[k]|} \qquad \textbf{Equation 4-22}$$

With R_{MD} a resistor constant, which must be chosen in such way that the actual current through the winding resembles the reference current as much as possible. If the motor driver is in the slow decay mode, the bridge resistance should be equal to the output on resistance supplied by the driver chip manufacturer. To implement the current decay mode bridge resistor, the current equation 4.17 should now be changed to:

$$\begin{cases} I_A[k+1] = \dfrac{1}{N \cdot L_w}\left(V_A[k] - V_{A,emf}[k]\right) + \dfrac{N \cdot L_w - R_w - R_{A,b}[k]}{N \cdot L_w} I_A[k] \\ I_B[k+1] = \dfrac{1}{N \cdot L_w}\left(V_B[k] - V_{B,emf}[k]\right) + \dfrac{N \cdot L_w - R_w - R_{B,b}[k]}{N \cdot L_w} I_B[k] \end{cases} \qquad \textbf{Equation 4-23}$$

Note that when the reference current is equal to zero, the bridge resistor can no longer be calculated with equation 4.22. To avoid problems at zero current levels, the bridge resistor is clipped to a finite value. Also remember that the decay modes, as implemented in the simulation model, do not have any physical relevance. It is just a way to emulate the current waves of a chopper.

4.4 *Simulating with the algorithm*

The proposed simulation algorithm has many simulation parameters. Table 4.1 gives a summary of these parameters. Most of these parameters can be directly found in the datasheets supplied by the manufacturer. The exceptions are: ψ_M, R_{MD} and all parameters which must be chosen by the user. The way the parameter R_{MD} should be chosen is explained in the previous section.

The parameter ψ_M can be acquired by two means. The preferred method is to measure the back emf voltage of the stepping motor at a certain angular speed of the rotor, and calculate ψ_M with the following expression:

$$\psi_M = \frac{\sqrt{2} \cdot V_{emf,RMS}}{p \cdot \omega_m} \qquad \textbf{Equation 4-24}$$

Sometimes the manufacturer already supplies the back emf voltage at a certain angular speed, making this measurement obsolete. Of course the maximum flux linkage can also be calculated with equation 4.8. But this results in an estimate of the maximum flux linkage.

Table 4-1: simulation parameters and their sources

Parameter	Unit	Explanation
T_{pk}	Nm	Peak static torque, often referred to as holding torque
J_R	Kg m^2	Rotor inertia
R_W	Ω	Winding resistance
L_W	H	Winding inductance
I_0	A	Rated current
p	-	Number of rotor teeth
ψ_M	Vs^{-1}	Maximum flux linking each winding
Supplied by motor manufacturer		
$R_{b,on}$	Ω	output on resistance
R_{MD}	-	Mixed decay resistor constant
Supplied by motor driver manufacturer		
V_m	V	Voltage over H-bridge
I_{ref}	A	Peak reference current
M	-	Stepping mode
N	s^{-1}	Sample rate
T_{fp}	Nm	Friction parameters
Must be chosen by user		

The parameter T_{pk} must be chosen carefully. Most manufacturers supply this parameter for both phases on. The model has been slightly changed, so it will also expect a T_{pk} for both phases on. The relation between the peak static torque for both phases on and for only one phase on is:

$$T_{pk,2\,phases} = \sqrt{2} \cdot T_{pk,A} = \sqrt{2} \cdot T_{pk,B} \qquad \textbf{Equation 4-25}$$

As at the beginning of this chapter was stated, this model can also be used with ordinary PM stepper motors. For correct implementation, the parameter p, describing the number of rotor teeth, must describe the number of north/south pole pairs of the rotor.

In appendix A is the first draft of the simulation algorithm, working with the methods described in the current chapter. The next chapter will analyse the performance and simulation limits of the model.

5 Measurements for the validation of the simulation model

The previous chapter already warned for some limitations of the simulation model of the bipolar (hybrid) stepper motor:

- The torque is assumed to be linearly dependent on the current through the winding
- The relation between the torque and the rotor angle is assumed to be sinusoidal
- The emf voltage amplitude is assumed to be linearly dependent on the angular speed of the rotor
- The relation between the emf voltage and the rotor angle is assumed to be sinusoidal
- The model does not take into account the magnetic saturation of the stator poles, eddy currents, skin effect and hysteresis
- The model only makes an numerical estimation of the motor behaviour, and the accuracy depends on the chosen sample rate

To see the impact of these limitations, a series of tests have been performed to validate the simulation algorithm and asses the accuracy and reliability of the model. This has been done by six experiments:

1. The relation between peak static torque and winding current
2. The relation between angular speed and emf voltage
3. The angular speed at different stepping rates
4. The winding current at different stepping rates
5. The motor efficiency at different stepping rates
6. The dynamical performance of the motor

The measured data from 3, 4, 5 and 6 will be compared with simulation results at different sample rates. The data from 1 and 2 will be used to verify some basic assumptions made during the design of the simulation model. All simulations will be performed with a sample rate of N = 50000 samples per second. The behaviour of the stepping motor can then be calculated for stepping rates up to 5 kHz (a sample rate of 10 times the input stepping rate has been proven to be acceptable).

At the end of this chapter is a small evaluation of the measurement results.

5.1 Torque versus winding current

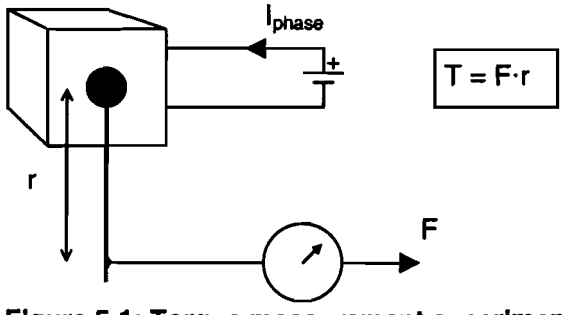

Figure 5-1: Torque measurement experiment

Figure 5.1 shows the experimental set-up to measure the peak static torque for different winding currents. The measurement is intended to investigate the linearity between the peak static torque and the current through the winding. It will show the limitations of the simulation model, as the model assumes, without restraints, a linear relation between the current and the torque.

The experiment is conducted by measuring the maximum force applied on the lever, before the stepping motor is released from its step position. By repeating this procedure for different winding currents, a relationship between the torque and current is revealed. Figure 5.2 shows the result for four different types of hybrid stepping motors.

The results of this experiment show that the linearity between the torque and current is not true. But as long as the current is below the rated current supplied by the manufacturer, this should not be a problem. For currents higher then the rated current, the motor becomes

magnetically saturated, impairing the further build-up of torque. Only the PK266M-E2.0B from figure 5.2b is already magnetically saturated before reaching the rated current.

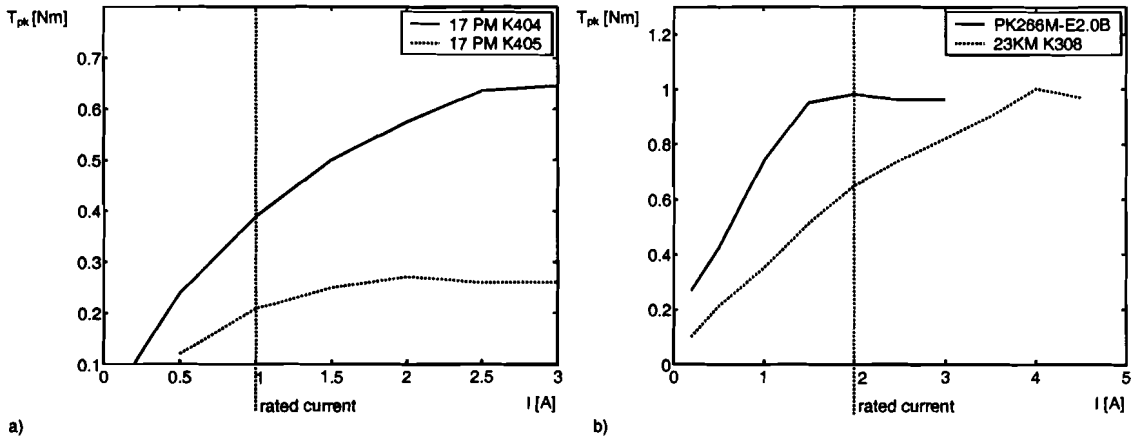

Figure 5-2: Static peak torque versus current for I_{rated} = 1A (a) and I_{rated} = 2A (b)

Although the magnetic saturation starts to play a significant role in the total torque current relationship when the winding current is higher then the rated current, it is obvious that a reasonable increase of torque can be achieved by doing so (at least for the 17PM-K404, 17PM-K405 and the 23KM-K308 from figure 5.2). The only disadvantage is the increased heat production, but for short motor operations this should not be a problem.

5.2 *EMF voltage versus angular speed*

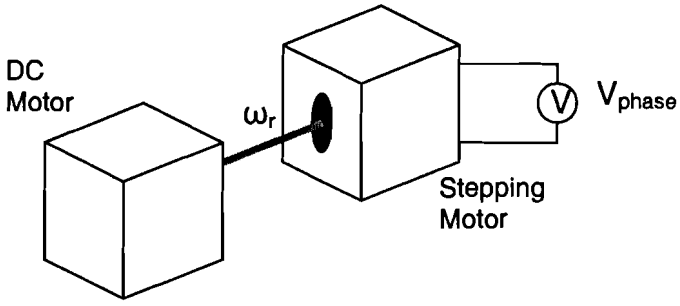

Figure 5-3: Emf voltage measurement

Besides the assumption of a linear relation between the torque and the current, also a linear relation between the emf voltage and the angular speed is assumed. The way to determine the emf voltage is already outlined in chapter 4.4. Figure 5.3 shows the experimental set-up to measure the emf voltage at different angular speeds.

Figure 5.4 shows the results of two measurements. The relation between the angular speed and the emf voltage is linear for both measurements. As stated in part 4.4 the emf voltage should be a function of the rotor angular speed and the parameters p and ψ_M. From the measurements the parameter ψ_M can be determined:

Table 5-1: Three ways to get parameter ψ_M (for three stepping motors)

Stepping motor	$\psi_{M,measured}$ [Vs^{-1}]	$\psi_{M,ideal}$ [Vs^{-1}]	$\psi_{M,manufacturer}$ [Vs^{-1}]
17PM-K404	$7{,}3 \cdot 10^{-3}$	$7.8 \cdot 10^{-3}$	$7.6 \cdot 10^{-3}$
17PM-K542	$4.4 \cdot 10^{-3}$	$4.5 \cdot 10^{-3}$	$4.5 \cdot 10^{-3}$
23KM-K308	$6.2 \cdot 10^{-3}$	$6.1 \cdot 10^{-3}$	$6.3 \cdot 10^{-3}$

As the results in table 5.1 show, the parameter ψ_M from the manufacturer is very close to the parameter obtained by the simulations and the measurements.

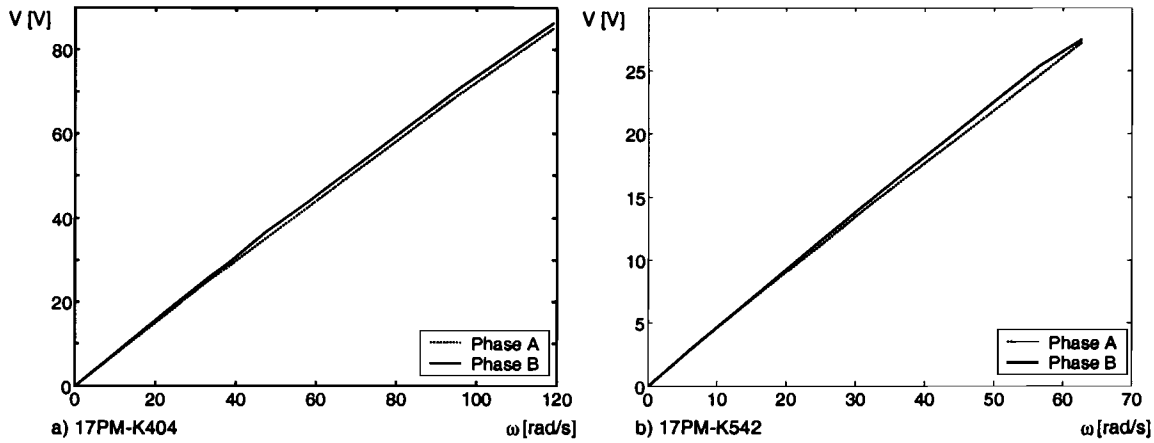

Figure 5-4: Two measurements of the emf voltage

5.3 *Rotor position and angular speed*

The first measurement to determine the accuracy of the simulation model, is a set of rotor movement tests. For these experiments the angle between the rotor and stator is measured by a quadrature encoder with 1000 slits, resulting in a resolution of 4000 samples per revolution. This resolution should be sufficient for accurately measuring the rotor angle of the stepping motors, used during the experiments (200 steps per revolution).

The first test is to calibrate the simulation model with the real motor. In chapter 4 the friction opposing the rotor movement was described by equation 4.3:

$$T_f = b_f \cdot \omega_m + c_f \cdot sign(\omega_m)$$

This expression contains two unknown parameters, the coulomb friction c_f, and the viscous damping b_f. These parameters can be estimated by a single step response of the stepping motor. Figure 5.5 shows the effects on an single step response by each part of the frictions separately. Notice that the response with coulomb friction, shows a linear decay of the rotor angle position error in time, and the viscous damped response shows an exponential decay of the rotor angle position error in time.

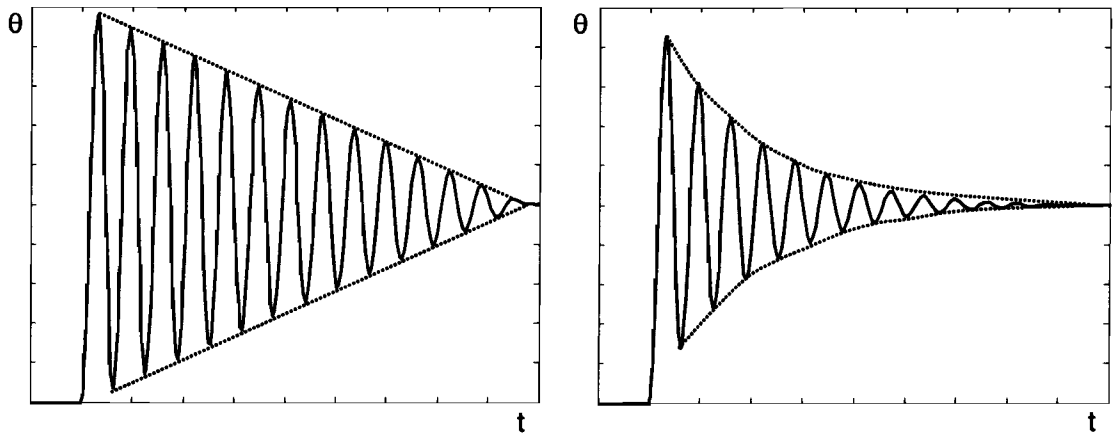

a) Coulomb friction only b) Viscous damping only

Figure 5-5: Simulation of the effect of coulomb friction and viscous damping on a single step response

The two friction parameters will be estimated by fitting the simulations of a single step response of the stepping motors, to the actual responses measured during the tests.

Figure 5.6 shows the single step responses measured from two stepping motors, the 17PM-K404 and the 23KM-K308 (See appendix G for motor specifications). As can be observed

from the figures, the fundamental part of the damping seems to be produced by the viscous damping (because the two single step curves have an exponential decay of the rotor angle position error in time). So the obvious way to estimate the friction parameters, is by first fitting the simulation curve, by changing the viscous damping. When the fit seems to be acceptable, the coulomb friction will be used to possibly improve the fit.

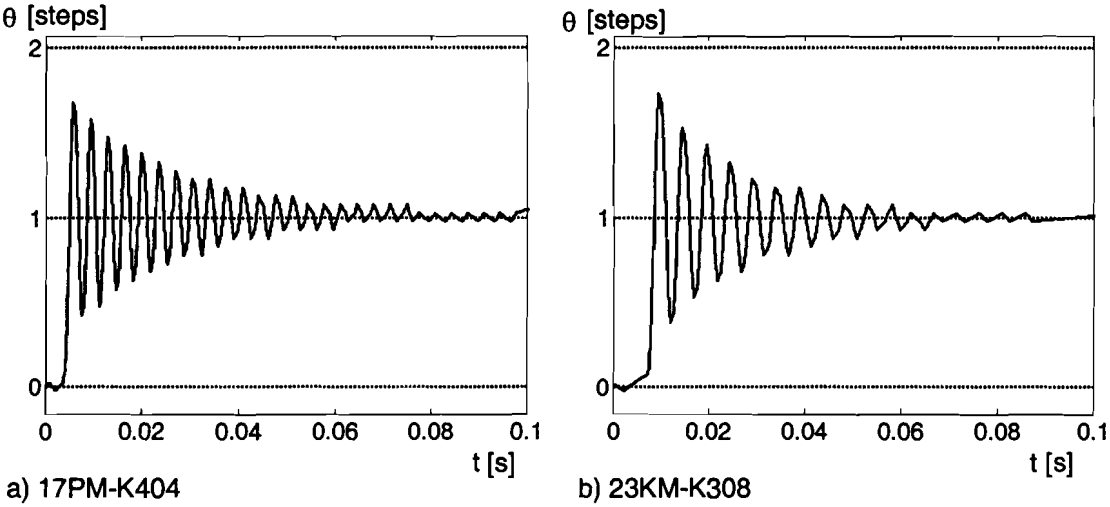

a) 17PM-K404 b) 23KM-K308

Figure 5-6: Measured single step responses

After changing the friction parameters by trial and error, the following estimates have resulted in satisfactory fits:

	17PM-K404	23KM-K308	unit
c_f	0.1	0.2	mN m
b_f	0.8	1.8	mN m s rad^{-1}

Figure 5.7 shows the resulting fit for both stepping motor.

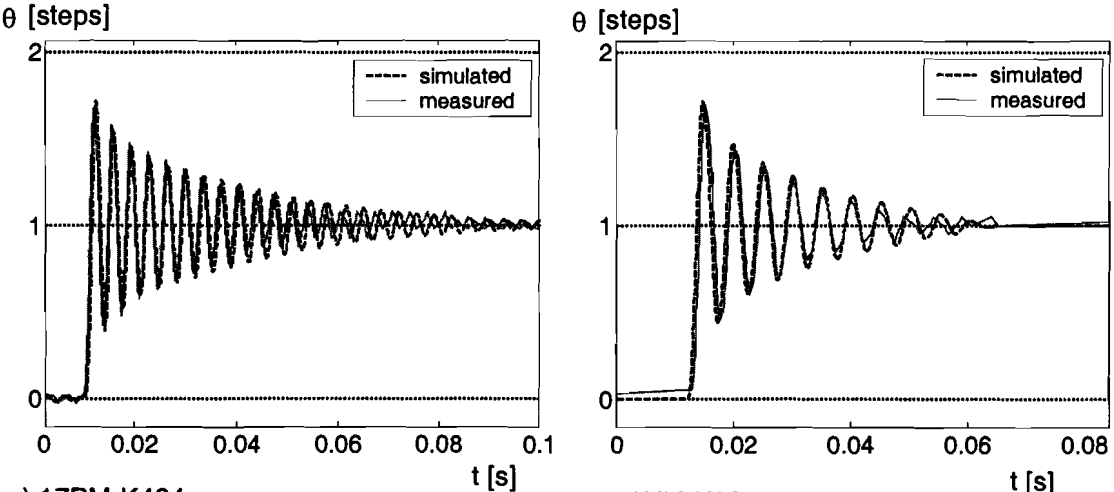

a) 17PM-K404 b) 23KM-K308

Figure 5-7: Simulation step responses calibrated with the measurements

Now that the stepping motor simulation parameters of the 17PM-K404 and the 23KM-K308 are calibrated with their real behaviour, some angular speed tests can be performed to compare the simulation model motor behaviour with the true motor behaviour. Figure 5.8 shows a plot of the 17PM-K404, running at a stepping rate of 100 Hz. The simulation model results seem to be close to the true motor behaviour, but after a close examination of the plot, one sees rectangular glitches in the measured data plot. These glitches are not produced by the motor, but by the encoder.

At higher step rates the encoder noise becomes even a bigger problem. That is why the measurement and simulation data will be examined in the frequency domain. Because the

glitches are rectangular, major part of their energy will be in high frequencies. The frequency dynamics of the rotor movement depends on the inertia of the rotor, and the natural frequencies of both motors are in-between 100 and 400 Hz, far below the encoder introduced noise.

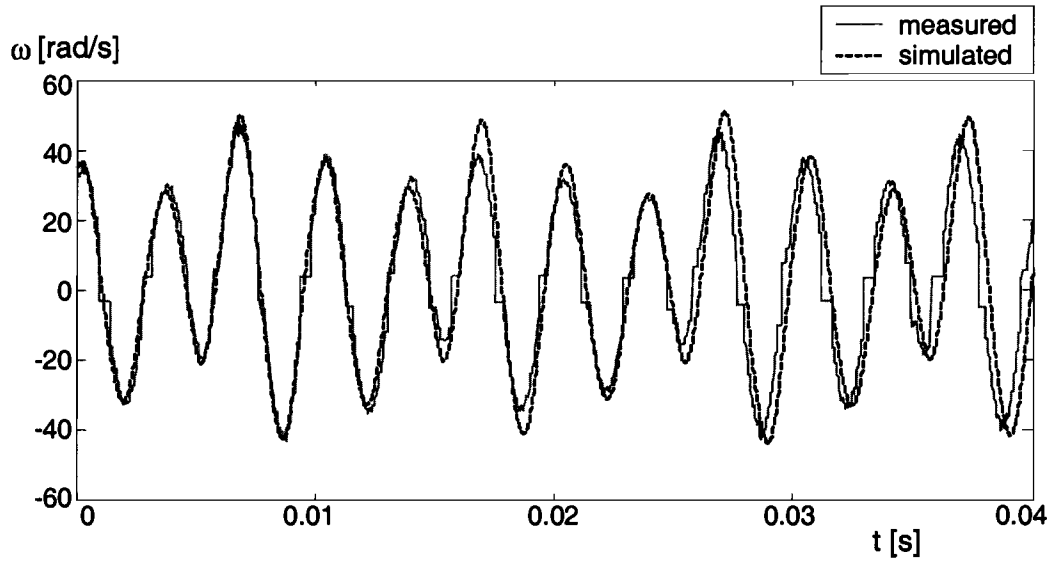

Figure 5-8: Angular speed of the 17PM-K404 at f_s = 100 Hz

Figure 5.9 and 5.10 show the measured versus simulated angular speeds for the 17PM-K404. For a step rate of 100 Hz (5.9a) the measurements and simulations produce nearly similar frequency spectra. The same can be said for the 500 Hz step rate plot (5.9b), when considering that the encircled peaks are encoder attributes (the encircled peaks can be identified as encoder noise, see Appendix B.1).

The f_s = 1 kHz measurement (5.10a) shows peaks which can not be predicted by the stepper motor simulation. Also the encoder analysis of Appendix B.1 does not predict any encoder attribute at these peak locations. The first peak is the natural frequency of the mechanical system (located at ±250 Hz). The f_s = 500 Hz simulation already shows a small difference between the simulated and measured peak at the natural frequency, indicating a model mismatch in the simulation model.

The 250 Hz peak does not show in the simulation result, but the 2 peaks at 500 Hz and 750 Hz are encoder attributes. Appendix B.1 again shows that new frequency peaks emerge when using an encoder to record a 250 Hz angular speed oscillation. So in fact the only missing peak is the natural frequency peak. This means that the simulated rotor movement is better damped as the real rotor movement.

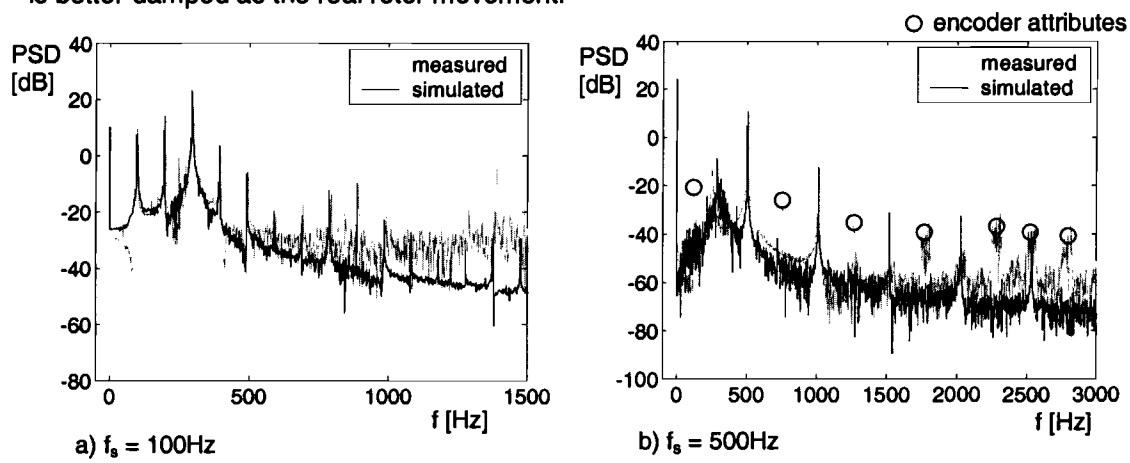

Figure 5-9: Frequency spectrum of angular speeds for f_s = 100Hz and f_s = 500 Hz

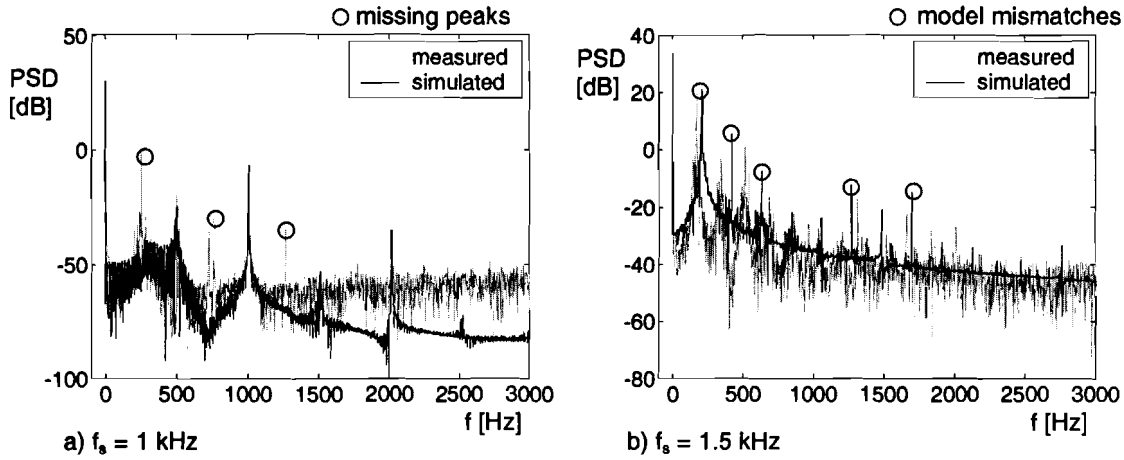

Figure 5-10: Frequency spectrum of angular speeds for f_s = 1 kHz and f_s = 1.5 kHz

The last simulation (figure 5.10b, f_s = 1.5 kHz) shows the frequency differences between the different peaks. The natural frequency peak of the simulation (again at a frequency of ±250 Hz) is slightly to the right of the measured peak. This shows that the simulated system is stiffer then the measured system, meaning that the difference between the real torque produced by the motor, and the predicted torque by the simulation model is increasing.

The definition of the natural frequency of the stepper motor oscillations (equation 3.5) show that the real stepper motor stiffness at f_s = 1500 Hz must be between 9.1 and 9.5 Nm rad^{-1}, the simulated natural frequency result to a stiffness between the 13.9 and 14.6 Nm rad^{-1}, a 55% prediction error. Unfortunately the stiffness as f_s = 1 kHz cannot be analysed, because the simulation does not show a resonance peak at the natural frequency. At f_s = 100 Hz and f_s = 500 Hz the natural frequency peak locations of both the simulations and the measurements are very close to each other.

The measurements and simulations of the 23KM-K308 show the same results as for the 17PM-K404. These results can be found in appendix B.2. Higher stepping frequencies have not been used for model validation, because the stepping motors could not be set above the instability rate, without being damped (both simulation model and the actual motor stall).

5.4 *The winding current, measurements versus simulations*

As explained in chapter 3.3 the stepping motor behaviour can be divided in two different situations, because of the current build-up in the windings:

- At low speeds the winding current has enough time to reach its reference current, before having to change polarity.
- At high speeds the winding current is no longer capable of reaching its reference value, before changing from polarity.

Besides these regions of normal operation, the stepping motor also suffers from instabilities:

- At low speeds because of the resonance of the rotor, resulting in a mechanical instability region.
- At high speeds because of electrical resonance's, resulting in an electrical instability region.

These regions will be used to analyse the stepping motor currents, for both the cases with no external load connected to the motor, and the motor connected to a brake torque producing motor. The results will be compared with results from the simulation model.

5.4.1 No load connected to the motor

A series of measurements have been performed on the 17PM-K404 stepping motor to get an idea of the way the winding current suffers from different parasitic effects like winding inductance, eddy currents etc. Comparing the results of the measurements with simulation

results will give an indication of the simulation model accuracy, and the impact of neglecting several motor impairments.

The basic wave-form of the currents measured and simulated are displayed by figure 5.11 and 5.12. As can be seen from figures 5.11, the difference between the simulations and the measurements is small for low stepping rates. The step rate of 273 Hz (figure 5.11a) is near the natural frequency of the motor. The little peaks on top of the constant current levels are emf attributes, which can also be found in the simulation results. The simulation of the stable stepping rate of 505Hz is very close to the measurements.

Figure 5.12 shows, that at medium stepping rates the simulation results begin to differ from the measured results. The angular speed measurements already showed that simulations near the electrical instability rate showed a difference in stator rotor stiffness. This indicates that the simulation model torque predictions are to optimistic. The currents measurements show the same trend.

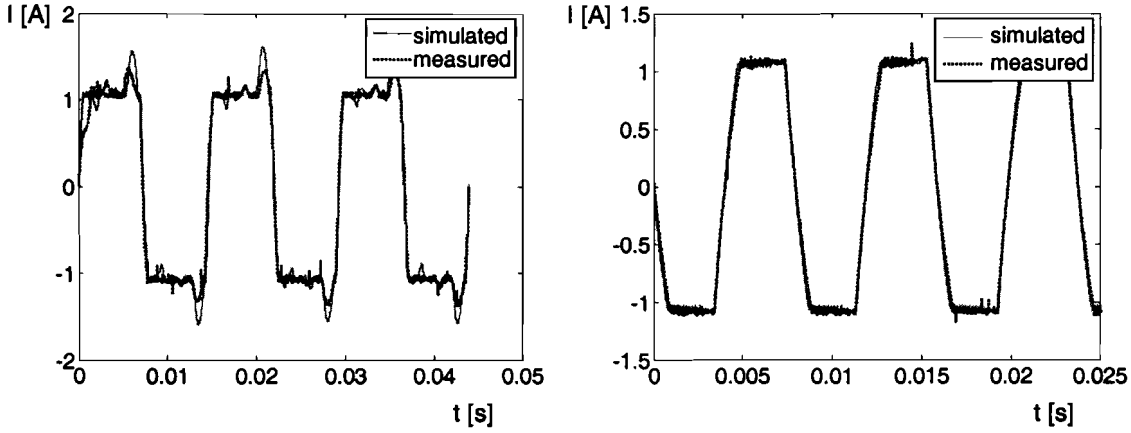

a) f_s = 273 Hz b) f_s = 505 Hz

Figure 5-11: Winding currents at low stepping rates

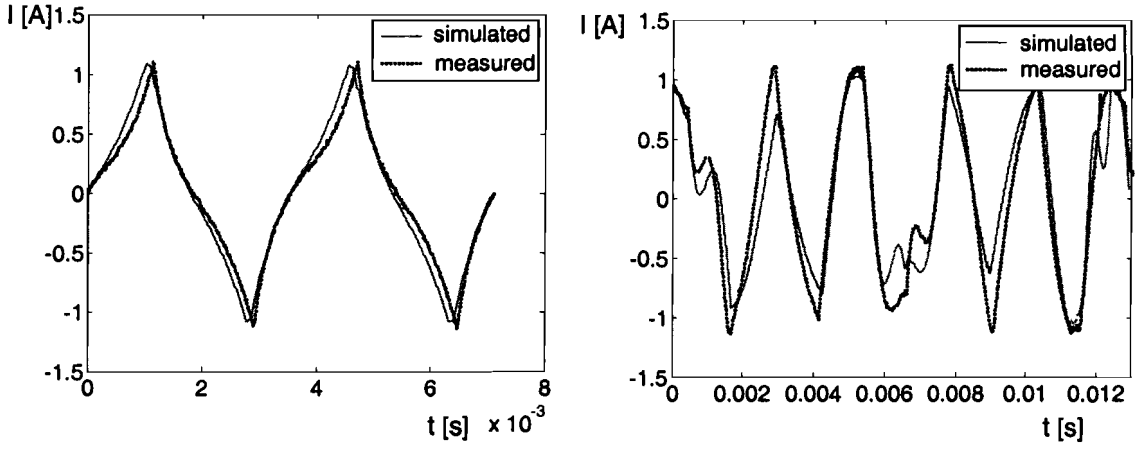

a) f_s = 1124 Hz b) f_s = 1617 Hz measured, f_s = 1750 simulated

Figure 5-12: Winding currents at medium stepping rates

Performing the simulation of the stepping rate 1124Hz shows that the winding resistance should increase with 8Ω (above the 4.7Ω the winding has at stepping rate zero), to get the same results as the measurements.

Figure 5.12b shows the stepper motor currents at 1617 Hz. This stepping rate is in the middle of the electrical instability region. To match the simulated current waveforms with the measured waveforms, the simulation step rate had to be increased to 1750. This again shows a model impairment Hz (the current wave of 1750Hz form of 5.12b has been normalised to 1617Hz).

A list of the rms values of the measured and simulated currents is shown in table 5.2. Again the results show an increasing model prediction error, when simulating higher step rates.

The currents at 1617 Hz are also unstable, making the error analysis impossible. Currents of higher stepping rates could not be measured, because of motor failure (without any form of damping, the motor could not maintain angle synchronisation above 1800 Hz).

Table 5-2: RMS of currents, and simulation error

Step rate [Hz]	Measured I_{rms} [A]	Simulated I_{rms} [A]	Simulation error [%]
273	1.06	1.09	-3
505	0.94	0.95	-1
1124	0.53	0.59	-10
1617	-	-	-

5.4.2 Measurements with known load

Using a stepper motor without driving any load is not very useful, so measurements of a stepper motor driving a known mechanical load will give a better idea of the simulation model performance in realistic situations. A series of measurements have been performed, using a brake torque bench to analyse the winding currents when the stepper motor has to produce torque.

Again no simulations could be performed above the 1.1 kHz, because of electrical instability. The rms values of the measured and simulated winding currents are described by table 5.3. The variable T_x stands for the brake torque produced by the bench. Again the measurements become less reliable when increasing the stepping rate. But the error remains of the same order, when increasing the brake torque.

The plots of the results are displayed in appendix C, but to get an idea of the difference between simulations and measurements, two plots of measurements and simulations at a stepping rate of 505 Hz are displayed by figure 5.15. As can be seen from the figure, only the rising part of the winding currents are different (encircled parts in figure 5.15a and 5.15b). To make the simulation currents match the measured currents, an extra loss resistance of 8Ω must be placed in series with the winding (figure 5.16 shows the match for the 505 Hz, 250 mNm situation.

Table 5-3: Winding current measurements of 17PM-K404

	Measured I_{rms} [A]	Simulated I_{rms} [A]	Simulation error [%]
Step rate = 284Hz			
T_x = 50 mNm	1.03	1.00	3
T_x = 100 mNm	0.96	1.00	-4
T_x = 250 mNm	-	-	-
Step rate = 505 Hz			
T_x = 50 mNm	0.89	0.93	-4
T_x = 100 mNm	0.89	0.93	-4
T_x = 250 mNm	0.91	0.94	-3
Step rate = 1115 Hz			
T_x = 50 mNm	0.51	0.59	-15
T_x = 100 mNm	0.51	0.59	-15
T_x = 250 mNm	0.57	0.66	-17

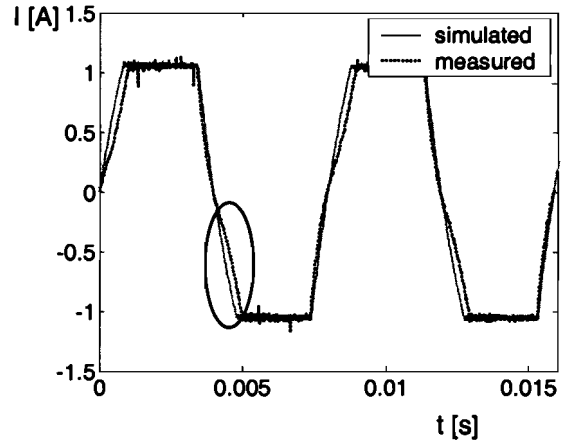

a) f_s = 505 Hz, T_x = 100mNm

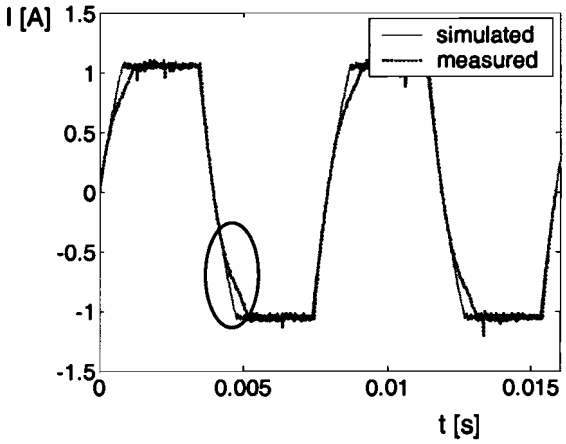

b) f_s = 505 Hz, T_x = 250mNm

Figure 5-13: Winding current plots at f_s = 505 Hz

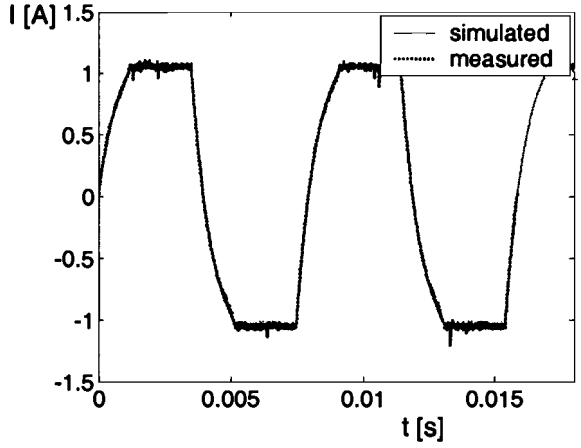

Figure 5-14: Matched winding current at f_s = 505 Hz, T_x = 250 (R_x = 8Ω)

5.5 *Efficiency and torque measurements*

The current measurements from the previous section show the motor suffers from losses, not implemented in the model. These losses can be implemented by adding an extra winding resistance, as done for two situations in the previous section. But a better way to analysis differences between the simulation model and the real world would be to look at the power flow through the motor. This analysis has been performed with the 17PM-K404 driving the brake torque bench, at stepping rates where the chopper can no longer maintain its reference current (this ensures nice square wave voltages from the H bridge).

Figure 5.15 shows the power flow from the measured system. The measured variables are the DC voltage of the two H bridges (V_{dc}), the average current dissipated by the H bridges ($I_{average}$), the winding current, the mechanical torque produced by the brake torque bench (T_m) and the mean angular speed of the motor and brake torque bench (ω_m).

The bridge resistance and sense resistance of the H bridge are also known, so a approximation of the bridge losses $P_{loss,bridge}$ can be made by:

$$P_{loss,bridge} = 2 \cdot I_w^2 (R_{bridge} + R_{sense}) \qquad \textbf{Equation 5-1}$$

With I_w the winding current of one phase, R_{bridge} the bridge resistance and R_{sense} the sense resistance. The processing of the measurements are done with the assumption that the H-bridge switching losses are negligible small (no chopping, so the switching frequencies of the H bridges are at half of the stepping rate).

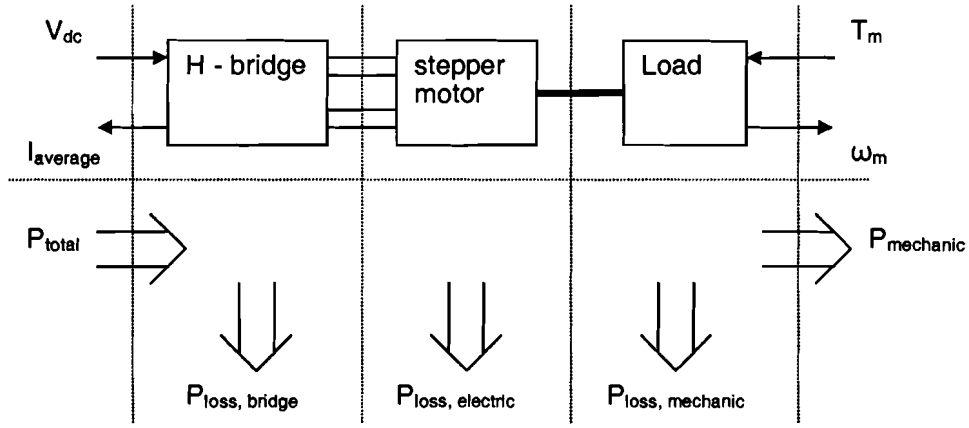

Figure 5-15: Power flow situation of measurements with the brake torque bench

The electrical power losses of the stepping motor are partly from the winding resistance, and partly of higher order effects as iron losses. The second part of the losses is unknown (the model from chapter 4 does not incorporate these losses), but the winding resistance losses $P_{loss,winding}$ can be expressed with:

$$P_{loss,winding} = 2 \cdot I_w^2 \cdot R_w \qquad \textbf{Equation 5-2}$$

The last losses are the mechanical losses from coulomb and viscous frictions in the system. These mechanical losses ($P_{loss,mechanic}$) can be expressed with:

$$P_{loss,mechanic} = b_f \cdot \omega_m^2 + c_f \cdot \omega_m \qquad \textbf{Equation 5-3}$$

With b_f the viscous friction and c_f the coulomb friction measured in section 5.3. The friction of the brake torque bench is assumed to be negligible small.

The only losses which cannot be determined are the higher order electrical losses. These remain an unknown variable for the power flow analysis. Figure 5.16 shows the measured motor efficiencies at different step rates and brake torque's. The motor efficiency is defined as:

$$efficiency = \frac{P_{mechanical}}{P_{total} - P_{loss,bridge}} \cdot 100\% \qquad \textbf{Equation 5-4}$$

With $P_{mechanical}$ the mechanical energy dissipated by the brake torque bench, and P_{total} the total electrical power produced by the H bridge voltage source (= $V_{dc} \cdot I_{average}$). The $P_{loss,mechanic}$ are considered a part of the total stepper motor losses.-+

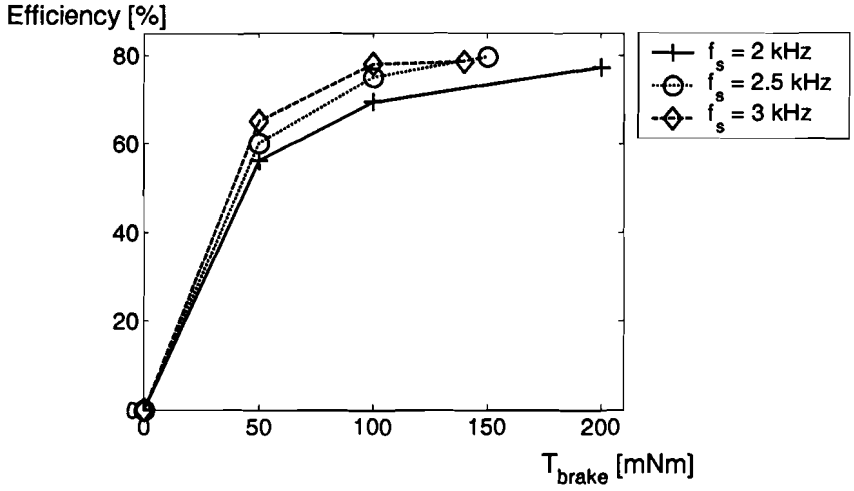

Figure 5-16: Measured efficiency of the 17PM-K404

The measurements from above also have been simulated. The results are shown by figure 5.17. These simulations have been performed under the following circumstances:

R_{bridge}	0.81 Ω/phase	from datasheet
R_{sense}	0.25 Ω/phase	from datasheet
$R_{winding}$	4.7 Ω/phase	from datasheet
b_f	0.8 mN m s rad^{-1}	from measurements section 5.3
c_f	0.1 mN	from measurements section 5.3

The simulated efficiency curves show a different trend as the measured curves. Most striking is the constant decay of the efficiency for increasing step rates. This means that the viscous friction estimation from section 5.3 is chosen to high. But as section 5.3 showed, the viscous friction parameter did enable the simulation model to produce a similar single step response as the measured one. This means that the chosen friction parameter includes a power loss in the stepper motor, not implemented in the simulation model.

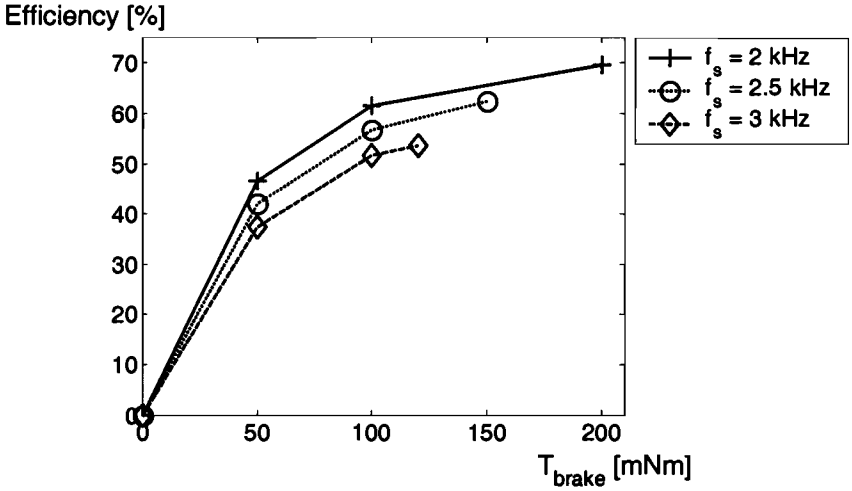

Figure 5-17: Simulated efficiency of the 17PM-K404

But besides the inaccuracy of the results, they do give an impression of the efficiency of the motor. For getting better results, the real origin of the power losses should be investigated.

Besides the motor efficiency, the results from these measurements also show the relationship between the torque and the current of the motor for different stepping rates. Figure 5.18 shows these results. As can be seen, the torque current ratio decreases for higher stepping rates. A part of this decay is produced by the viscous frictions. But the gradient of the three curves are also different (lower for higher stepping rates). This indicates that the motor has a decreasing torque production for higher stepping rates.

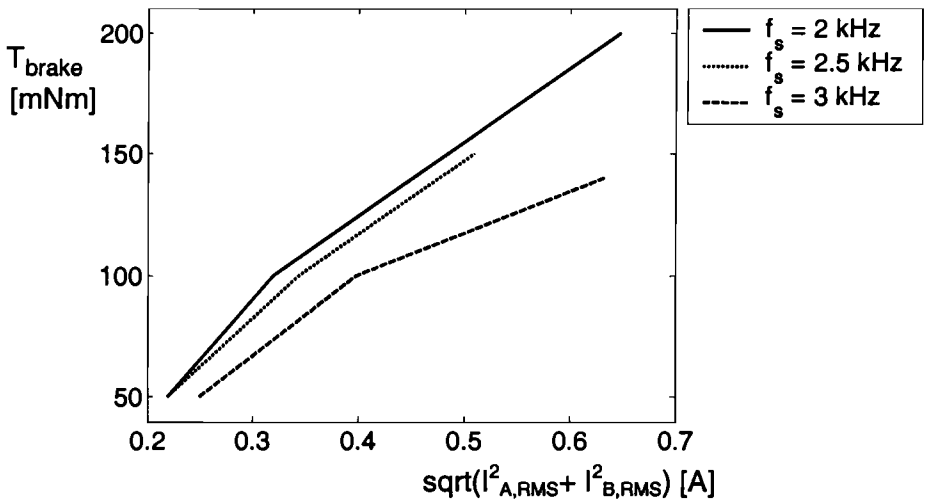

Figure 5-18: Torque current relation ship

5.6 *Dynamical performance.*

This part of the chapter deals with the performance of the 17PM-K404 stepper motor. The rotor angle has been measured during acceleration to and deceleration from a series of stepping rates. The measurement results will be compared with simulations of the stepper motor. The main aim is to compare the following properties of both the measurement and simulation results:

1. Angular speed overshoot or undershoot during acceleration or deceleration
2. Settling time of the angular speed (both at reference speed and at zero)
3. Time to failure, if the stepper motor fails

Five sets of measurements have been performed, at stepping rates of 500, 1000, 1500, 2000 and 2500 Hz. Each of the results are analysed separately.

f_s = 500 Hz:
At 500 Hz the motor has no risk of failure, so only the first two items will be checked. Figure 5.19 shows the two plots of both the measurements and simulations. As figure 5.19a shows, both the measurement and the simulation have a very similar acceleration, the same overshoot and undershoot, and except for some small mismatches, the same final speed. Also the deceleration plot shows a big similarity between the measurement and the simulation.

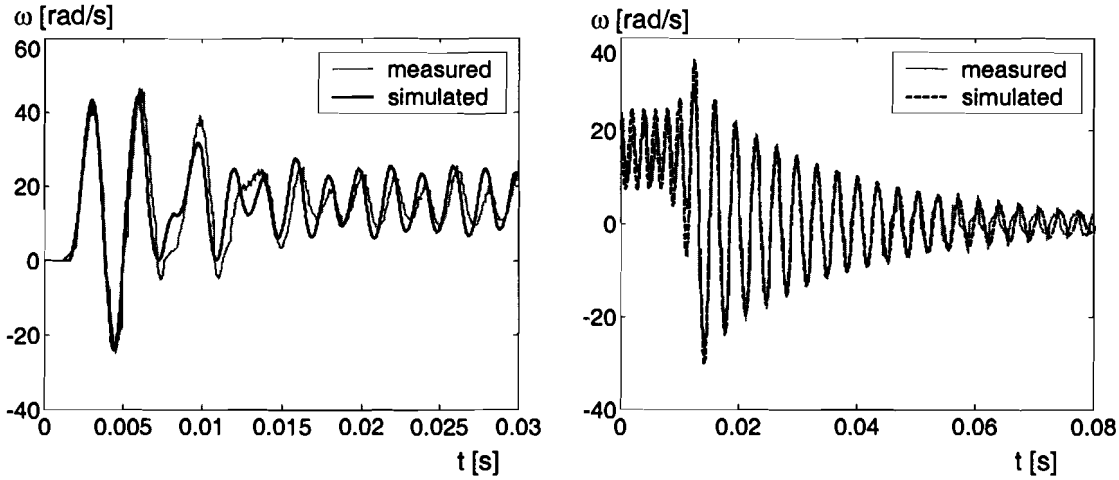

a) Acceleration b) Deceleration

Figure 5-19: Acceleration to and deceleration from f_s = 500Hz

f_s = 1000 Hz:
The motor will not fail at this stepping rate, so again only the acceleration and deceleration are analysed. The acceleration and deceleration plots are shown by figure 5.20. Again the simulations are very close to the measurements, but notice that the simulated rotor movement seems to be better damped then the measured rotor movement. Part of the difference may come from the encoder measurement errors (the speed is determined by differentiating the measured angle). But also the frequency of the rotor oscillation shows a greater decay for the measured data. This indicates a decrease in torque production for the stepper motor.

f_s = 1500Hz:
At this stepping rate the rotor movement already begins to get unstable (electrical instabilities). Figure 5.21 shows the measurement of a full start-up – slowdown cycle, and notice the oscillatory behaviour of the rotor. The oscillatory behaviour of the rotor itself has already been investigated in part 5.3. But the rotor does not stall during operation, so again no failure test. Figure 5.22 shows the acceleration and deceleration plots. Again the simulated rotor oscillation has a higher frequency, and also the damping is higher. Beside that, the simulated motor behaviour resembles the real behaviour.

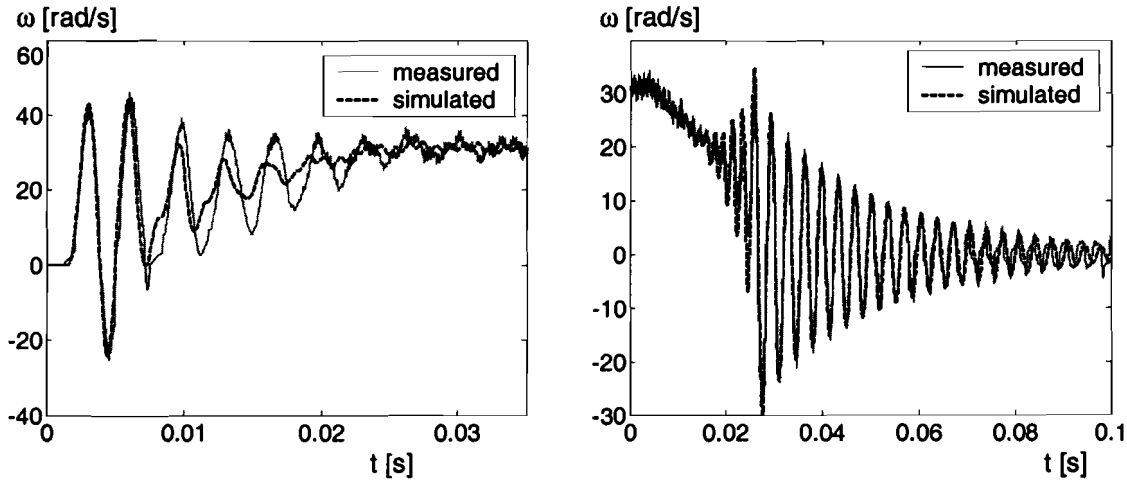

a) Acceleration b) Deceleration

Figure 5-20: Acceleration to and deceleration from f_s = 1000Hz

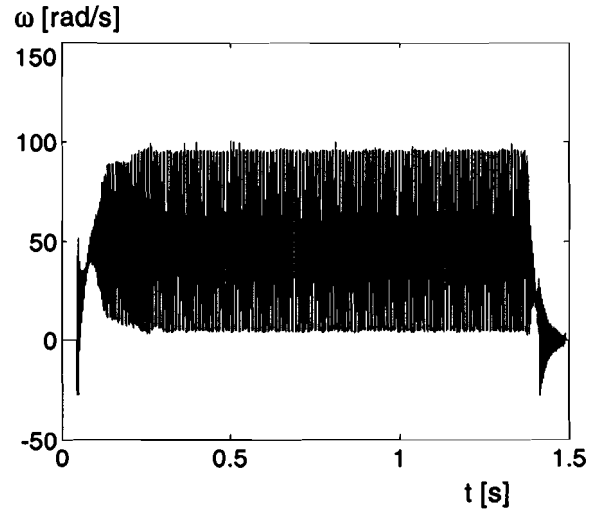

Figure 5-21: The 17PM-K404 at f_s = 1500 Hz

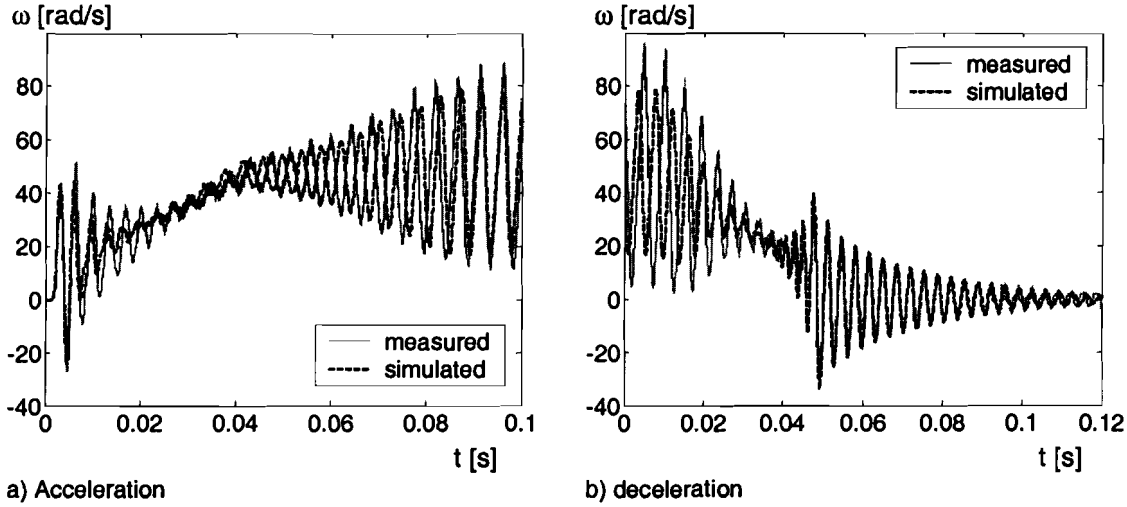

a) Acceleration b) deceleration

Figure 5-22: Acceleration to and deceleration from f_s = 1500Hz

f_s = 2000Hz and f_s = 2500Hz:
The stepper motor model has proven to be optimistic, when predicting the motor torque for higher stepping rates. Also the damping of the rotor oscillations is too high. So investigating the acceleration and deceleration of higher stepping rates will not reveal new information. At stepping rates of 2000 and 2500 Hz, the stepper motor is in, or has to pass through, the electrical instability region.

Figure 5.23 shows the plots of the measured angular speed at f_s = 2000Hz and f_s = 2500Hz. As the plots show, the motor fails to maintain a stepping rate of 2000Hz (figure 2.23a), and does not even reach the 2500 Hz (figure 2.23b, measured with a different angular speed reference ramp, but that does not affect the measurement results). The motor failure is a result of the electrical instability of the stepper motor.

Figure 5.24 shows the simulation of these angular speed ramps. At a stepping rate of 2000 Hz (figure 5.26a), the simulation model also predicts a motor failure, but after 0.22 seconds instead of 0.15 seconds. At 2500 Hz (figure 5.24b) the model does not predict a motor failure. For both cases the difference is the damping of the rotor oscillations. The damping measured in section 5.3 is not a result of friction, but of not modelled phenomena of the stepper motor.

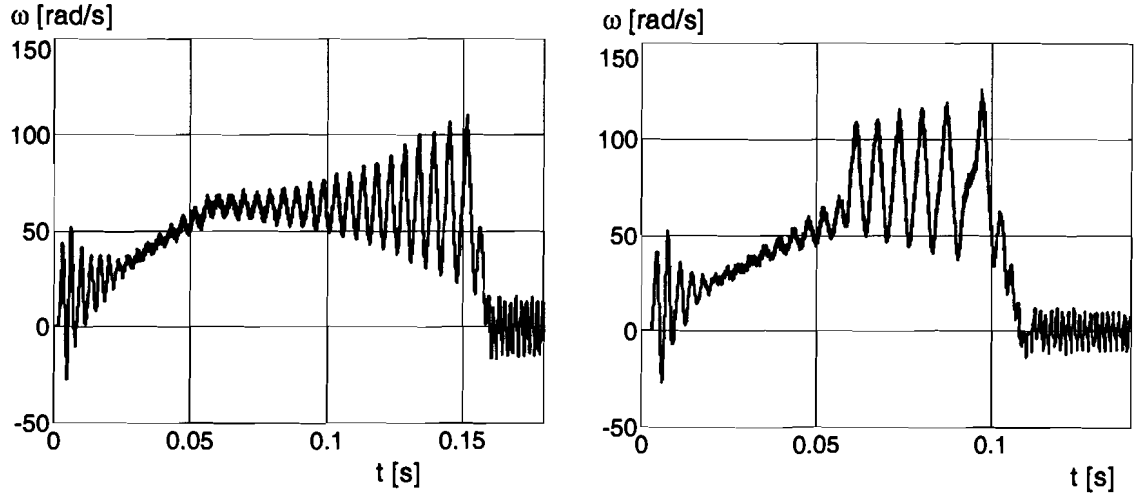

a) f_s = 2000 Hz b) f_s = 2500 Hz

Figure 5-23: Measured motor failure at 2000Hz and 2500Hz

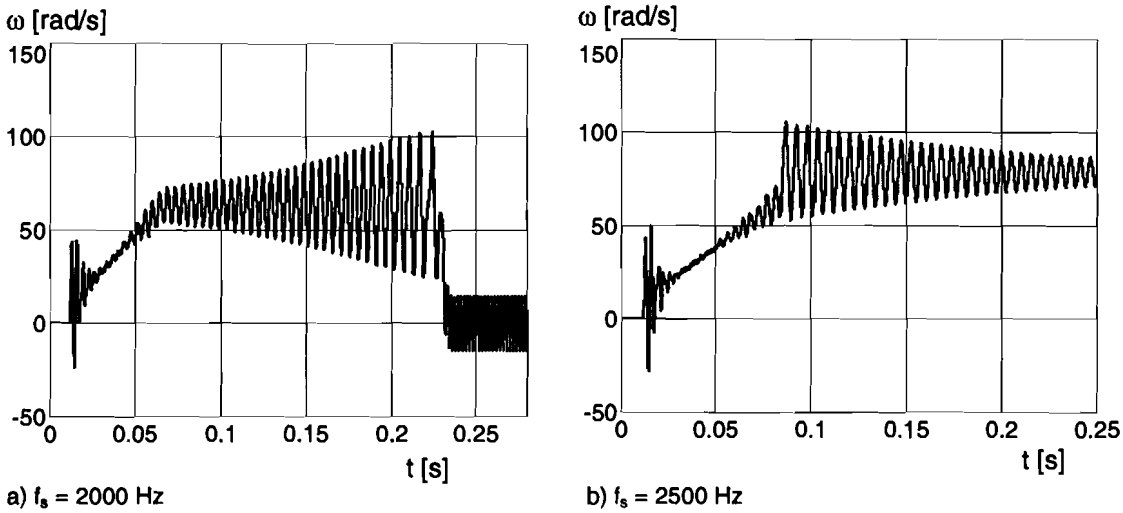

a) f_s = 2000 Hz b) f_s = 2500 Hz

Figure 5-24: Motor behaviour prediction at 2000Hz and 2500Hz

5.7 *Interpretation of measurement results*

The main aim of the measurements is to asses the predictive quality of the stepper motor simulation model. The measurements from section 5.1 show that the basic assumptions of a linear relation between static torque and winding current is acceptable, if the winding current does not exceed the rated current. Although using a higher then rated current increases the motor torque, the relation between the current and torque are no longer linear, making the simulation results unreliable.

The measurements of section 5.2 show a linear relation between the emf voltage and the angular speed, so no problems are expected from the emf voltage modelling.

The results from Sections 5.3, 5.4, 5.5 and 5.6 show some model mismatches. The most striking mismatch is the motor torque at higher speeds. All the measurements show a decay of motor torque for higher speeds, resulting into a reduced stiffness between the stator and rotor of the motor.

The exact origin of this torque drop is not known, but investigations at the university of technology in Eindhoven show that this problem is not due to mutual inductance losses or magnetic hysteresis losses. Further investigation in these losses are performed by the university in Eindhoven [].

Because the unknown losses can not be derived from the basic datasheet information supplied by stepper motor manufacturers, the stepper motor model design will not be adapted to account for these losses. Easy use of the model is more important then very accurate simulation results. And even with the inaccuracies of the model, it still proves to be a acceptable tool for stepper motor design, as long as the user knows the model impairments.

The next step in improving the model is done by expanding the simulation model to accept complex mechanical systems to driven by the stepper motor. And finally creating a graphic user interface to make the model more accessible for inexperienced matlab users. The next chapter will deal with the mechanical expansion of the stepper motor model. Appendix D contains the layout of the graphic user interface of the stepper motor toolbox, together with an instruction manual.

6 Expanding model: enhancing mechanical dynamics in model

The stepping motor is a feed-forward actuator, and this demands a thorough knowledge of the system dynamics driven by the stepping motor, to make an acceptable prediction of its behaviour. Until now, the simulation model uses a very simple mechanical system. In reality the model of the mechanical system should describe the behaviour of complex mechanical dynamics. Take for example the system shown in figure 6.1a and a schematic representation of the system in figure 6.1b.

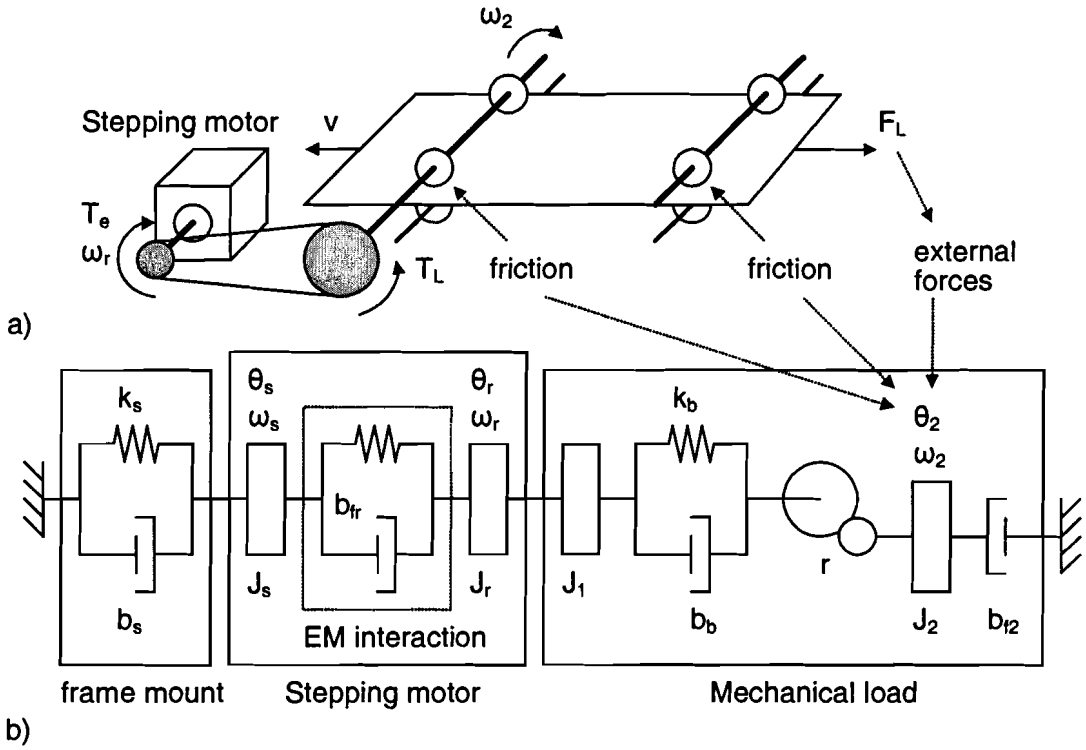

Figure 6-1: a) A stepping motor connected to a paper path
b) Possible schematic representation of system a)

The dynamics of a mechanical system as displayed by figure 6.1 can no longer be described by the simple dynamics used by the first stepping motor simulation model (figure 4.1). So the model must be enhanced to accept different mechanical configurations.

The complete mechanical system of figure 6.1 can be divided into three parts:

- The dynamics of the stepping motor
- The dynamics of the load
- The dynamics of the mount between stepping motor and frame

Each of these parts will be converted to separate MIMO systems, which partly incorporate non-linear behaviour. The separation of each system makes it possible to design a simulation model, in which the user can implement higher order dynamical properties for both the mechanical load and frame mount. He will also be able to change small parts of the model, without having to redefine other parts of the system dynamics.

The next sections will deal with the design of a state space lay-out for each dynamic part, and the way these parts interact. At the end is a small analysis to demonstrate how to acquire the dynamics of a mechanical system, needed for the implementation of the higher order mechanical dynamics in the simulation model.

6.1 State space description of the stepping motor

Because of the new description for the mechanical system, the stepping motor dynamics also have to be rewritten. The torque can be described with:

$$T_e = -k\{I_A \sin(p(\theta_r - \theta_s)) - I_B \cos(p(\theta_r - \theta_s))\} \qquad \textbf{Equation 6-1}$$

With θ_r the rotor angle, and θ_s the stator angle.

Also the emf voltage equation has to be rewritten:

$$\begin{cases} V_{A,emf} = -k \sin(p(\theta_r - \theta_s))(\omega_r - \omega_s) \\ V_{B,emf} = k \cos(p(\theta_r - \theta_s))(\omega_r - \omega_s) \end{cases} \qquad \textbf{Equation 6-2}$$

Both the torque and emf voltage equations are non-linear, making it impossible to create one linear state space representation of the stepping motor dynamics. That is why the stepping motor dynamical system will be divided into two different state spaces, connected to each other by these equations. Figure 6.2 show the required layout.

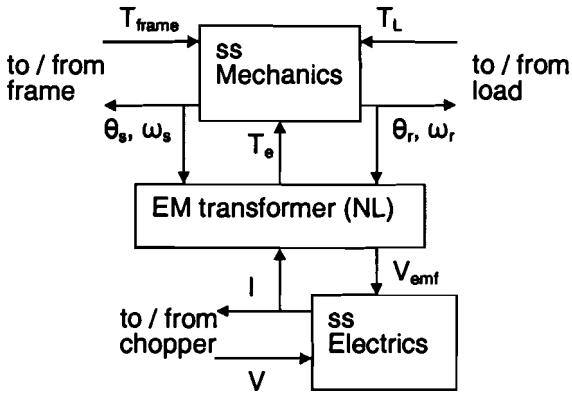

Figure 6-2: Dynamical lay-out of the stepping motor

Equations 6.1 and 6.2 connect the state spaces of the electrical and mechanical parts of the motor. The electrical state space (the winding dynamics) can be directly derived from equation 4.4:

$$\dot{I}_{phase} = -\frac{R}{L} I_{phase} + \begin{pmatrix} 1/L & -1/L \end{pmatrix} \begin{pmatrix} V_{phase} \\ V_{emf,phase} \end{pmatrix} \qquad \textbf{Equation 6-3}$$

With I_{phase} the winding current (also directly the output), L the winding inductance, and R the total winding resistance (including the bridge resistance).

The mechanical dynamics are a bit more complicated to describe, because all the inertia's directly connected to the rotor must be included in this state space (these inertia's are coupled with an infinite stiffness, instantaneously influencing the rotor behaviour). For example the situation from figure 6.1, inertia J_1 is directly connected to the stepping motor, resulting in the following differential equations:

$$\begin{cases} \dot{\theta}_s = \omega_s \\ J_s \dot{\omega}_s = -k_s \theta_s - b_s \omega_s - b_{fr}(\omega_s - \omega_r) - T_e \\ \dot{\theta}_r = \omega_r \\ (J_r + J_1)\dot{\omega}_r = -k_b(\theta_r - r \cdot \theta_2) - b_b(\omega_r - r \cdot \omega_2) - b_{fr}(\omega_r - \omega_s) + T_e \end{cases} \qquad \textbf{Equation 6-4}$$

In these equations, the parameter r is the transmission ratio. To make the state space independent from the load variables θ_2, ω_2 the following substitutions will be performed:

$$T_L = k_b(\theta_r - r\cdot\theta_2) + b_b(\omega_r - r\cdot\omega_2)$$ **Equation 6-5**

And also the frame mount dynamics will be excluded, by defining:

$$T_{frame} = k_s\theta_s + b_s\omega_s$$ **Equation 6-6**

After these substitutions the state space for the stepping motor mechanical dynamics is:

Equation 6-7

$$\begin{pmatrix}\dot\theta_s\\ \dot\omega_s\\ \dot\theta_r\\ \dot\omega_r\end{pmatrix} = \begin{pmatrix}0 & 1 & 0 & 0\\ 0 & -b_{fr}/J_s & 0 & b_{fr}/J_s\\ 0 & 0 & 0 & 1\\ 0 & b_{fr}/J_r+J_1 & 0 & -b_{fr}/J_r+J_1\end{pmatrix}\begin{pmatrix}\theta_s\\ \omega_s\\ \theta_r\\ \omega_r\end{pmatrix} + \begin{pmatrix}0 & 0 & 0\\ -1/J_s & 0 & -1/J_s\\ 0 & 0 & 0\\ 1/J_r+J_1 & -1/J_r+J_1 & 0\end{pmatrix}\begin{pmatrix}T_e\\ T_L\\ T_{frame}\end{pmatrix}$$

And the output vector is defined as:

$$\underline{y}_{SM} = \mathbf{I}\underline{x}_{SM} + \mathbf{0}\cdot\underline{u}_{SM}$$ **Equation 6-8**

With $\underline{y}_{SM}$ the output vector, $\underline{x}_{SM}$ the state vector, $\underline{u}_{SM}$ the input vector, and **I** the identity matrix:

$$\underline{y}_{SM} = (\theta_s, \omega_s, \theta_r, \omega_r)^t$$
$$\underline{x}_{SM} = (\theta_s, \omega_s, \theta_r, \omega_r)^t$$
$$\underline{u}_{SM} = (T_e, T_L, T_{frame})^t$$

Additional non-linear behaviour like a coulomb friction between the stator and rotor can be subtracted as a torque loss from the electric torque T_e:

$$T_{eff} = T_e - sign(\omega_r - \omega_s)\cdot c_{fr}$$
$$\underline{u}_{SM} = (T_{eff}, T_L, T_{frame})$$ **Equation 6-9**

6.2 *State space description of the load*

The state space framework for the stepping motor puts some restraints on the design of a state space for the load dynamics. The input vector must at least contain the rotor angle and rotor angular speed (see figure 6.2, the chosen lay-out for the stepping motor dynamics). And the output vector must contain the torque demand of the load. Figure 6.3 shows the chosen layout for the load dynamics.

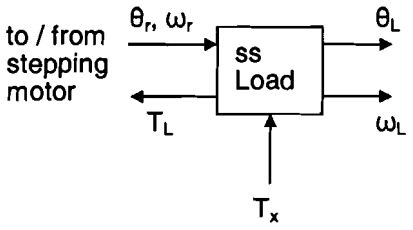

Figure 6-3: Lay-out for load state space

Again for the example from figure 6.1, the differential equations must comply with:

$$\begin{cases} \dot{\theta}_2 = \omega \\ J_2 \cdot \dot{\omega}_2 = r \cdot k_b(\theta_r - r \cdot \theta_2) + r \cdot b_b(\omega_r - r \cdot \omega_2) - b_{f2}\omega_2 - T_x \end{cases}$$ **Equation 6-10**

In which T_x describes torque resulting from the disturbances. The state space vectors are now defined as:

$$\underline{x}_L = (\theta_2, \omega_2)^t$$

$$\underline{u}_L = (\theta_r, \omega_r, T_x)^t$$

$$\underline{y}_L = (T_L, \theta_2, \omega_2)^t$$

And the state space description of the load must be:

$$\dot{\underline{x}}_L = \begin{pmatrix} 0 & 1 \\ -\frac{r^2 \cdot k_b}{J_2} & -\frac{r^2 \cdot b_b + b_{f2}}{J_2} \end{pmatrix} \underline{x}_L + \begin{pmatrix} 0 & 0 & 0 \\ \frac{r \cdot k_b}{J_2} & \frac{r \cdot b_b}{J_2} & -\frac{1}{J_2} \end{pmatrix} \underline{u}_L$$ **Equation 6-11**

With the output vector defined as (making use of equation 6.5, the definition of the torque required for the load):

$$\underline{y}_L = \begin{pmatrix} -r \cdot k_b & -r \cdot b_b \\ 1 & 0 \\ 0 & 1 \end{pmatrix} \underline{x}_L + \begin{pmatrix} k_b & b_b & 0 \\ 0 & 0 & 0 \\ 0 & 0 & 0 \end{pmatrix} \underline{u}_L$$ **Equation 6-12**

This is just an example of how the load could be defined. In practice, by using state spaces, the load could be as complicated as necessary. Also a state space derived from measurements could be used, as long as the relationship between the load torque and the load angle and angular speed is known.

6.3 *State space description of the frame mount*

The description of the frame mount must be of the same form as that from the mechanical load (because of the stepping motor state space description. The resulting lay-out for the frame mount is shown in figure 6.4.

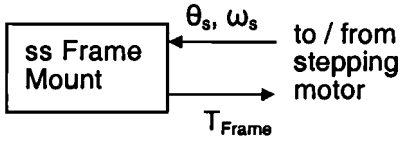

Figure 6-4: lay out for frame mount state space

For the example defined in figure 6.1 the dynamics already have been defined in equation 6.6. The resulting state space only has an input vector and an output scalar:

$$\underline{u}_{FM} = (\theta_s, \omega_s)^t$$

$$y_{FM} = T_{frame}$$

The resulting state space is a static gain, defined as:

$$y_{FM} = (k_s \quad b_s)\underline{u}_{FM}$$ **Equation 6-13**

Again, this is only an example.

6.4 *Resulting simulation model*

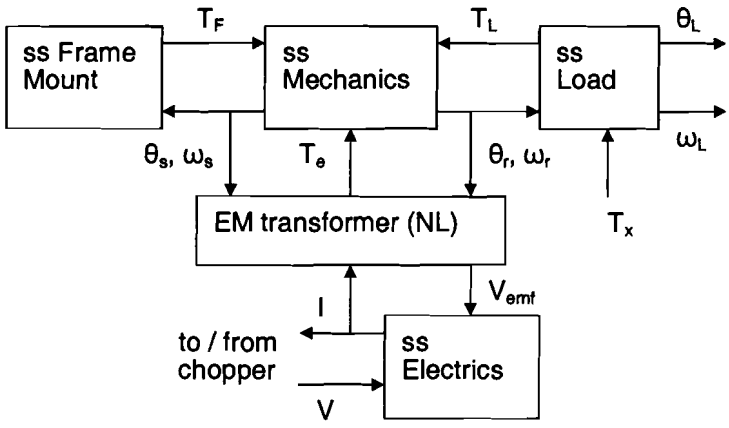

Figure 6-5: The complete stepping motor dynamics after upgrade

Figure 6.5 shows the combination of the three state spaces. The fact that the total model consist out of different parts, makes it possible to change the dynamical properties of the mechanics, without altering the simulation code, but by changing input parameters for the simulation algorithm. The three systems can then be merged to one big mechanical state space, connected to the electronic state space via the two non linear relations between the stepping motor electronics and mechanics.

For the combination of the state spaces, first a formalised description should be given for each part. The general state space equations are described by two equations:

$$\begin{cases} \dot{\underline{x}} = \mathbf{A}\underline{x} + \mathbf{B}\underline{u} \\ \underline{y} = \mathbf{C}\underline{x} + \mathbf{D}\underline{u} \end{cases} \qquad \textbf{Equation 6-14}$$

For each system the **A**, **B**, **C** and **D** matrices and the state, input and output vectors are indexed with the following strings:
FM: Frame mount
SM: Stepping motor
ML: Mechanical load

The resulting state space of the complete mechanical dynamics can be constructed by creating the following state space:

$$\begin{cases} \dot{\underline{x}}_t = \begin{pmatrix} A_{FM} & 0 & 0 \\ 0 & A_{SM} & 0 \\ 0 & 0 & A_{ML} \end{pmatrix} \underline{x}_t + \begin{pmatrix} B_{FM} & 0 & 0 \\ 0 & B_{SM} & 0 \\ 0 & 0 & B_{ML} \end{pmatrix} \underline{u}_t \\ \underline{y}_t = \begin{pmatrix} C_{FM} & 0 & 0 \\ 0 & C_{SM} & 0 \\ 0 & 0 & C_{ML} \end{pmatrix} \underline{x}_t + \begin{pmatrix} D_{FM} & 0 & 0 \\ 0 & D_{SM} & 0 \\ 0 & 0 & D_{ML} \end{pmatrix} \underline{u}_t \end{cases} \qquad \textbf{Equation 6-15}$$

With $\underline{x}_t$ the combination of the state vectors of the three systems:

$$\underline{x}_t = (\underline{x}_{FM}, \underline{x}_{SM}, \underline{x}_{ML})^t$$

The input vector is:

$$\underline{u}_t = (\theta_s, \omega_s, T_e, T_L, T_{frame}, \theta_r, \omega_r, T_x)^t$$

And the output vector is:

$$\underline{y}_t = (T_{frame}, \theta_s, \omega_s, \theta_r, \omega_r, T_L, \theta_2, \omega_2)'$$

To complete the state space, some outputs have to directed to their inputs (sharing the same name), just like figure 6.5 shows. After making the right connections, the input vector should be:

$$\underline{u}_{mech} = (T_e, T_x)'$$

And the new output vector is:

$$\underline{y}_{mech} = (\theta_s, \omega_s, \theta_r, \omega_r, T_L, \omega_2)'$$

From the output vector, the variables θ_s, ω_s, θ_r and ω_r must be directed to the emf calculation, and the torque calculation for the stepping motor, completing the frame / motor / load dynamics.

As can be seen from the input and output vectors, the layout forces them to be always the same. The state vector does not matter. So the resulting model has a limited amount of inputs or outputs, but an unlimited order for the mechanical system dynamics.

6.5 *Method to acquire the model dynamics of a mechanical system*

The former sections describe a way to implement dynamical systems into a simulation environment for stepping motors. But in order to do this, first the dynamics of the mechanical system must be known. In general there are two ways to accomplish this:

- Describing the mechanics by the parameters of every part of the system separately, as has been done for the example in figure 6.1 (although for this example the dynamics have been heavily simplified). The difficulty of this procedure is the fact that it is hard to identify every part of the process, and also to understand the impact of every aspect. The advantage is the fact, that once the system has been identified, the knowledge can be used in different systems with resembling mechanical configurations.
- Creating a black-box model of the system, only extracting the most important aspects required to simulate the system dynamics. Black box models are accurate models of particular systems, ignoring (actually hiding) the dynamics which do not really contribute to the process dynamics. The big disadvantage of this procedure is the fact that virtually no new knowledge about the system is acquired (depending on the way the black box is constructed), making it obligatory to repeat the identification procedure for every variation of the mechanical system.

Either way, the resulting model will always be a simplified representation of the real dynamics. Because mechanical engineering is not really part of the scope of this investigation, the second identification method will be used for simulation purposes. Report [11] uses the first approach to mechanical system identification.

The basic procedure for the black box system identifications is:

- Constant input test: For identifying trends, measurement drifts and measurement noise
  » After this step signal can be cleaned from trends and measurement drifts
- Staircase test: For identifying linear and non linear ranges of operation, identifying lowest time constant of system.

» Regions of heavy non-linear behaviour can be avoided during further identification process

- Pseudo random noise test: For extracting the linear dynamics
  » Creating model dynamics at chosen working regions

For the mechanical systems of Océ applications such a thorough identification process is not necessary. A fair amount of information about the mechanics is already known. Figure 6.6 shows the basic schematic of 6.1b, but with the well known properties described. So the frame mount properties the transmission effects, and the frictions should be investigated.

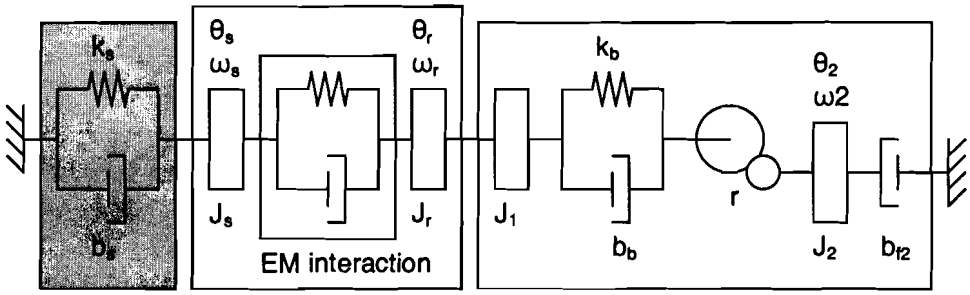

frame mount	Stepping motor	Mechanical load
Unknown To be investigated in chapter 7	Known See chapter 4	Known: Inertias / transmission ratios / external forces Unknown: Frictions / stiffnes and play transmission

Figure 6-6: Schematic with known and unknown properties

Making good choices with the frame mount, can result into cheap and effective ways to damp the rotor oscillations of a stepper motor. Chapter 7 will deal with this part of the unknown dynamics. For the mechanical load part, a Matlab simulink simulation has been created, to predict the results to be obtained when identifying the mechanical load. This section will deal with a method to identify mechanical dynamics, using the simulation model. Chapter 8 will show the results of this method with real measurements, and will also analyse the described method of this section.

The identification of the load must be done with a motor which has a very predictable behaviour, and is easy to understand. A DC motor seems most fitted for the task, because of its more or less linear relation between voltage and speed, and current and torque. The motor chosen for the investigations is a Parvex RS220XR, the properties are shown by table 6.1.

Table 6-1: Parvex RS220XR motor properties

Physical property	Value	Description
R [Ω]	1.1	Winding resistance
L [H]	$3.2 \cdot 10^{-4}$	Winding inductance
k_t [Nm A^{-1}, V s rad^{-1}]	$4.6 \cdot 10^{-2}$	Motor constant
J_{rotor} [kg m^2]	$1.95 \cdot 10^{-5}$	Rotor inertia (including gear J_1)
G_1 [teeth]	18	Number of rotor gear teeth
c_{fr} [Nm]	$1.7 \cdot 10^{-2}$	Coulomb friction between stator and rotor
b_{fr} [Nm s rad^{-1}]	$1.3 \cdot 10^{-5}$	Viscous friction between stator and rotor

Table 6.2 shows the typical known data for the "stopper wals" mechanical configuration. This configuration will be simulated with simulink, to get a better understanding of the impact of the missing knowledge about the system. The different unknown parameters will be varied, to see their influence on system dynamics.

Table 6-2: Mechanical data from the "stopper wals"

Mechanical property	Value	Description
G_2 [teeth]	29	Number of load gear teeth
k_b [Nm rad^{-1}]	-	Transmission stiffness
b_b [Nm s rad^{-1}]	-	Transmission damping
J_{load} [kg m^2]	$4.15 \cdot 10^{-5}$	Load total inertia
c_{f2} [Nm]	0.026	Coulomb friction at load estimate
b_{f2} [Nm s rad^{-1}]	-	Viscous friction at load

Because DC motor dynamics change when running hot, all real measurements should be short. When performing simulations, this will also be taken into account. The constant input test is no longer interesting, when a motor cannot run at a desired speed for a longer time span. The stair-case test will be changed to a series of single step responses with different voltages, and pseudo random noise test is still possible, but should have a short time duration.

Figure 6.7 shows the simulation test set-up. The measurable variables are the winding current of the DC motor (I [A]), and the angles of the rotor (θ_r [rad]) and load (θ_2 [rad]). For maintaining realism during simulations the measured data will be disturbed by white noise, to simulate the measurement disturbances like encoder noise and AD conversion noise.

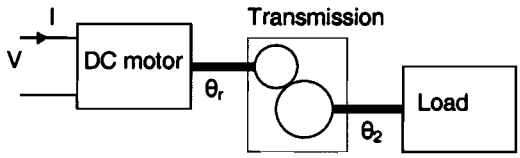

Figure 6-7: Simulation set-up

6.5.1 Simulating single step responses

The transmission belt should have little effect on the single step responses, so the parameters concerning this transmission belt are not analysed during these simulations (k_b, b_b). The parameters to be investigated are the coulomb and viscous friction at the load.

An example of the single step responses simulation results is shown by the phase diagram of figure 6.8. The DC motor has made three single steps, from zero to three different fixed voltages. For each step the speed and current also stabilises to a fixed value (the arrows), and these stationary locations in the phase diagram are a measure for the total coulomb and viscous friction as seen from the motor rotor (inertia's and springs only demand torque when the system is accelerating or decelerating).

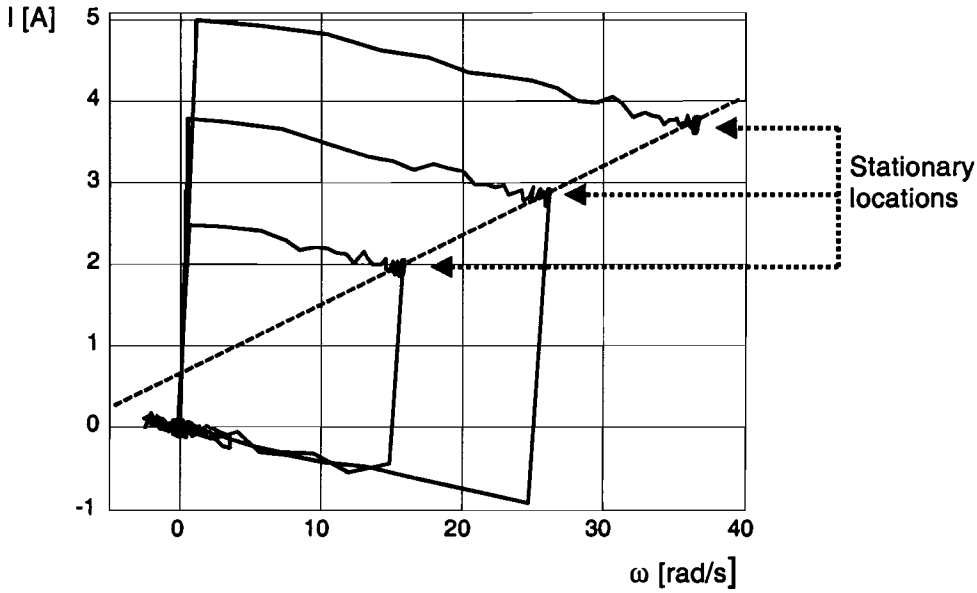

Figure 6-8: A simulation current / speed phase diagram

The dotted line through the three stationary points shows a linear relationship between the stationary angular speeds and currents. The gradient of this relationship determines the total viscous friction on the rotor (b_{ft} [Nm s rad^{-1}]):

$$b_{ft} = k_T \frac{dI_{interp}(\omega)}{d\omega}$$ **Equation 6-16**

With $I_{interp}(\omega)$ the linear interpolated stationary current expression as function of the stationary angular speeds. The viscous friction of the motor is known, so the viscous friction of the load should be:

$$b_{f2} = \left(\frac{G_2}{G_1}\right)^2 (b_{ft} - b_{fr})$$ **Equation 6-17**

The current offset for the stationary angular speed zero is the total coulomb friction c_{ft}:

$$c_{ft} = k_T \cdot I_{interp}(0) \qquad \textbf{Equation 6-18}$$

and the coulomb friction at the load must be:

$$c_{f2} = \frac{G_2}{G_1}(c_{ft} - c_{fr}) \qquad \textbf{Equation 6-19}$$

Knowing these expressions a series of simulations have been performed. First a simulation where the coulomb frictions of the "stopper wals" example vary between 0.02 Nm and 0.1 Nm, while the viscous friction of the load remains zero. The resulting estimates for both frictions after simulation are put in table 6.3.

Table 6-3: Simulation results for coulomb frictions

real c_{f2} [Nm]	c_{f2} estimate [Nm]	b_{f2} estimate [Nm s rad^{-1}]
0.02	0.019	$2.4 \cdot 10^{-5}$
0.026	0.026	$2.9 \cdot 10^{-5}$
0.05	0.050	$2.4 \cdot 10^{-5}$
0.10	0.10	$0.5 \cdot 10^{-5}$

Estimating the coulomb friction from the single step responses seems to be quite successful. The estimate of the viscous friction is inaccurate. A series of simulations have been performed to analyse when a viscous friction is measurable. Table 6.4 shows the results, when only the viscous friction is altered between $1.0 \cdot 10^{-5}$ and $1.0 \cdot 10^{-3}$, and the coulomb friction is set to 0.026 Nm.

As the simulation results show, only viscous frictions higher then $5.0 \cdot 10^{-5}$ Nm s rad^{-1} can be identified. Lower frictions get lost in the measurement noise. So the results depend on the measurement accuracy. It is better to analyse a phase diagram like figure 6.8. If the interpolated current has virtually no slope, it is better to assume that the load does not suffer from any viscous friction.

The main aim of the single step simulations is to identify non linear attributes. The pseudo random noise test has no use when the measurements suffer from non linear attributes like coulomb friction. In the case of a mechanical system it is advisable to remove the coulomb friction from future measurements, and only measure the dynamics when the angular speed of the DC motor is not zero (only then the coulomb friction may be removed as a torque offset).

Table 6-4: Simulation results for viscous friction

real b_{f2} [Nm s rad^{-1}]	b_{f2} estimate [Nm s rad^{-1}]	estimate c_{f2} [Nm]
$1.0 \cdot 10^{-5}$	$0.5 \cdot 10^{-5}$	0.026
$5.0 \cdot 10^{-5}$	$4.4 \cdot 10^{-5}$	0.026
$1.0 \cdot 10^{-4}$	$1.0 \cdot 10^{-4}$	0.026
$5.0 \cdot 10^{-4}$	$4.7 \cdot 10^{-4}$	0.027
$1.0 \cdot 10^{-3}$	$9.8 \cdot 10^{-4}$	0.027

6.5.2 Simulating the pseudo random noise test

Before extracting system dynamics with a pseudo random noise test, the effects of the transmission must be analysed. A series of pseudo random simulations have been performed to asses the impact of the transmission stiffness and transmission damping to the load angular speed, when the motor is in operation. These simulations have been performed with the mechanical data from the "stopper wals".

First the stiffness and damping of the transmission have been varied during the pseudo random noise test. Table 6.5 shows the simulation results. The table shows the match between the motor (ω_1) and load (ω_2) angular speed recordings during the whole pseudo random noise test, when describing the transmission dynamics as:

$$\omega_2 = \frac{G_1}{G_2}\omega_r$$ **Equation 6-20**

When the two angular speed recordings are closely matched, the transmission can be seen as a stiff transmission, with only the gear ratio as variable. The load inertia may then be seen as an integral part of the rotor inertia (the same state), reducing the complexity of the system dynamics.

Table 6-5: Ratio match between angular speed and load angular speed

	b_b [Nm s rad^{-1}]		
k_b [Nm rad^{-1}]	10	0.1	0.001
1000	99.9%	99.9%	99.9%
100	99.9%	99.7%	98.6%
10	99.9%	99.3%	94.1%
1	99.9%	99.1%	79.8%

Table 6.5 shows that the stiffness and damping of the transmission has barely any effect on the relation between the motor and load angular speeds. Only the k_b = 1 Nm rad^{-1} and b_b = 0.001 Nm s rad^{-1} situation shows a considerable difference between the motor and load angular speed. But this value for the stiffness is very low. Suppose the rotor angle may differ from the load angle with 0.1º at a torque difference of 0.1 Nm, the stiffness should be at least 57 Nm rad^{-1}.

For most Océ applications this estimate would rather be too low then too high, because the transmission is often a toothed belt with an iron core (very stiff in rotational sense). When using gears, the transmission has an even higher stiffness. But for further pseudo random noise simulations a transmission with a stiffness of 57 Nm rad^{-1} and a damping of 0.01 Nm s rad^{-1} will be used.

By using a pseudo random noise test wisely, the full dynamics of a mechanical system can be identified. For the situation with a stiff transmission, the identification can be simplified. When the relationship between the motor torque and the angular speed of the rotor is known, all the dynamics for the state space can be derived:

$$\begin{cases} \dfrac{d\theta_r}{dt} = \omega_r \\ \dfrac{d\theta_2}{dt} = \omega_2 \\ \omega_2 = \dfrac{G_1}{G_2}\omega_r \end{cases}$$ **Equation 6-21**

For the "stopper wals" the viscous friction at the load will be set to 10^{-4} Nm s rad^{-1}. The motor voltage will be randomly switched between 2.5 and 7 volts. The measured motor current and rotor speed are displayed in figure 6.9. The currents are a measure for the total torque produced by the motor:

$$T_{total} = k_T \cdot I$$ **Equation 6-22**

But for the identification non linearity's like coulomb friction should be removed. The total coulomb friction as seen from the motor must be 0.033 Nm, which can be subtracted of the total torque produced by the motor (because the rotor speed is always set greater then zero during the pseudo random noise test).

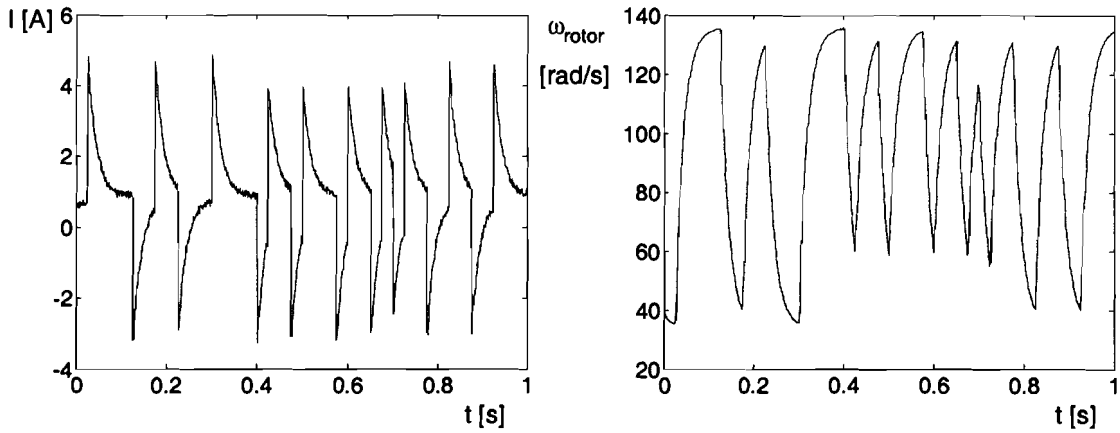

a) DC motor current

b) DC rotor current angular speed

Figure 6-9: A pseudo random noise test with the "stopper wals" simulation

After this procedure, the relation between the effective torque available for rotation and angular speed can be determined. This has been done for the "stopper wals", with the identification toolbox of Matlab. Not surprisingly the toolbox recommends a first order state space for describing the dynamics, resulting into a 96.4% match between measurements and state space. The resulting state space for the complete mechanic dynamics is:

$$\begin{pmatrix} \dot{\theta}_r \\ \dot{\omega}_r \end{pmatrix} = \begin{pmatrix} 0 & 1 \\ 0 & -1.46 \end{pmatrix} \begin{pmatrix} \theta_r \\ \omega_r \end{pmatrix} + \begin{pmatrix} 0 \\ 1.84 \cdot 10^4 \end{pmatrix} T_{eff}$$ **Equation 6-23**

And the output expression for this state space is:

$$\begin{pmatrix} \theta_r \\ \omega_r \\ \theta_2 \\ \omega_2 \end{pmatrix} = \begin{pmatrix} 1 & 0 \\ 0 & 1 \\ \frac{G_1}{G_2} & 0 \\ 0 & \frac{G_1}{G_2} \end{pmatrix} \begin{pmatrix} \theta_r \\ \omega_r \end{pmatrix}$$ **Equation 6-24**

The following relation applies:

$$\dot{\omega}_r = \frac{b_{fr} + \left(\frac{G_1}{G_2}\right)^2 b_{f2}}{J_{rotor} + \left(\frac{G_1}{G_2}\right)^2 J_2} \omega_r + \frac{1}{J_{rotor} + \left(\frac{G_1}{G_2}\right)^2 J_2} T_{eff}$$ **Equation 6-25**

Because the inertia's, gear ratio and rotor viscous friction are known, the viscous friction from the measurements should be $1.01 \cdot 10^{-4}$ Nm s rad^{-1}. To check if the real inertia's are equal to the calculated values, the second part of equation 6.25 can be used. The calculated total inertia is equal to $3.55 \cdot 10^{-5}$ kg m^2, while the measured total inertia results to $3.52 \cdot 10^{-5}$ kg m^2.

All measured values are very close to the simulation parameters. Chapter 8 will use the method described in this chapter, to analyse the "stopper wals" mechanical system with real measurements, which will be used for evaluating the stepper motor simulation model.

7 Analysis of mechanical dampers to improve motor behaviour

During the investigation of stepper motors, some damping of rotor oscillations could be obtained, by using (simple) mechanical dampers. Basically mechanical dampers come in three types:

- A plastic suspension ring, to be placed between frame and motor
- A elastically coupled inertia damper, to be placed on the rotor
- A viscously coupled inertia damper, to be placed on the rotor

Figure 7.1 shows schematic sketches for each of the three dampers. The basic way each damper works is the same, dissipating the energy of rotor oscillations. The way each damper is able to do this, is explained in the next sessions. Also some measurements have been performed to show the effects on the rotor movement of stepper motors.

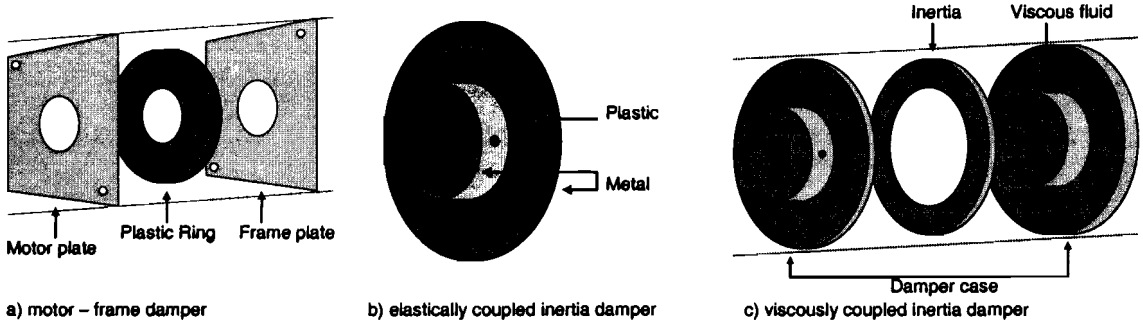

a) motor – frame damper b) elastically coupled inertia damper c) viscously coupled inertia damper

Figure 7-1: Schematic sketches of mechanical dampers

7.1 The motor - frame suspension ring

In chapter 4 the stepper motor stator was directly connected to the earth, making the stator inertia infinitely big. Chapter 6 already showed that normally the stepper motor is connected to the earth via a frame mount. In practise the frame mounts for electrical motors are chosen stiff, but in the case of a stepper motor this is not always the best solution. When lowering the stiffness between the frame and the motor, by using a special frame mount as in figure 7.1a, a part of the movement energy between the rotor and the stator, can be absorbed by the frame mount.

The motor – frame damper acts as a damped spring between the stator and the frame, as figure 7.2 shows. Because the oscillatory part of the rotor movement is at frequencies well above zero, the constant speed part of the rotor movement may be discarded. So the stepper motor has been modelled as a stator inertia connected to a rotor inertia by a damped spring, a model well suited to analyse high frequency effects on the rotor angle and speed.

For analysis, an external torque T_x can be produced between the rotor and the stator, to see the effects of changing the frame – motor damper properties on the rotor angle and angular speed. The state space model of this mechanical system is:

$$\begin{pmatrix} \dot{\theta}_r \\ \dot{\omega}_r \\ \dot{\theta}_s \\ \dot{\omega}_s \end{pmatrix} = \begin{pmatrix} 0 & 1 & 0 & 0 \\ -\frac{k_e}{J_r} & -\frac{b_e}{J_r} & \frac{k_e}{J_r} & \frac{b_e}{J_r} \\ 0 & 0 & 0 & 1 \\ \frac{k_e}{J_s} & \frac{b_e}{J_s} & -\frac{k_e + k_s}{J_s} & -\frac{b_e + b_s}{J_s} \end{pmatrix} \begin{pmatrix} \theta_r \\ \omega_r \\ \theta_s \\ \omega_s \end{pmatrix} + \begin{pmatrix} 0 \\ \frac{1}{J_r} \\ 0 \\ -\frac{1}{J_s} \end{pmatrix} T_x \qquad \textbf{Equation 7-1}$$

With k_s and b_s the stiffness and damping between the frame and stator, and k_e and b_e the stiffness and damping between the stator and the rotor. As output function, the rotor angle and speed relative to the stator angle and speed has been chosen (θ_{rs}, ω_{rs}):

$$\begin{pmatrix}\theta_{rs}\\ \omega_{rs}\end{pmatrix}=\begin{pmatrix}1 & 0 & -1 & 0\\ 0 & 1 & 0 & -1\end{pmatrix}\begin{pmatrix}\theta_r\\ \omega_r\\ \theta_s\\ \omega_s\end{pmatrix}$$

Equation 7-2

For analysis purposes, the stiffness k_e is chosen as the rotor - stator stiffness defined by equations 3.1 and 3.3 (chapter 3) for the 17PM-K404 at rated current:

$$k_e=\left.\frac{dT}{d\theta}\right|_{\theta=0}=p\cdot T_{pk}=27\,{}^{Nm}/_{rad}$$

The electrical damping is chosen as the damping measured for the 17PM-K404 in chapter 5.2, b_e = 0.8 mNm s rad^{-1}.

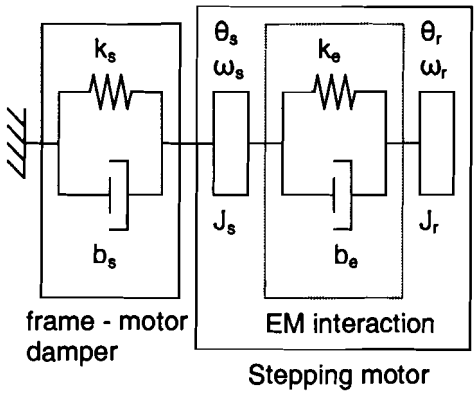

Figure 7-2: Mechanical model frame – motor damper

First, analyse the rotor stator behaviour, when the stator has virtually no rotational freedom relative to the frame. Figure 7.3a shows the zero-pole plot of the mechanical system. The two poles are poorly damped, resulting to an angular speed oscillation frequency of f = 1837 rad s^{-1} (See figure 7.3b for the bode magnitude plot).

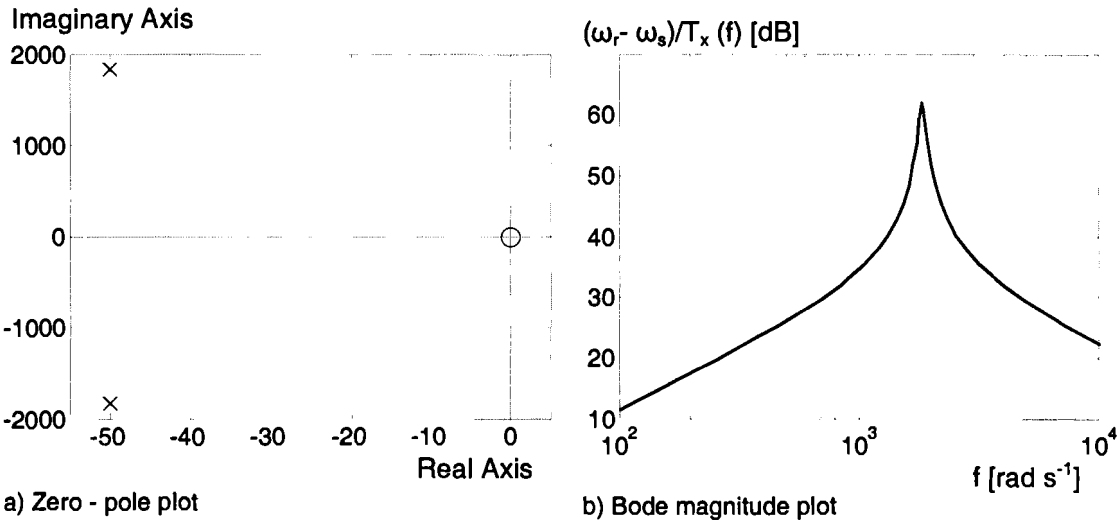

a) Zero - pole plot

b) Bode magnitude plot

Figure 7-3: Dynamical characteristics of the stepper motor

The poles of the stepper motor directly connected to the frame have a damping factor of 0.028 (a damped pole has a damping factor of one). Now when introducing a damped spring between the stator and frame, the mechanical dynamics change. The new mechanical system has two new zeros, and two new poles.

The use of an alternative frame mount does not always result to improved motor behaviour. The logic choice would be a damper ring which can dissipate the movement energy around the oscillation frequency of the rotor - stator system. This would result to a damper stiffness:

$$k_s = \frac{J_s}{J_r} k_e \qquad \textbf{Equation 7-3}$$

The damper stiffness is now matched with the motor stiffness, so that the stator - frame natural frequency is equal to the rotor - stator natural frequency. The stator inertia of the 17PM-K404 is not supplied by the manufacturer, but calculations showed a stator inertia of approximately ten times the rotor inertia: $J_s = 10 \cdot J_r$. So the damper stiffness must be: k_s = 270 Nm rad^{-1}.

Besides the stiffness, also a damping must be chosen for the frame mount. This is more complicated, because the damper b_s actually dissipates the energy of the rotor - stator oscillations around the natural frequency. Chosen too high, it will obstruct the free movement between the stator and the frame, and chosen to low it will not dissipate enough energy to damp the oscillations.

To show the relationship between the frame mount damping performance, and its basic two properties k_s and b_s, a three dimensional surface plot of the damping is shown by figure 7.4 (actually, the damping factor of the two worst damped poles is plotted along the z-axis). Although this plot shows a clear optimum for the frame mount performance, it does not help with making the best choice for the k_s and b_s.

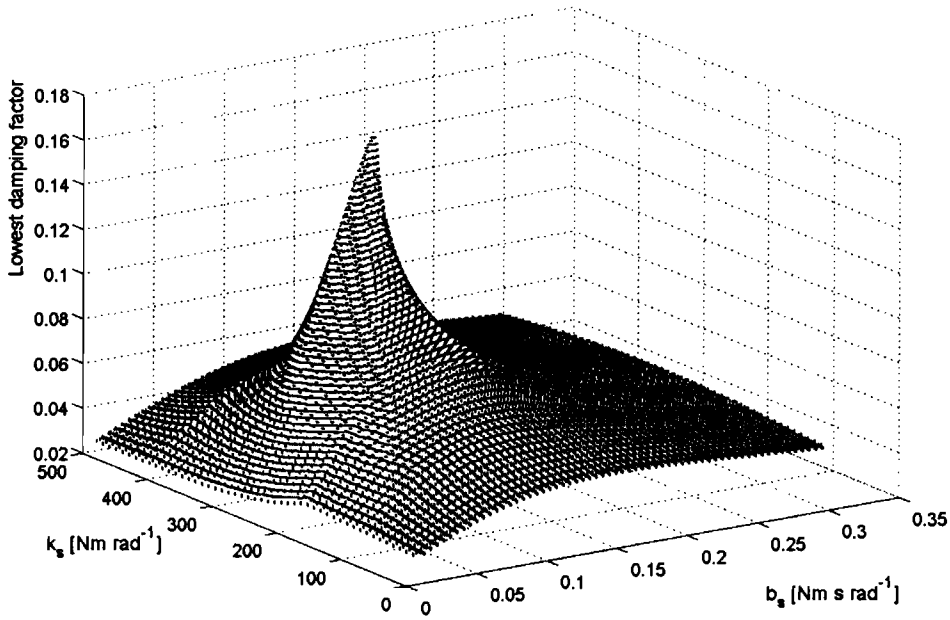

Figure 7-4: Surface plot of the damping as function of k_s and b_s

The contour plot shown by figure 7.5 shows the ideal values for k_s and b_s. The optimal frame mount must be:

- k_s = 265 Nm rad^{-1}
- b_s = 0.098 Nm s rad^{-1}
- Damping factor worst damped poles: 0.18, with f_n = 301 Hz

The stiffness is slightly lower as when calculated by equation 7.3, that is because equation 7.3 assumes that the frame mount does not influence the motor dynamics, which is not true. For comparing the behaviour of the damped motor with the undamped motor, figure 7.6 shows the step responses for both the damped and undamped situations. As the figure shows, the maximum overshoot remains almost the same, but the settling time drastically shortens when damping the motor with the frame mount.

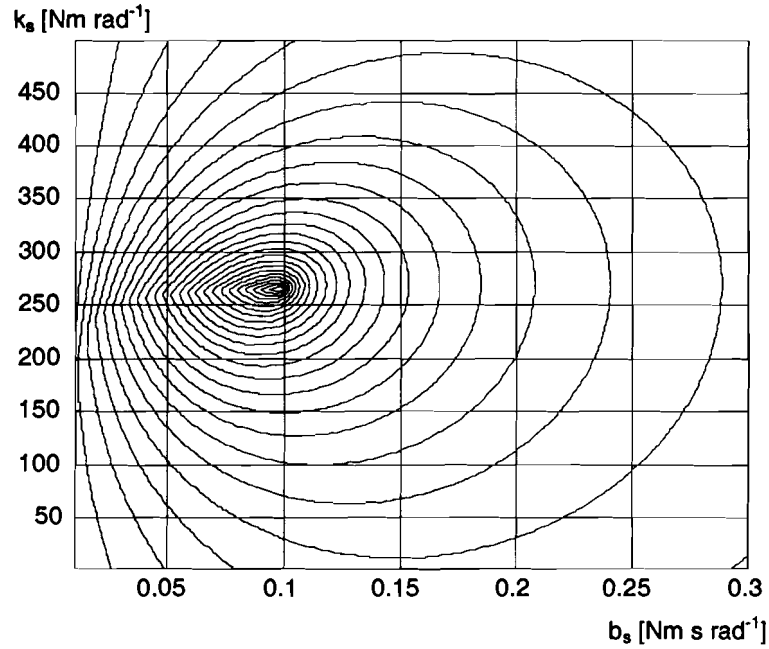

Figure 7-5: Contour plot of the damping as function of k_s and b_s

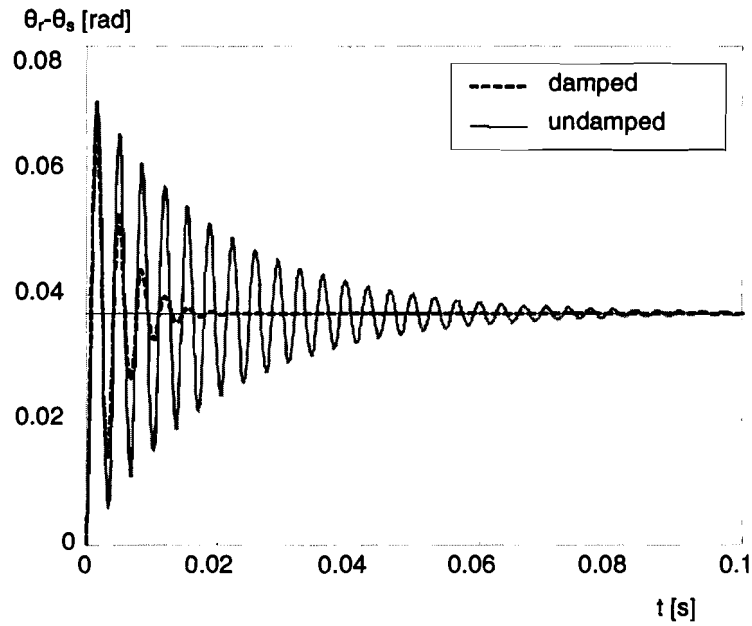

Figure 7-6: Damped and undamped step responses

When analysing the new zero pole plot shown by figure 7.7a, it is obvious that the optimum damper has better damped poles, although the damped situation now has two undamped pole pairs. The bode magnitude plot of figure 7.7b shows a 11.3 dB reduction of the oscillation frequency.

The improvement in motor behaviour seems to be impressive, when using a simple frame mount damper. There are some considerations to be taken, when choosing a frame mount damper by the way described in this section. The analysis of this section has linearised the rotor - stator behaviour of the motor around an equilibrium position of the stepper motor. Unfortunately when using a stepper motor, the rotor – stator position depends on the load to be driven. So the stiffness between the rotor and the stator is not constant.

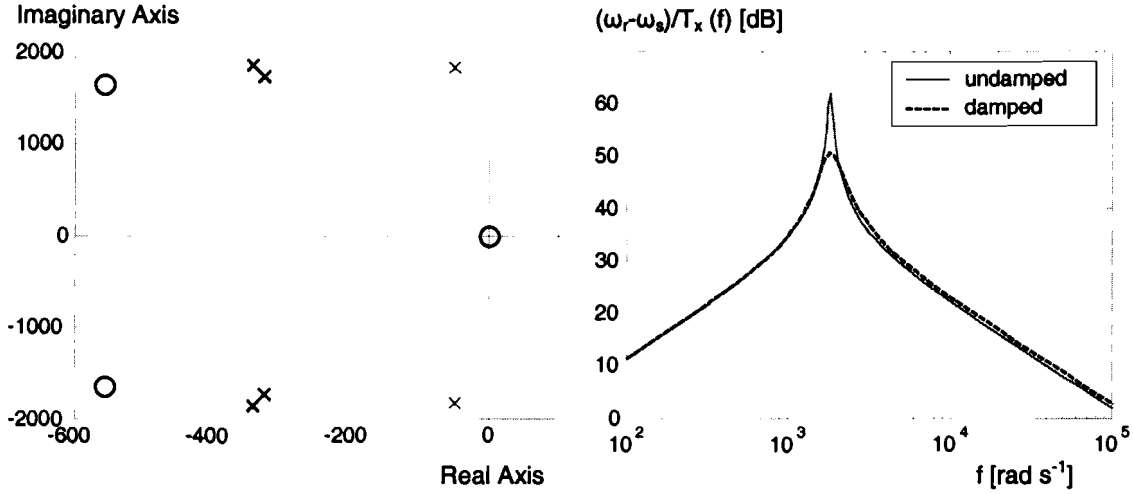

a) Zero - pole plot b) Bode magnitude plot

Figure 7-7: Dynamical characteristics of the (un)damped stepper motor

Besides the position, also the peak static torque is a function of the angular speed of the rotor (relative to the stator). For higher stepping rates, the winding currents can no longer maintain the rated current, making the peak static torque drop. Also the magnetic losses in the stepper motor result in torque drops at high stepping rates. All these effects lower the stiffness between the stator and rotor.

Because of these problems, an ideal frame mount can only be chosen when the mechanical dynamics of the load are known with a very high certainty. Figure 7.8 shows the damping effects of the frame mount, when the calculated stiffness $k_{e,calc}$ is not equal to the real stiffness $k_{e,real}$. Notice that when the stiffness of the frame mount is not optimally tuned, a lower then optimal damping would be worse then a higher then optimal damping.

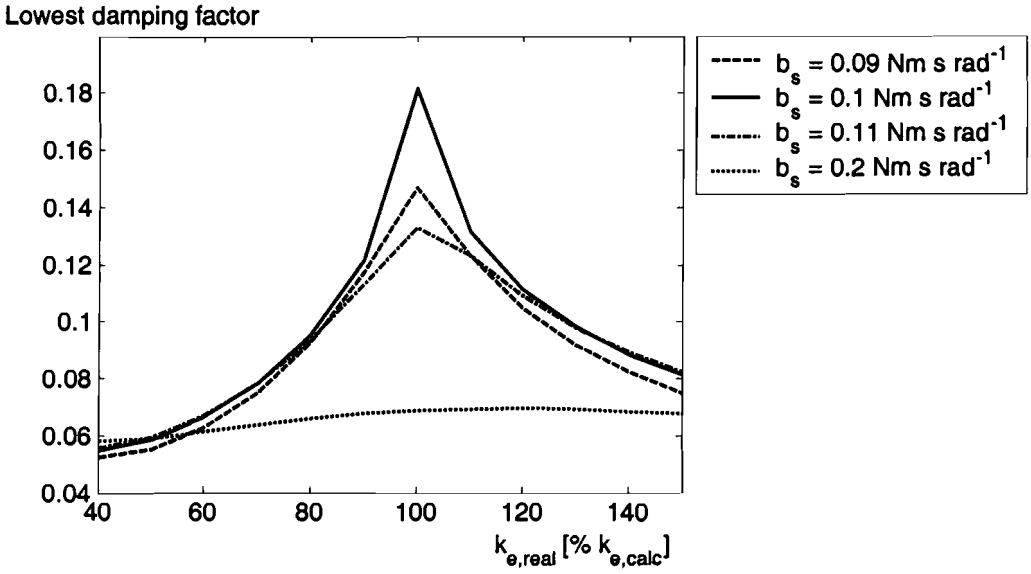

Figure 7-8: damping as function of $k_{e,real}$ and b_s

7.2 *The viscously and elastically coupled inertia dampers*

The viscously and elastically coupled inertia dampers are in essence the same. The elastically coupled damper is basically two inertia, coupled with a plastic material (figure 7.1b). The viscous damper consists out of a damper housing filled with a viscous fluid, and within this fluid is an inertia as shown by figure 7.1c.

The mechanical schematics for each damper are shown by figure 7.9a and b. For each case the stator of the motor is directly coupled to the earth. An housing inertia J_H is directly

coupled to the rotor, and the damping inertia J_D is connected to the housing inertia via a damped spring (elastically coupled, figure 7.9a) or a damper only (viscously connected, figure 7.9b).

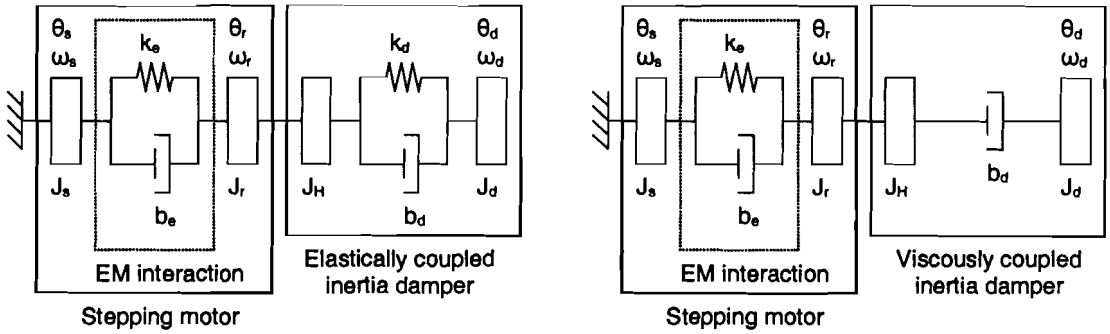

Figure 7-9: Mechanical schematics for elastically and viscously coupled dampers

The viscously coupled inertia damper can be seen as the elastically coupled inertia damper with no stiffness between the two inertia's (k_d = 0 Nm rad^{-1}), so the same state space can be used for both dampers:

Equation 7-4

$$\begin{pmatrix} \dot{\theta}_r \\ \dot{\omega}_r \\ \dot{\theta}_d \\ \dot{\omega}_d \end{pmatrix} = \begin{pmatrix} 0 & 1 & 0 & 0 \\ -\frac{k_e}{J_r + J_H} & -\frac{b_e}{J_r + J_H} & \frac{k_d}{J_r + J_H} & \frac{b_d}{J_r + J_H} \\ 0 & 0 & 0 & 1 \\ \frac{k_d}{J_d} & \frac{b_d}{J_d} & -\frac{k_d}{J_d} & -\frac{b_d}{J_d} \end{pmatrix} \begin{pmatrix} \theta_r \\ \omega_r \\ \theta_d \\ \omega_d \end{pmatrix} + \begin{pmatrix} 0 \\ \frac{1}{J_r + J_H} \\ 0 \\ 0 \end{pmatrix} T_x$$

With k_e and b_e as defined in the previous section, b_d the damping between the inertia's J_H and J_d, and k_d the stiffness between the inertia's J_H and J_d. The output function is now:

$$\begin{pmatrix} \theta_r \\ \omega_r \end{pmatrix} = \begin{pmatrix} 1 & 0 & 0 & 0 \\ 0 & 1 & 0 & 0 \end{pmatrix} \begin{pmatrix} \theta_r \\ \omega_r \\ \theta_d \\ \omega_d \end{pmatrix}$$

Equation 7-5

With θ_r the rotor angle, and ω_r the rotor angular speed.

Without the damper the motor dynamics would be the same as shown by figure 7.3 in the previous section. Again calculating the optimal damper is the objective. Now the choice can be made on the basis of three damper parameters: k_d, b_d and J_d. Lets first analyse the viscously coupled inertia damper, reducing the search area to the parameters b_d and J_d (k_d = 0 Nm rad^{-1}, because the inertia's J_H and J_d are only viscously coupled). For analysis the motor data of the 17PM-K404 is used, as for the previous section has been done.

The viscously coupled inertia damper only produces a torque when the angular speed of the rotor is not equal to the angular speed of the damper inertia (check the space state with k_d = 0 Nm rad^{-1}). This torque is opposed to the speed difference between the rotor and the inertia damper ($\omega_r - \omega_d$). Because of this property the damper will only effect the rotor angular speed oscillations, and not the constant part of the rotor angular speed, making the motor less sensitive for electrical instabilities and mechanical resonance.

The optimal tuning for the damper will be done by the same way as for the frame mount damper, by analysing the worst damped pole(s) of the mechanical system. Figure 7.10 shows the worst damped pole(s) as function of the damping between inertia's J_H and J_d, and the size of the inertia J_d. Again this plot does not give much information about the location of

an optimal value, but it shows that the all the poles can be optimally damped for a series of inertia and damping values (if the worst damped pole has a damping factor equal to one, then all the poles have a damping value of one).

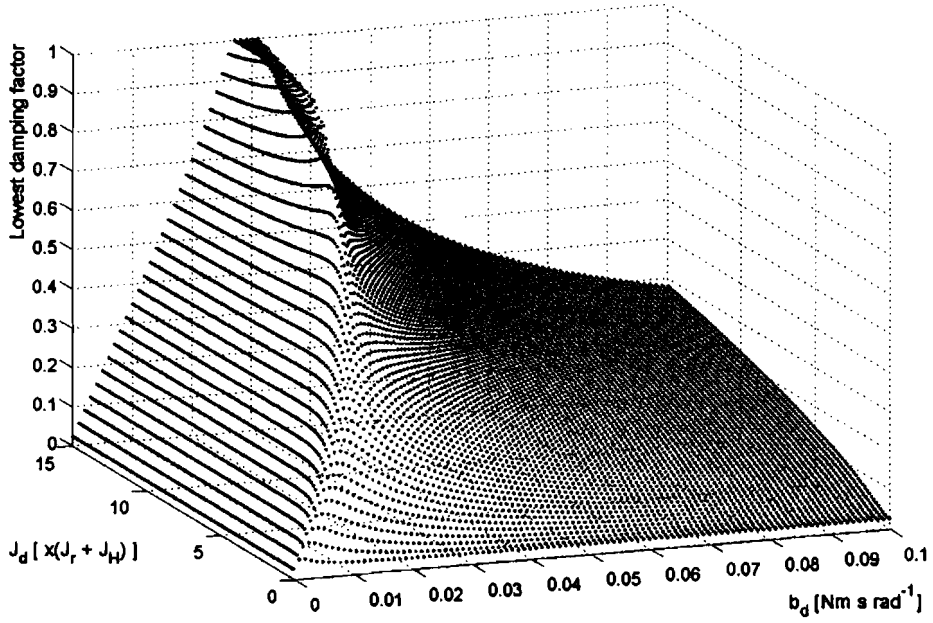

Figure 7-10: Surface plot of the damping as function of J_d and b_d

To get a better impression of the optimal values for the damper inertia J_d and damping b_d, figure 7.11 shows the contour plot of figure 7.10. The highest plateau represent the values in-between 0.95 and 1 for the worst damped pole. To be sure that the situation to be analysed has the optimal damping of one, the following values have been chosen:

- $J_d = 10 \cdot (J_r + J_H) = 9.9 \cdot 10^{-5}$ kg m^2
- $b_d = 0.025$ Nm s rad^{-1}
- Damping factor worst damped pole: 1, with $f_n = 75$ Hz

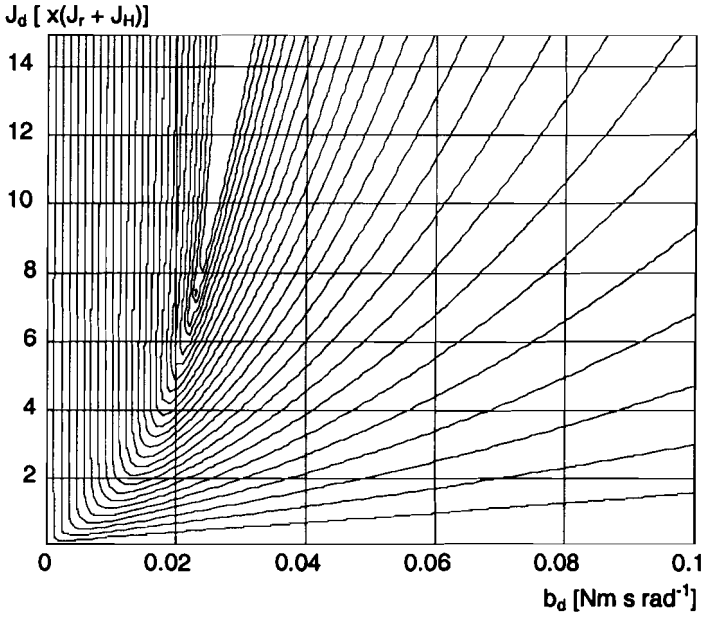

Figure 7-11: Contour plot of the damping as function of J_d and b_d

Figure 7.12 shows the single step response of the undamped and viscously damped mechanical systems. Notice that both the overshoot as the settling time are drastically decreased when using the viscously coupled inertia damper. But the damper also slows

down the rotor motion. The damped system has a rise time, comparable to the undamped mechanical system with an additional inertia of 3.5 times the rotor inertia.

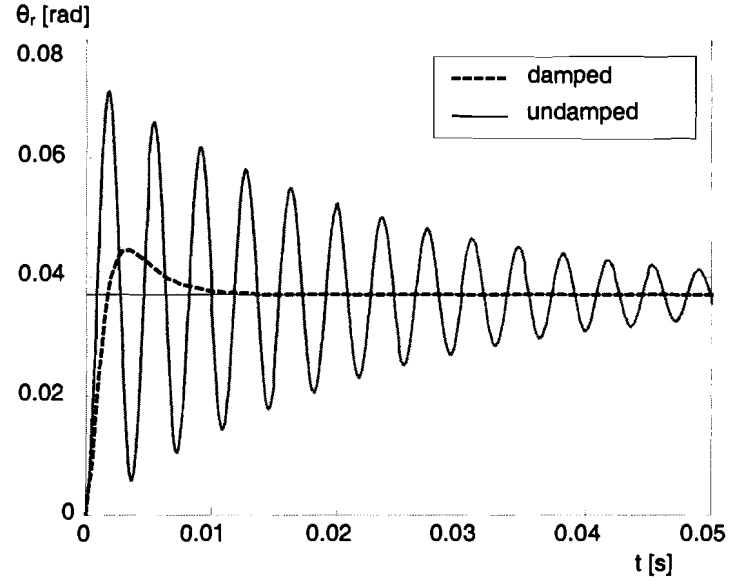

Figure 7-12: Damped and undamped step responses

The zero pole and bode magnitude plots are shown by figure 7.13. The zero pole plot shows that all poles are along the real axis, meaning that they are well damped. The improvement is also noticeable in the bode magnitude plot. The oscillation frequency has been damped with an impressive 29.8 dB.

As with the frame mount damper, the torque loss of the motor itself has influence on the performance of the damper. To analyse the impact, figure 7.14 shows a plot of the damping as function of the stiffness mismatch (real stiffness $k_{e,real}$ as percentage of $k_{e,calc}$). When the real stiffness has a little deviation from the calculated, the damper still has a good performance. For great deviations the damper loses its efficiency, but still gives the rotor much better damping, as when no damper was used at all.

The viscously coupled inertia damper outperforms the frame mount damper. But disadvantages are the complexity of the damper (resulting to high costs), and the loss of acceleration (because of the additional inertia to accelerate).

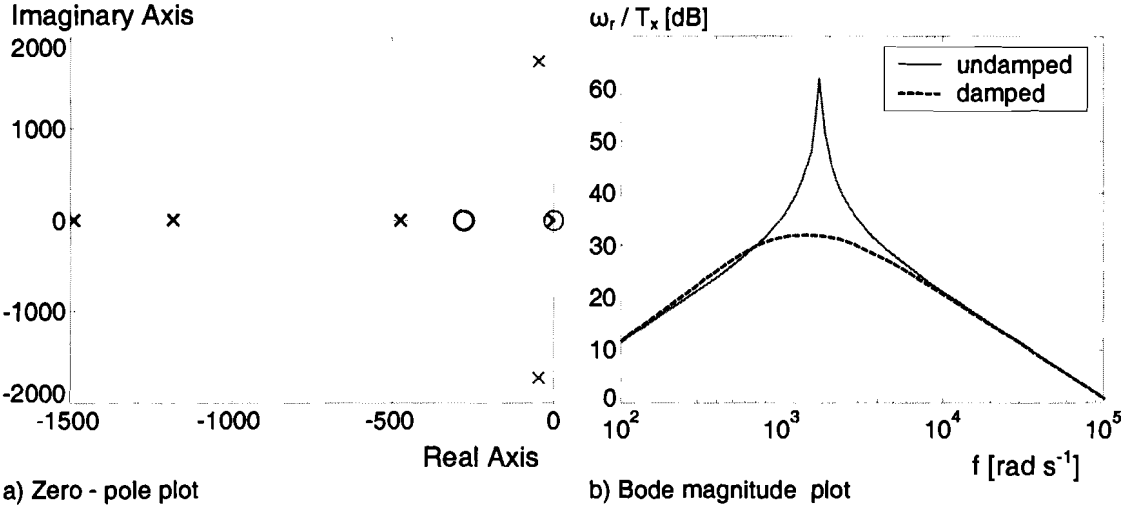

Figure 7-13: Dynamical characteristics of the (un)damped stepper motor

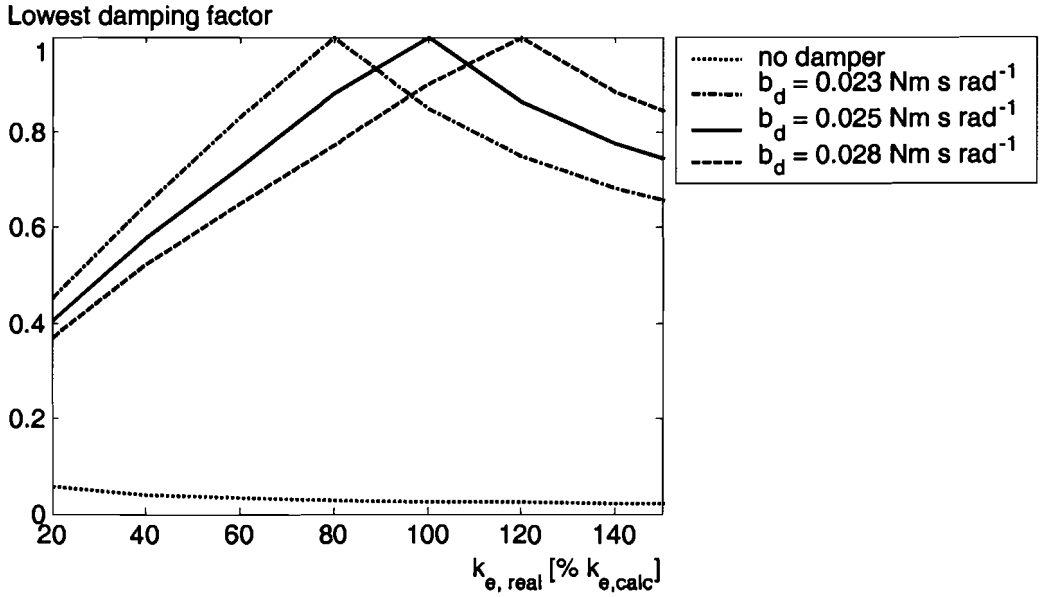

Figure 7-14: damping as function of $k_{e,real}$ and b_d

The elastically coupled inertia damper has basically the same way of damping as the viscously coupled inertia damper. Only now also the stiffness between the housing inertia and the damper inertia has influence on the damper performance. This makes the search to an optimal damper a bit more complicated. In an effort to search for the optimal damper, a series of simulations have been performed, looking for the optimal stiffness and damping when the inertia of the damper already is chosen (again the 17PM-K404 is used as stepper motor).

Figure 7.15 shows the contour plots for the damper inertia's $J_d = 2 \cdot J_r$ and $J_d = 4 \cdot J_r$. As can be seen from the plots, the worst damped pole has a maximal damping factor of 0.63 for $J_d = 2 \cdot J_r$ and 0.93 for $J_d = 4 \cdot J_r$. The maximum damping factor of the worst damped pole reaches a value of one for the inertia $J_d = 6 \cdot J_r$. Figure 7.16a shows the contour plot of damping as function of the stiffness and damping of the damper, and 7.16b shows the step response of the mechanical system damped with the optimal values retrieved from figure 7.16a:

- $k_d = 3.5$
- $b_d = 0.024$
- Damping factor worst damped pole: 1, with $f_n = 50.3$ Hz

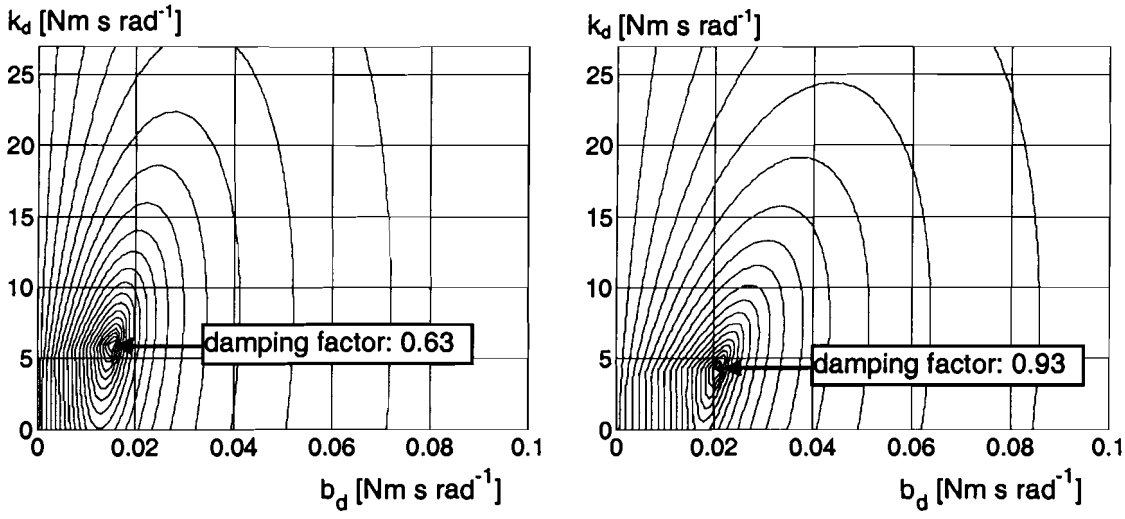

a) $J_d = 2 \cdot J_r$ b) $J_d = 4 \cdot J_r$

Figure 7-15: Contour plots of the worst damped poles

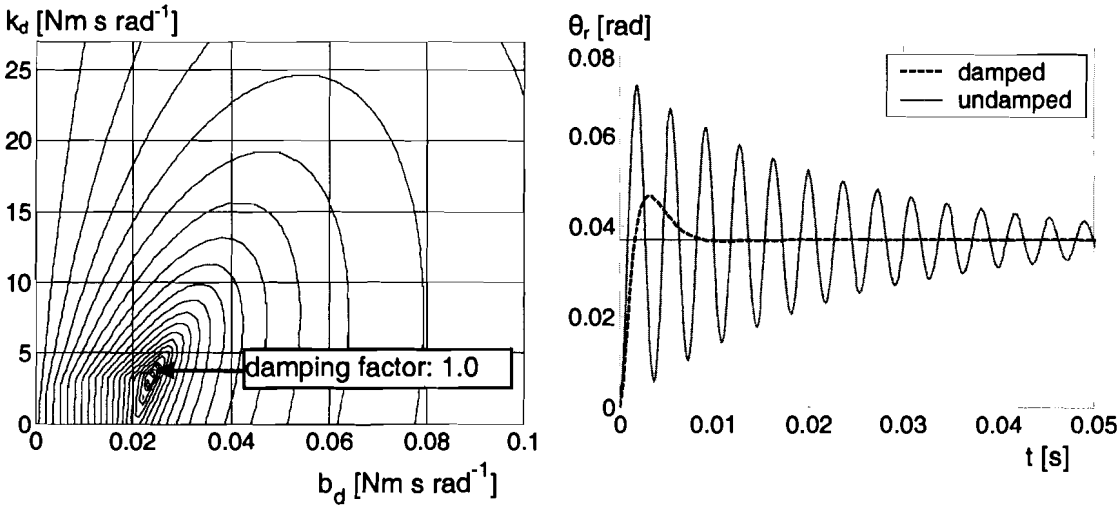

a) Contour plot of worst damped pole b) Step response

Figure 7-16: Simulation results for $J_d = 6 \cdot J_r$

For any inertia $J_d \geq 6 \cdot J_r$ exists a combination of stiffness and damping resulting in a damping factor of one for the worst damped pole. But as with the viscously coupled damper, the damper inertia results in a longer rise time for the step response, and higher damper inertia's result in longer rise times. The damped response of the system with $J_d = 6 \cdot J_r$ has a rise time comparable with an undamped system with an additional inertia of four times the rotor inertia J_r.

The impact of the damper on the pole zero map of the complete mechanical system is shown by figure 7.17a. As can be seen from the plot, all poles are on the real axis. The bode magnitude plot of the mechanical system is shown by figure 7.17b, the oscillation frequency peak has been lowered by 29.4 dB. Figure 7.18 shows the impact of a motor stiffness mismatch on the performance of the damper. Just as the viscously coupled inertia damper, the overall damping is higher as when no damper is used, but tuning is more critical as when using a viscously coupled inertia damper.

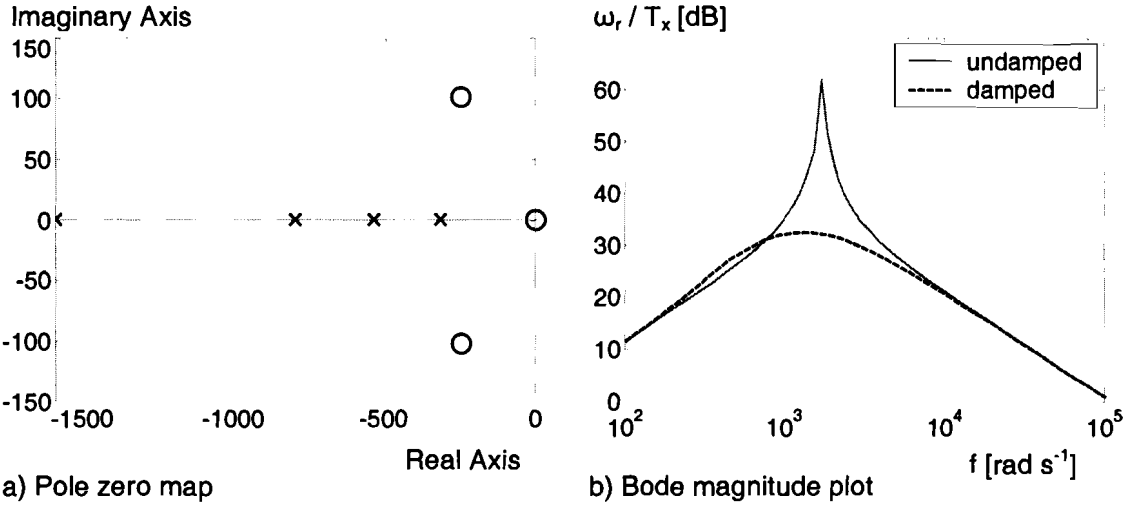

a) Pole zero map b) Bode magnitude plot

Figure 7-17: Simulation results for $J_d = 6 \cdot J_r$

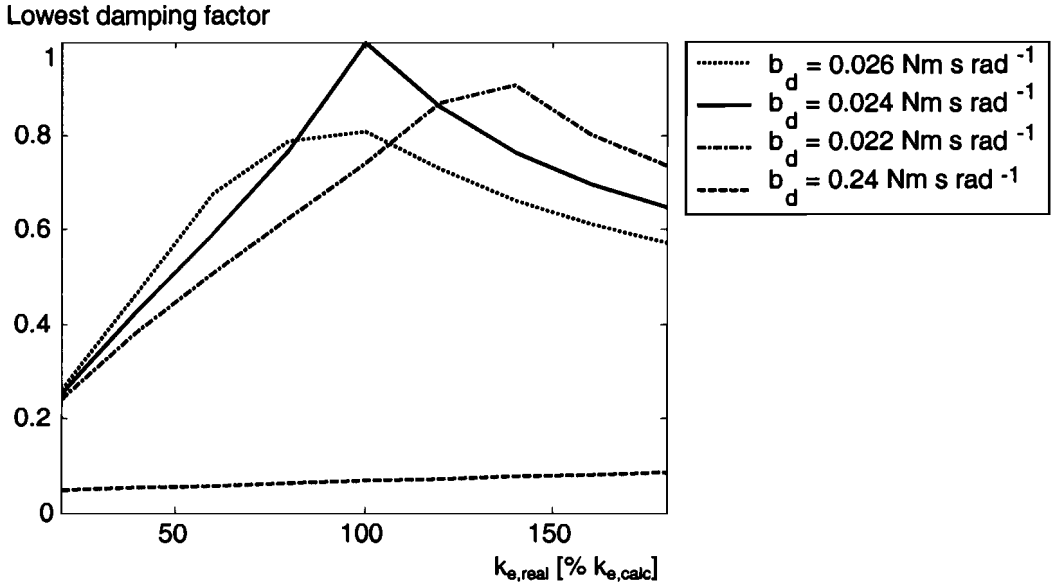

Figure 7-18 damping as function of $k_{e,real}$ and b_d

7.3 Practical implementation of mechanical dampers

The analyses of the previous two sections assumes complete freedom with the design or choice of mechanical dampers. This is not true when choosing dampers for practical applications. All dampers are limited by the materials they are made from (each material has typical damping and stiffness properties, limiting the design possibilities), and share a limited availability. Another problem with choosing a damper is the fact that manufacturers are not very generous with sharing specifications of their products.

The frame mount damper is often supplied by the motor manufacturer, with no specifications at all. These dampers seem to be tuned for the motor they are delivered with, resulting to a noticeable improvement when using the damper. Figure 7.19 shows a single step response of the 17PM-K404 stepper motor with and without the frame damper.

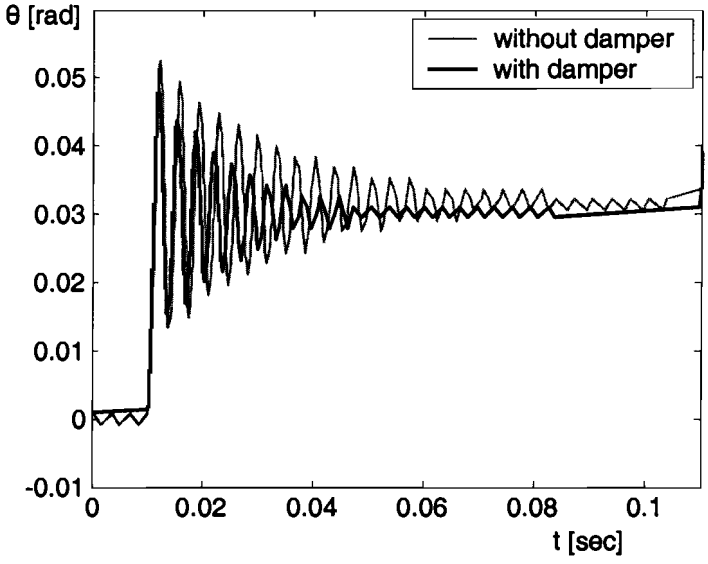

Figure 7-19: Single step response of 17PM-K404 with and without frame damper

The elastically coupled inertia damper should have a greater design freedom as the frame mount damper, as it has only one function, damping the rotor movement. The frame mount damper must also sustain the motor to the frame, restricting the choice of stiffness and damping. Also the choice of damper inertia should make the elastically coupled inertia damper more versatile. Unfortunately the damper is restricted by the plastic material providing the stiffness and damping between the housing inertia and damper inertia. Plastics

have their own typical material properties restricting the freedom of choice for damping and stiffness.

The viscously coupled damper consist out of two inertia's and a viscous fluid providing the damping. This damper has by far the most freedom in design, but also is the most expensive of the three. This damper would only be interesting when very precise movements are required.

For "normal" use of stepper motors, only the frame mount damper could be interesting, because of its low price and the fact that the damper does not influence the acceleration. But in general, when the motor needs additional damping, it is better to choose a smaller motor, instead of using all kinds of dampers. Only when very precise movements are required, the use of one of the inertia dampers may be the solution.

The inertia dampers have not been available during the investigation, and will not be further analysed. The frame mount damper supplied by the manufacturer together with the 17PM-K404 will be analysed. The improvement of damping has already been shown by the single step response of figure 7.19. The next section will deal with a series of measurements and simulations to determine the motor behaviour improvement when no load is attached to the motor.

Chapter 8 will also deal with a series of measurements and simulations when the damper and motor are used to drive a known load, and compared with measurements and simulations of the motor without frame damper.

7.4 Measurements and simulations with the frame mount damper

As figure 7.19 already shows, using the frame mount damper results to a damped single step response for the stepper motor. The stiffness of the frame damper has been measured, $k_s = 65$ Nm rad^{-1} [11]. The stator inertia has again been set at the calculated value of ten times the rotor inertia.

For getting the damping parameter of the frame damper, several simulations have been performed, to match a simulated step response to the measured step response of figure 7.19. From the simulation the damping has been set to : $b_s = 0.08$ Nm s rad^{-1}. Figure 7.20 shows both the measured and simulated step responses, for : $k_s = 65$ Nm rad^{-1} and $b_s = 0.08$ Nm s rad^{-1}.

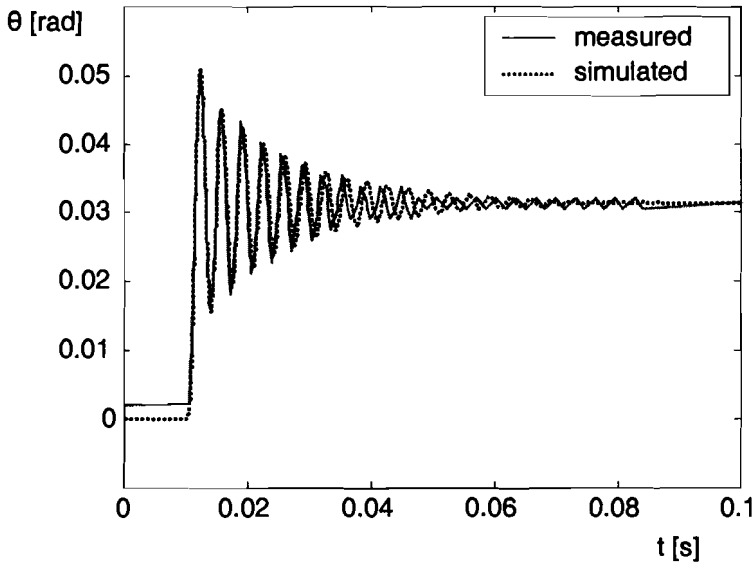

Figure 7-20: Measured and simulated damped step responses of 17PM-K404

Besides the single step responses, also some dynamical measurements have been performed, the same way as the measurements from section 5.6. The stepping rates that have been analysed are: 500, 1000, 1500, 2000 and 2500 steps per second. At stepping rates of 500 and 1000 steps per second little differences have been encountered between the damped and undamped stepper motor measurements.

At 1500 Hz, the electrical unstable stepping frequency, the improvement of the frame mount on the rotor movement is obvious. Figure 7.21 shows the measurements for both the damped and the undamped rotor speed, at 1500 Hz. Undamped the rotor instantaneously starts to oscillate between 4 and 96 rad s^{-1}, almost getting to a complete stand still. Damped the oscillation is reduced to 26 and 69 rad s^{-1}, with a slow build-up.

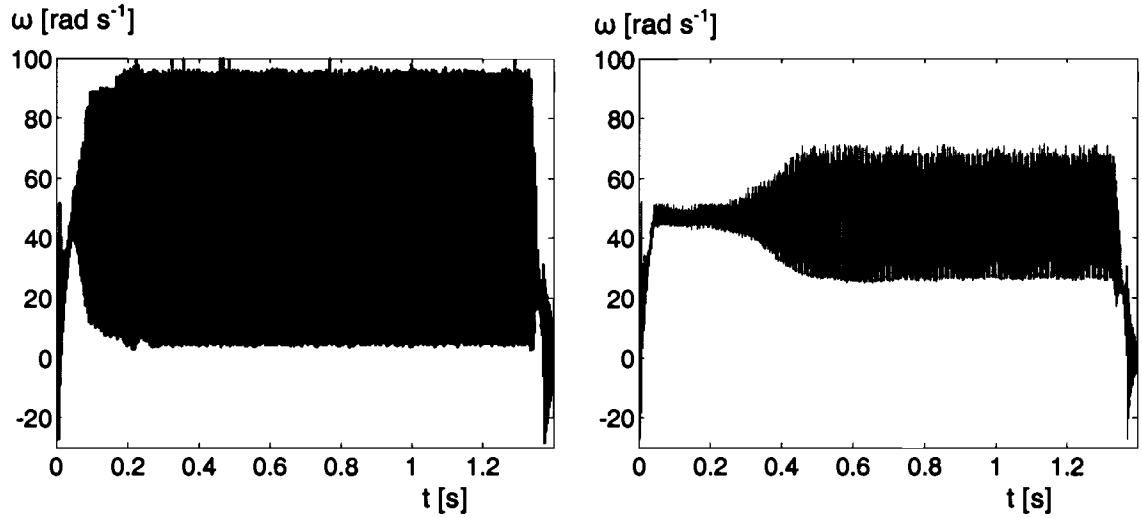

a) undamped b) damped

Figure 7-21: 17PM-K404 turning at 1500 steps per second

The oscillation at 1500 steps per second is still quite big, but the damper provides enough damping to enable the stepper motor to pass through the electrical instability region (section 5.6 shows that the undamped stepper motor failed to get to speeds above the 1500 Hz). Figure 7.22 show the plots of the damped stepper motor at 2000 and 2500 Hz. The speed profiles are exactly the same as the speed profiles used for the measurements of section 5.6, but now the motor has no problem passing through the electrical instability region.

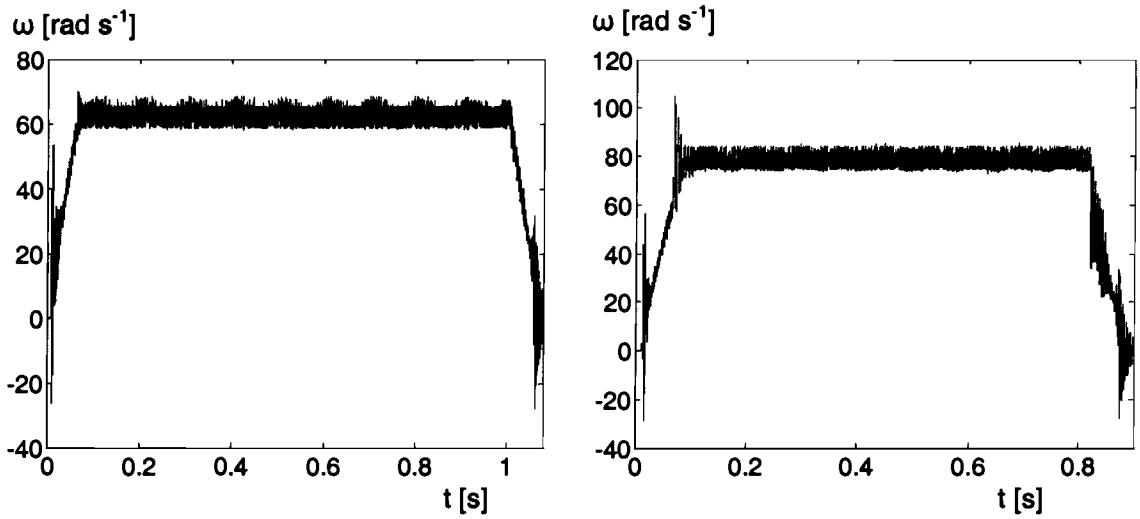

a) f_s = 2000 Hz b) f_s = 2500 Hz

Figure 7-22: The damped 17PM-K404 above f_s = 1500 Hz

Figure 7.23 shows the simulated stepper motor response with the ramp of figure 7.21b, the measured stiffness, and the damping derived from the single step response. The simulated response shows great similarity with the measured response. Again the oscillation has a

slow build-up, and also the amplitude is very similar (between the 35 and 60 rad s^{-1}). The simulation results for higher stepping rates show the same kind of behaviour as the measured responses.

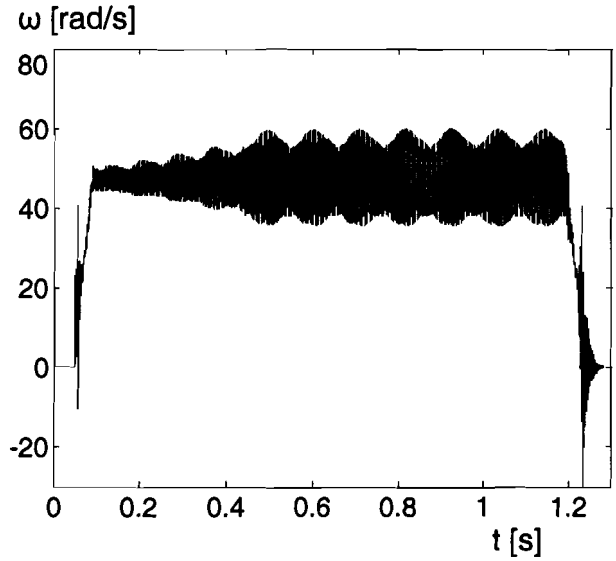

Figure 7-23: Simulation of damped 17PM-K404 at f_s = 1500Hz

8 Analysing the stepper motor driving a load

Until now the measurements with stepper motors had the primary objective to analyse the predictability of its behaviour. During the investigation of stepper motors, the mechanical load proved to drastically change the motor behaviour (for example the frame mount damper). This is not very surprising, since both systems interact with each other. This is not different with any other type of electrical motor, but the lack of feedback forces the designer to have a bigger a priori knowledge of the complete stepper motor and mechanical load dynamics.

Chapter 6 already dealt with enhancing the simulation model to accept different mechanical configurations. The way how to determine the dynamics of the mechanical configuration has also been outlined in chapter 6. The aim of this chapter is to analyse the stepper motor behaviour of the 17PM-K404 when being used with the "stopper wals" configuration described by chapter 6.

The simulation model of the stepper motor will be used to determine if decent predictions of the motor behaviour can be made, when the mechanical dynamics of the load are well known. These dynamics of the "stopper wals" will be acquired by a series of measurements as described by chapter 6.5.

And finally the motor behaviour of the 17PM-K404 will be compared with the behaviour when the motor is damped by a frame mount damper.

8.1 Identifying the "Stopper wals" dynamics

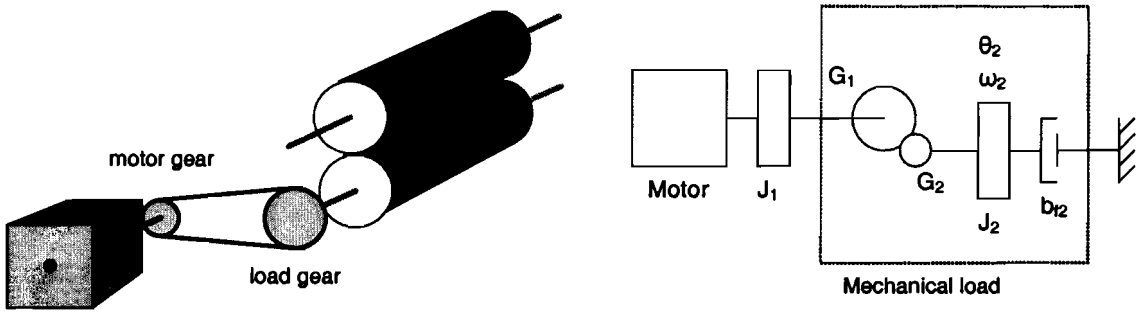

a) Schematic

b) Mechanical dynamics

Figure 8-1: The "stopper wals" schematic and dynamics

Figure 8.1 shows both the "stopper wals" schematics and the chosen dynamical representation for model identification. The known parameters for the "stopper wals" are:

Mechanical property	Value	Description
G_2 [teeth]	29	Number of load gear teeth
J_2 [kg m^2]	$4.15 \cdot 10^{-5}$	Load total inertia
c_{f2} [Nm]	0.026	Coulomb friction at load estimate

The load inertia has been calculated, with a high accuracy. The coulomb friction has been measured, but the measurement accuracy is very low. This parameters will be taken as unknown during the identification.

The DC motor used for driving the load is the Parvex RS220XR, also used for the simulations of chapter 6.5. The motor parameters are displayed in table 8.1. The parameters to identify are:

- By the single step method: Coulomb friction c_{f2} and viscous friction of load b_{f2}
- By the pseudo random noise test: Confirm order of dynamics and viscous friction b_{f2}

Table 8-1: Parvex RS220XR motor properties

Physical property	Value	Description
R [Ω]	1.1	Winding resistance
L [H]	$3.2 \cdot 10^{-4}$	Winding inductance
k_t [N A^{-1}, V s rad^{-1}]	$4.6 \cdot 10^{-2}$	Motor constant
J_{rotor} [kg m^2]	$1.95 \cdot 10^{-5}$	Rotor inertia (including gear J_1)
G_1 [teeth]	18	Number of rotor gear teeth
c_{fr} [Nm]	$1.7 \cdot 10^{-2}$	Measured coulomb friction between stator and rotor
b_{fr} [Nm s rad^{-1}]	$1.3 \cdot 10^{-5}$	Measured viscous friction between stator and rotor

Single step measurements:
The step response measurements have been performed as described in chapter 6.5. Figure 8.2 shows an example of such a single step. With a bit of imagination the measurements show a constant steady state for both the current (8.2a) and the angular speed (8.2b). This procedure has been repeated several times for different DC voltages (and thus different winding current and angular speeds).

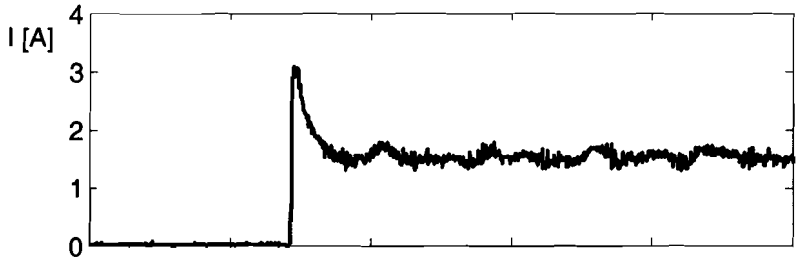

a) DC motor current

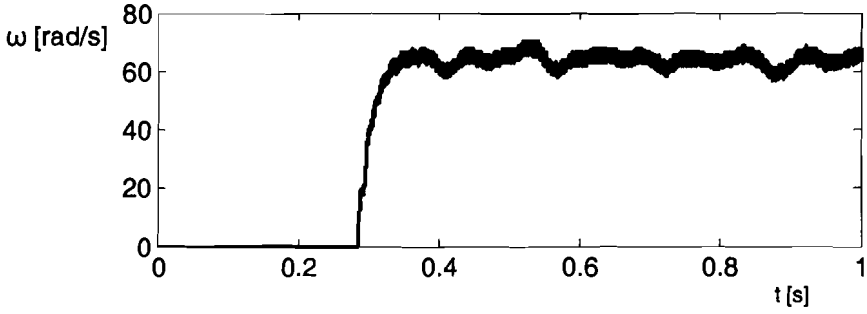

b) DC motor angular speed

Figure 8-2: Measurements of a single step response

Figure 8.3 shows the results from the measurements. The torque on the y-axis has been calculated from the measured steady state current values using the DC motor constant, and the x-axis shows the measured steady state angular speeds. Except for the lowest and highest values of the torque measurements, the relation between the torque and angular speed is fairly linear (roughly in between ω_{motor} = 30 – 90 rad s^{-1}). From the measurements the following parameters have been retrieved:

c_{f2} = 62 mNm
$b_{f2} = 3.4 \cdot 10^{-4}$ Nm s rad^{-1}

Notice that the coulomb friction measured with the single step response is more then two times the first coulomb friction estimate. The viscous friction is very small, but at speed above the 20 rad s^{-1} already results to a friction torque of more then 10% of the coulomb friction torque of the load.

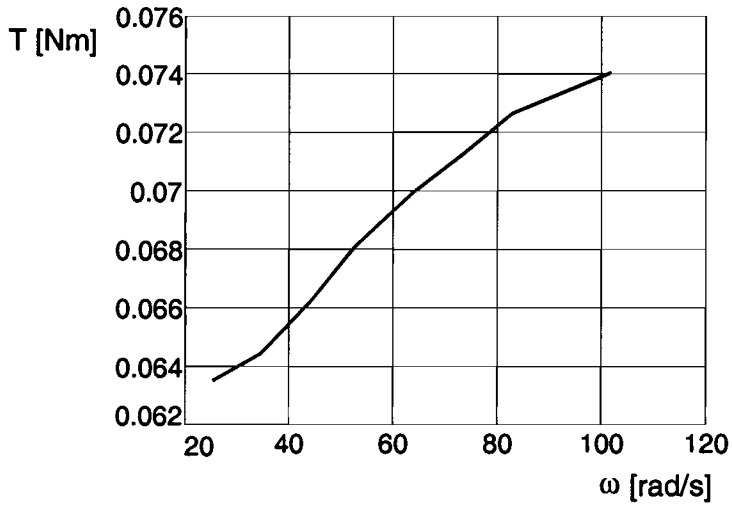

Figure 8-3: Measured torque vs. angular speed

The pseudo random noise (PRN) test:
When theoretically analysing the "stopper wals" in chapter 6.5, the conclusion was made that the stiffness between the motor gear and the load gear could not have a big impact on the total load dynamics, and were therefore ignored. The PRN test will show if this assumption is valid, as the test will reveal the total system dynamics as seen from the motor.

For the PRN test the voltage of the DC motor was randomly changed in such way that the angular speed of the motor remained in between the fairly linear region measured during the step responses (ω_{motor} = 30 – 90 rad s^{-1}). The currents and angular speeds have been measured during the test. The results are shown by figure 8.4. Again the dc motor torque has been calculated from the winding currents (8.4a).

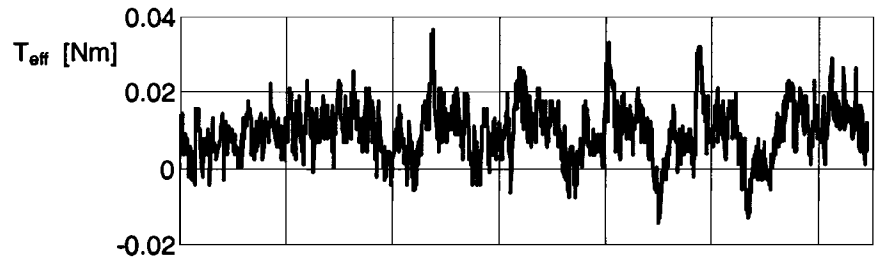

a) Effective torque produced by dc motor

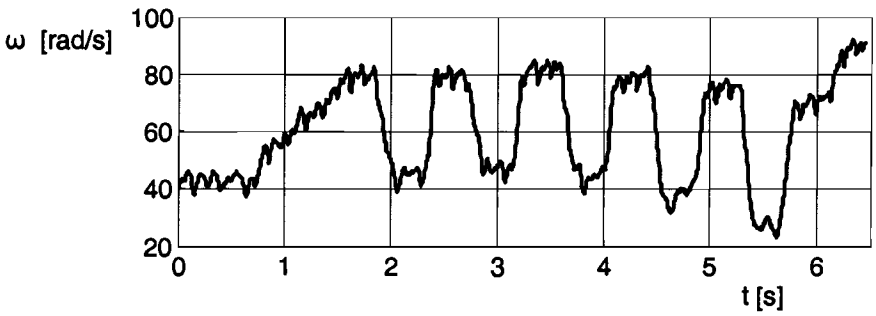

b) Angular speed of rotor

Figure 8-4: Measured data from the PRN test

The measured data is very noisy, and only a small amount of data is available (to prevent the DC motor from getting hot, changing the motor dynamics). It maybe seems hard to get any data about the load dynamics, but the matlab identification toolbox was still able to retrieve the load dynamics. A first order estimate of the system dynamics results to a 75% fit, while a second order estimate will result to a 77% fit. So a first order estimate should be sufficient. The resulting state space representation for the DC motor - load combination is:

$$\begin{pmatrix}\dot{\theta}\\ \dot{\omega}\end{pmatrix}=\begin{pmatrix}0 & 1\\ 0 & -3.9\end{pmatrix}\begin{pmatrix}\theta\\ \omega\end{pmatrix}+\begin{pmatrix}0\\ 2.5\cdot 10^{4}\end{pmatrix}T_{motor}$$

$$\begin{pmatrix}\theta_r\\ \omega_r\end{pmatrix}=\begin{pmatrix}1 & 0\\ 0 & 1\end{pmatrix}\begin{pmatrix}\theta\\ \omega\end{pmatrix}$$

Equation 8-1

With T_{motor} the torque produced by the motor, θ_r the rotor angle and ω_r the rotor angular speed. With help of equation 6.25, the representation of the state space in the parameters from figure 8.1b, the following estimates are made:

$b_{f2} = 3.1 \cdot 10^{-4}$ Nm s rad^{-1}
$J_2 = 4.5 \cdot 10^{-5}$ kg m^2

The measured inertia J_2 has a 8.4% difference with the calculated value (see "stopper wals" known parameters). When looking at the measurement results, this should not be a surprise. Figure 8.5 shows the performance of the estimated model versus the measured data from figure 8.4b. The first three seconds of the angular speed show a bigger simulation error as the last three seconds, because of a bad estimate for the initial states.

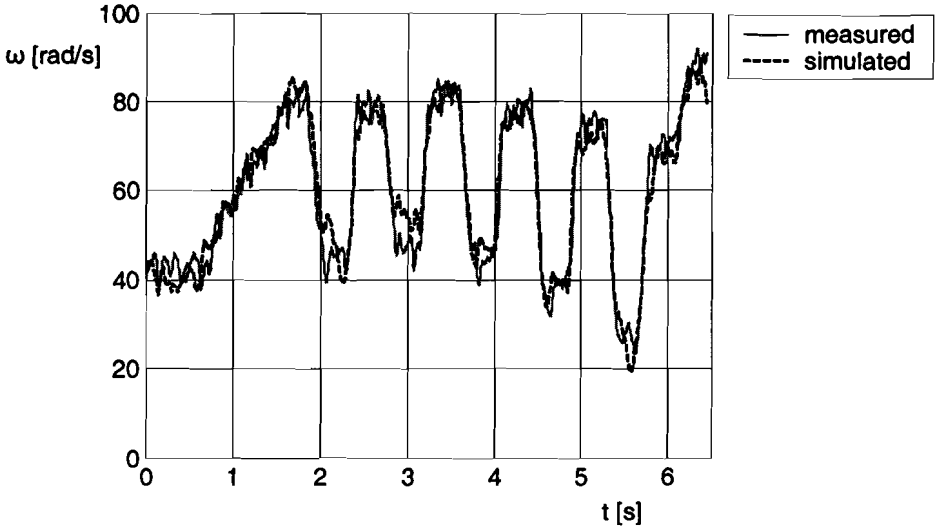

Figure 8-5: Measured versus simulated angular speed

8.2 Measurements and simulations of the "stopper wals" with the 17PM-K404

A series of measurements have been performed with the 17PM-K404 driving the "stopper wals". The measurements have been performed under the following conditions:

Stepper motor	Value	Description
I [A]	1.0	Chopper reference current
G_1 [teeth]	18	Number of motor gear teeth
J_1 [kg m^2]	$4 \cdot 10^{-7}$	Inertia motor gear

The load has been modelled with the parameters measured in the previous section. Both the stepper motor with and without the frame damper have been measured, performing a series of angular speed ramps, while an encoder measured the rotor angle. The measurements of the damped stepper motor will be compared with the undamped stepper motor in the next session.

To see if the 17PM-K404 is a good choice to drive the "stopper wals", consider the design rules from chapter 3.3:

- A rotor:load inertia ratio between 1:1 – 1:10, for the stopper wals the inertia ratio is 1:2, well between the recommended range, and even in the fast acceleration range of 1:1 – 1:3.

- The motor must deliver about 30% to 70% of its torque to drive the load. Figure 8.6 shows the load torque to pull out torque ratio for different stepping rates. The load ratio is only valid for stepping rates above the 2 kHz.

The measurements from chapter 5.6 will be repeated, so the stepping rates to be analysed are 500, 1000, 1500, 2000 and 2500 Hz. So only the situation of 2500 Hz complies with the design rules.

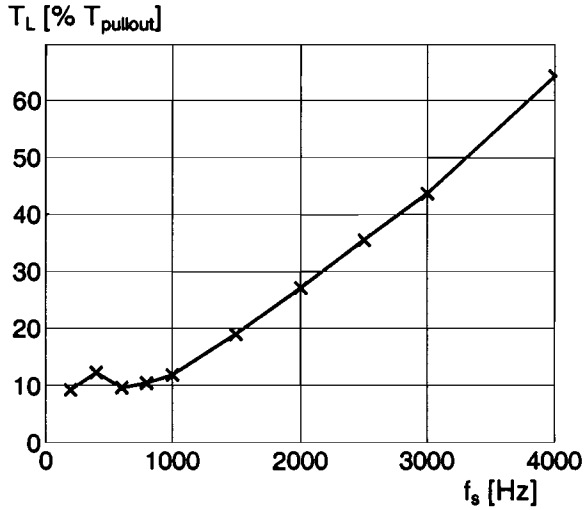

Figure 8-6: Load torque as percentage of the 17PM-K404 pull out torque

A measured speed ramp of the stepper motor accelerating to a stepping rate of 1500 Hz (ω_r = 47.1 rad s^{-1}) is shown by figure 8.7a. Notice the very fast accelerations and decelerations of the rotor during the first steps. This is an unexpected result, as the inertia of the stepper motor - load combination is three times that of the stepper motor without any load, and as figure 8.7b shows, yet the acceleration and decelerations are almost identical as the stepper motor without load. The only difference is the stability of the rotor motion at the stationary angular speed.

The simulated stepper motor response shown by figure 8.8 gives an idea of the expected response. The load inertia makes the rotor response far less aggressive during start-up, if the load is directly coupled to the stepper motor. It is obvious from the measurements, that this cannot be the case. The assumption of a stiff transmission between the load and the stepper motor from chapter 6.5.2 must be wrong.

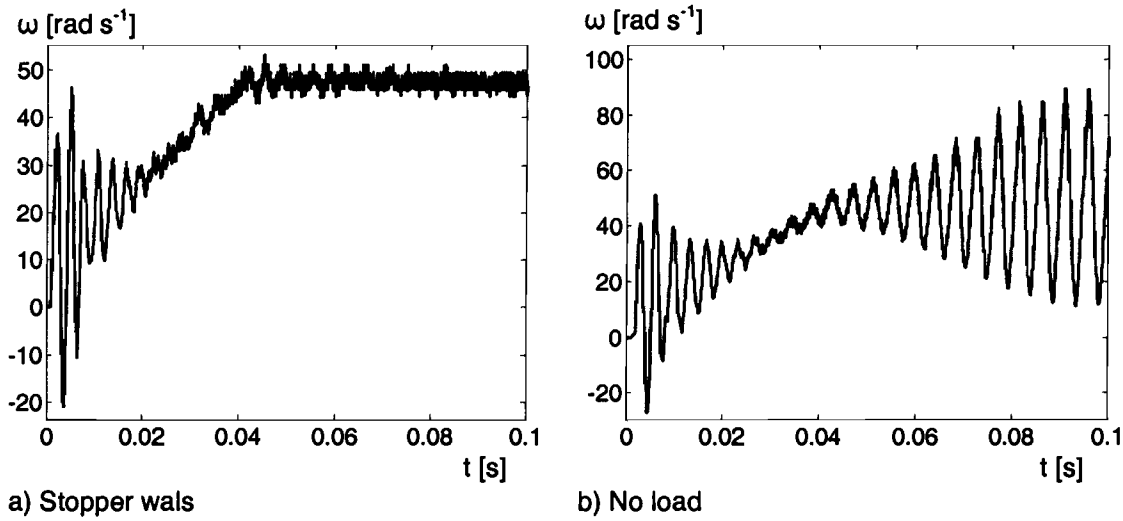

Figure 8-7: 17PM-K404 at F_s = 1500 Hz with and without "stopper wals" load

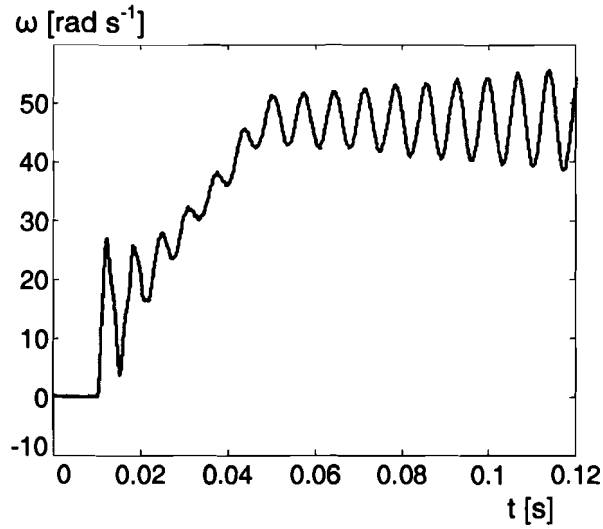

Figure 8-8: Simulation of "stopper wals" with stiff transmission

When modelling the "stopper wals", some parameters have not been included to the dynamics. Figure 8.9 shows some system variables which change the mechanical dynamics of the "stopper wals". The major contribution comes from the play between the load pulley and the load axle. This play will result in more freedom between the rotor and the load. Also the belt tension will influence the freedom between motor and load.

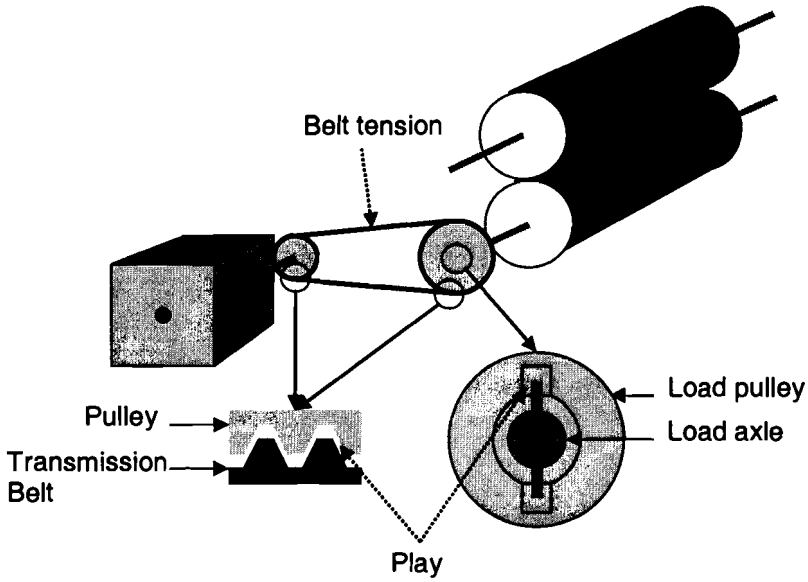

Figure 8-9: "Stopper wals" drive attributes

To demonstrate the effect of a greater freedom between the motor and the load, a new simulation has been performed. During simulation all the freedom between the rotor pulley and the load pulley has been simplified by dimensioning the transmission belt as a damped spring with a stiffness of k_b = 1 Nm rad^{-1}, and a damping $b_b = 10^{-3}$ Nm s rad^{-1} (using the notation of chapter 6). Figure 8.10a compares the simulation results with the actual measurements.

The new simulation predicts very similar motor behaviour as the actual behaviour measurements. During the analyses of chapter 6, a stiffness of 1 Nm was considered to be very unlikely, as the freedom of movement between load and play was to big. But as figure 8.10b demonstrates, during the simulation the angle difference between the rotor axle θ_{rotor} and the (normalised) load axle $\theta_{load,norm}$ just passed above the five degrees. After analyses of all the actual freedom between the load and the motor, this does not seem to be an exaggerated figure. Mechanical engineers at Océ have estimated the play between the two axles around three to five degrees.

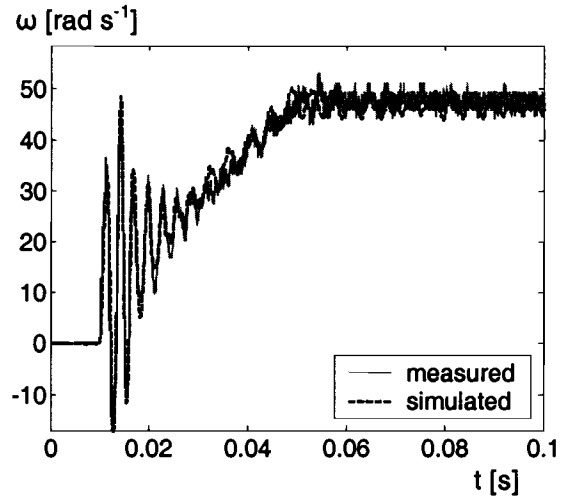

a) Simulation compared with measurement

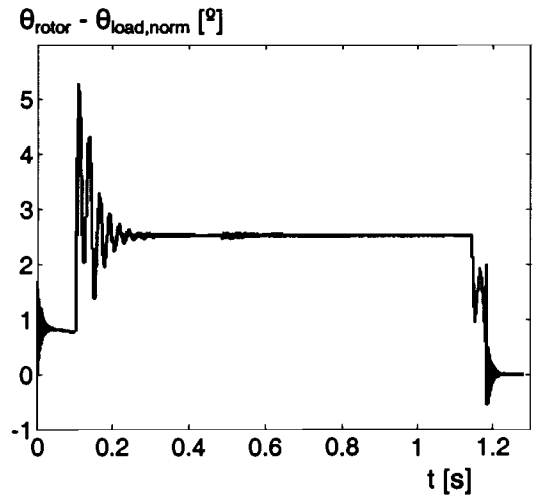

b) Simulated angle freedom between load and rotor

Figure 8-10: Simulation of "stopper wals" with k_b = 1 Nm rad^{-1}, b_b = 10^{-3} Nm s rad^{-1}

The other measurements performed with the "stopper wals" all show the same mechanical model mismatch. These experiments show the vital role of the mechanical dynamics for the motor behaviour. For the case of the "stopper wals" the transmission actually improved the motor behaviour, as the motor is completely stable at 1500 Hz, despite the fact that the stepping rate of 1500 Hz is within the electrical instability region of the motor (see the measurements from figure 8.7b). As a matter of fact, when driving the "stopper wals" the stepper had no problem with the electrical instability at all.

This sudden improvement of motor behaviour is a coincidence. Situations where the transmission seriously impeded motor behaviour are no rarity. A better (or more extensive) analysis of the load dynamics would result to better models. The identification process described by chapter 6.5 can still be useful, if the load angle is also recorded.

8.3 Measurements with the frame mount damper

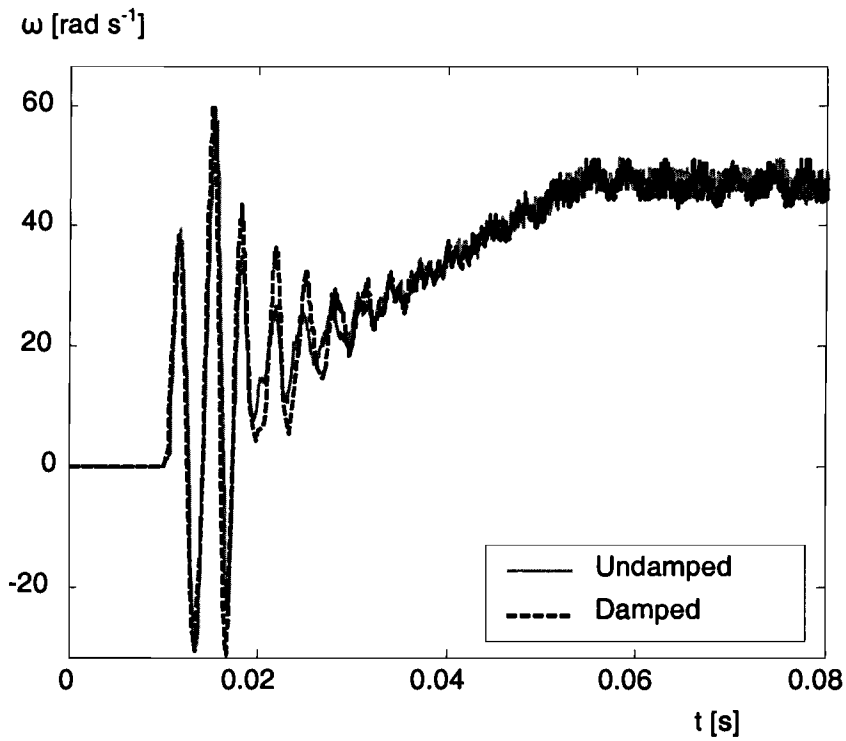

Figure 8-11: Damped vs Undamped response for the "stopper wals"

The measurement of the "stopper wals" at 1500 Hz show that the 17PM-K404 does not show any sign of instability. The same measurements have been performed with the motor mounted via the frame damper. Figure 8.11 shows the results of both the undamped and damped responses of the 17P-K404 for a stepping rate of 1500 Hz. The damper does not improve the motor behaviour. Actually, the response for the undamped situation has an lower oscillation at start-up. The responses for other stepping rates do not differ from the 1500 Hz situation.

9 Conclusions and recommendations

The investigation of stepper motors consists of two parts:

- Improving the predictability of stepping motors
- Improving the stepper motor behaviour

In an attempt to give an answer to the first item, a simulation model was created. The motor dynamics of this model have been kept simple, to make it accessible with limited information about the stepper motor itself. As a result of the simplicity, the model has a limited value for motor behaviour prediction. Comparing the measurement results with the simulation results show that the simulation model makes acceptable predictions for the following cases:

- Predicting the location of unstable stepping regions
- For stepping rates below the electrical instability region the measured data shows great similarity:
  - Current prediction errors below the 20%, depending on the motor load
  - Both dynamic and static encoder measurements show little differences
- The effects of higher order mechanical dynamics on the stepper motor behaviour, when driving a load
- At high speeds the estimates of motor efficiency have a 10% - 30% error, depending on the stepping rate

The value of the simulation model depends on the purpose. For the dynamical motor behaviour of a known stepper motor – load combination the model works fine. The problematic stepping rates of a stepper motor – load combination can be identified, and if necessary the use of mechanical dampers and higher stepping modes can be analysed with the simulation model.

The StepperGUi toolbox helps with analysing the stepper motor behaviour. An advantage is the fact that the toolbox is able to predict natural resonance's and electrical instabilities with the help of motor manufacturer datasheets. These datasheets contain little to no information about these problematic stepping regions.

The biggest model impairments are:

- Increasing inaccuracy at higher stepping rates
  - Dynamic and static simulation results have increasing prediction errors
  - Motor currents rely on load
- Mechanical dynamics have to be modelled well

The model mismatches for both the stepper motor and the mechanical load play a bigger role for higher stepping rates. Unlike feedback controlled DC motors, where the controller removes model uncertainties, stepper motors generally do not have this luxury. All the effects which have not been modelled, will only show up in measurements, making the simulations unreliable, specially when the chopper is no longer able to maintain a constant current through the motor windings. This should be no surprise, as the chopper itself is a current source which uses feedback to maintain a constant current, and thus minimising the effects of non modelled dynamics.

The second investigation item is the improvement of stepping motor behaviour. The effects of mechanical rotor dampers do have the potential to improve motor behaviour, but choosing the right motor for the load often results to the same effects, without further increasing the costs. Using a mechanical damper means dissipating energy from the rotor movement, resulting to both damping of the oscillations and a reduction of motor torque (as the motor speed is forced by the stepping frequency).

Getting better damping of rotor oscillations can also be acquired by:

- Using a smaller stepper motor, when acceleration and deceleration are not critical (smaller motors deliver less torque, and thus less mechanical power)
- Lowering the chopper current settings when operating at stationary speeds if acceleration and deceleration are critical (lower currents mean lower motor torque, and thus less mechanical power)
- Choosing a higher step mode, if motor operation at low speeds is critical

The basic stepper motor design rules stated in chapter 3.3, will help creating optimal motor – load combination.

To further facilitate the stepper motor usage, the recommended items to investigate are:

- The mechanical dynamics of Océ applications, what is the impact of:
  - Transmission belts
  - Gears

on motor behaviour. Can motor behaviour be improved by making use of the higher order (non linear) dynamics of these elements, or should these dynamics be suppressed during the design of stepper motor driven applications.

- How to adapt the mechanical dynamics to improve stepper motor performance:
  - From which mechanical configurations will the stepper motor behaviour benefit. Should motor choice be made in an early stage of the design process, partly adapting the mechanical properties of the complete system to improve the total performance
  - Does it help working with standardised mechanical modules. When a stepper motor driven mechanical configuration has proved to perform well, must this configuration be used for other but similar applications
- Investigation of cheap back emf voltage controlled stepper motor drivers:
  - What is the optimal structure for such controllers. A series of stepper motor models are now available to predict motor behaviour. These predictions can be used to create back emf feedback stepper motor controllers.
  - When is a back emf controlled stepper motor a better solutions? Taking the costs and performance demands of the application into account, when is this controller a better choice then the now available low cost commercial stepper motor drivers.

10 References

[1] Paul Acarnley, *Stepping motors : a guide to theory and practice*, 4th ed., London : The Institution of Electrical Engineers, 2002

[2] Takashi Kenjo and Akira Sugawara, *Stepping motors and their microprocessor controls*, 2nd ed., Oxford : Clarendon Press, 1994

[3] Russell Laidman, *Stepper Motors and Control Part IV: Microstepping of stepper motors*, http://65.36.151.149/steper/Tutorials/MicroTutor.htm, 2001

[4] NMB, *NMB Step motor engineering guide 2002*, no longer available via http://nmbtc.com/

[5] Reston Condit, Dr. Douglas W. Jones, *Stepping motor fundamentals*, http://ww1.microchip.com/downloads/en/AppNotes/00907a.pdf

[6] D.I. Jones, J.W. Finch, *Optimal Control Of a Voltage-driven Stepping Motor*, IEE proceedings, Vol 130, Pt. D 130, pag 175-182, July 1983

[7] Internal report, Océ-Technologies B.V.

[8] Internal report, Océ-Technologies B.V.

[9] R&D Research Report, Océ-Technologies B.V.

[10] R&D Research Report, Océ-Technologies B.V.

[11] R&D Research Report, Océ-Technologies B.V.

[12] R. Clarke, *Power losses in wound components*, http://www.ee.surrey.ac.uk/Workshop/advice/coils/power_loss.html

[13] A. Hughes, P.J. Lawrenson, *International conference on stepping motors ans systems, University of Leeds*, pp 127-135

11 Appendix A: First functional version of the simulation model

This is the raw matlab code for the stepping motor simulation algorithm, outlined in chapter 4. StepperGUI from appendix D uses an improved version of this algorithm, but the basic stepper motor dynamics remain the same.

```
function [theta, theta_s, w, Te, VIa, VIb]=
                        stappenmi(Iref0, Mp, Cp, fs, N, Jl, Tl, Tfp)

% usage: [theta, theta_s, w, Te, VIa, VIb]=
%                                 stappenmi(Iref0, Mp, Cp, fs, N, Jl, Tl, Tfp)
%
% Simulator of stepper motor with current control.
% See documentation for full explanation
%
% inputs:
% Iref0 Reference current
% Mp    Motor properties = [Tpk, Jr, R, L, I0, p, fluxm]
% Cp    Current driver parameters [Vm, M, Type, Rsd, Rmd]:
%       Vm:     On voltage (current will be chopped with voltages +Vm / -Vm)
%       M:      Stepmode (fs -> 1, hs -> 2, ....)
%       Type:   0 -> wave, 1 -> A3977
%       Rsd:    resistance to simulate slow decay for H bridge (is the total %
resistance of the H bridge, when turned on)
%       Rmd:    resistance to simulate mixed decay for H bridge
% fs    vector with pulses
% N     Sample rate, should be >> 10*fn,max
% Jl    Total inertia of Load (scalar)
% Tl    Load connected (scalar / sample based vector)
% Tfp   friction parameters:
%      Tfp = [alpha, beta], Tf = -df*w - cf*sign(w)
%
% outputs:
% theta     angle of rotor (vector)
% theta_s   required step angle (vector)
% w         angular speed of rotor (vector)
% Te        mechanic torque produced by motor (vector)
% Pe        Electrical power consumed by motor (vector)
% Pm        Mechanical power consumed by motor (vector)
% VIa       Voltage over / current through winding A (matrix)
% VIb       Voltage over / current through winding B (matrix)


% Written by:   Robert Vierbergen
% Oce initials: qvie
% Tue id:       447280
%
% Last updated: march 29, 2005
% Version:      3.3

echo off;


% checking the input arguments
if nargin == 8
    foff = 0;
end
if nargin < 8
    error('no sufficient input arguments')
end


% extracting motor parameters from Mp vector
Tpk = Mp(1);
Jr = Mp(2);
R = Mp(3);
L = Mp(4);
I0 = Mp(5);
```

```
p = Mp(6);
fluxm = Mp(7);


% extracting friction parameters from Tfp vector
alpha = Tfp(1);
beta = Tfp(2);


% preparing matrices and vectors
tend = length(fs);
VIa = zeros(tend+2,2);
VIb = zeros(tend+2,2);
theta_s = zeros(1, tend+1);
theta = zeros(1, tend+2);
Te = zeros(1, tend+1);
w = zeros(1, tend+2);


% extracting current driver parameters
Vm = Cp(1);
M = Cp(2);
if Cp(3) == 1       % Choosing allegro style driver chip
    dRefI = pi / 4;
    Iref0 = 2 * Iref0 / sqrt(2);
    theta_s(1) = pi/(4*p);
    theta(1) = pi/(4*p);
    theta(2) = pi/(4*p);
else                % Wave stepping
    dRefI = 0;
end
Rsd = Cp(4);
Rmd = Cp(5);


% initialisation of simulation variables:
i = 0;
Va = 0;
Vb = 0;
Ia = 0;
Ib = 0;
Vaemf = 0;
Vbemf = 0;
rtrdir = 1;


% preparing torque dynamics (filling heaps)
dt = tend - length(Tl) - 1;
if dt > 0
    Tl = [0, Tl, Tl(end)*ones(1, dt + 1)];
else
    Tl = [0, Tl];
end


% starting simulation
for k=2:tend + 1
% if a step is commanded, the step angle will be increased
    i = i + fs(k - 1);
    theta_s(k) = theta_s(k - 1) + fs(k - 1)* pi / (2*p*M);
    rtrdir = sign(rtrdir+2*sign(fs(k - 1)));
                % rotor direction (1 -> cw, -1 -> ccw)

% Setting the current reference values
    Iaref = Iref0*cos(pi / (2*M) * i + dRefI);
    Ibref = Iref0*sin(pi / (2*M) * i + dRefI);

% setting the decay mode (-1 / 0 => slow, 1 => mixed)
    dmodea = rtrdir*sign((M - 1) * sin(pi / (2*M) * (2*i - 1) + 2*dRefI));

    dmodeb = rtrdir*-sign((M - 1) * sin(pi / (2*M) * (2*i - 1) + 2*dRefI));
```

```
% calculating the emf voltages
    Vaemf = -p*fluxm*sin(p*theta(k))*w(k);
    Vbemf = p*fluxm*cos(p*theta(k))*w(k);

% Calculating the torque's
    Te(k) =  -Tpk / (I0 * sqrt(2)) * (Ia * sin(p * theta(k))
- Ib * cos(p * theta(k)));
    Tf = -beta * w(k-1) - sign(w(k-1)) * alpha;

% calculating voltage and future current
    [Va, Ia] = curctrl(Ia, Iaref, I0, Va, Vm, Vaemf, R, L, dmodea, Rsd, ...
                       Rmd, N);
    VIa(k+1,:) = [Va, Ia]; % Phase A, Voltage / current output

    [Vb, Ib] = curctrl(Ib, Ibref, I0, Vb, Vm, Vbemf, R, L, dmodeb, Rsd, ...
  Rmd, N);
    VIb(k+1,:) = [Vb, Ib]; % Phase B, voltage / current output

% calculating future values for the rotor angular speed, rotor angle, and emf
voltages
    w(k+1) = (Te(k) + Tf - Tl(k)) / ((Jr + Jl) * N) + w(k);
    theta(k+1) = w(k) / N + theta(k);
end


% ------------------------------------------------------------------------
% Chopper functions
%-------------------------------------------------------------------------

function [Vr, Ik] = curctrl(Ik1, Iref, I0, Vk, Vm, Vemf, R, L, dmode, ...
                            Rsd, Rmd, N)

% current control with voltage chopping

% ctrl parameters
alpha = 0.01;
dIref = alpha*I0;

% Voltage setpoint regulator
% Positive current situation
if Iref > alpha*I0
    if Ik1 > Iref + dIref
        Vr = 0;
    elseif Ik1 < Iref - dIref
        Vr = Vm;
    else
        Vr = Vk;
    end

    % Choosing current decay
    if (dmode == 1) & (Vr == 0)
        Rt = R + Rmd / abs(Iref);
    else
        Rt = R + Rsd;
    end

% Negative current situation
elseif Iref < -alpha*I0
    if Ik1 > Iref + dIref
        Vr = -Vm;
    elseif Ik1 < Iref - dIref
        Vr = 0;
    else
        Vr = Vk;
    end

    % Choosing current decay
    if (dmode == 1) & (Vr == 0)
        Rt = R + Rmd / abs(Iref);
    else
```

```
        Rt = R + Rsd;
    end;

% passive zero-ing
else
    Vr = 0;
    Rt = R + 5 * Rmd;
end

% Calculating new current
Ik = 1/(N*L)*(Vr - Vemf) + (N*L-Rt)/(N*L)*Ik1;
```

12 Appendix B: Angular speed measurement

12.1 Spectral noise introduced by encoders

Before performing a spectral analysis on angular speeds measured with an encoder, the effects of an encoder on the measured angular speed must be determined. A simple simulation can give more information about the spectral noise introduced by an encoder. For this experiment a 1000 slit quadrature encoder has been modelled in matlab, the same as the encoder used for the angular speed measurements in chapter 5.3 and Appendix B.2.

For analysing the stepper motor simulation model, the following stepping rates / angular speeds have been observed:

f_s [Hz]	ω [rad s^{-1}]
100	3.14
500	15.7
1000	31.4
1500	47.1

The encoder simulation will show the noise effects, when an encoder is used to measure these constant angular speeds. When converting a constant signal to the frequency domain, the frequency spectrum contains one peak at frequency zero. Figure 12.1 shows the frequency spectrum of the 4 angular speeds, when being recorded by the 1000 slit encoder.

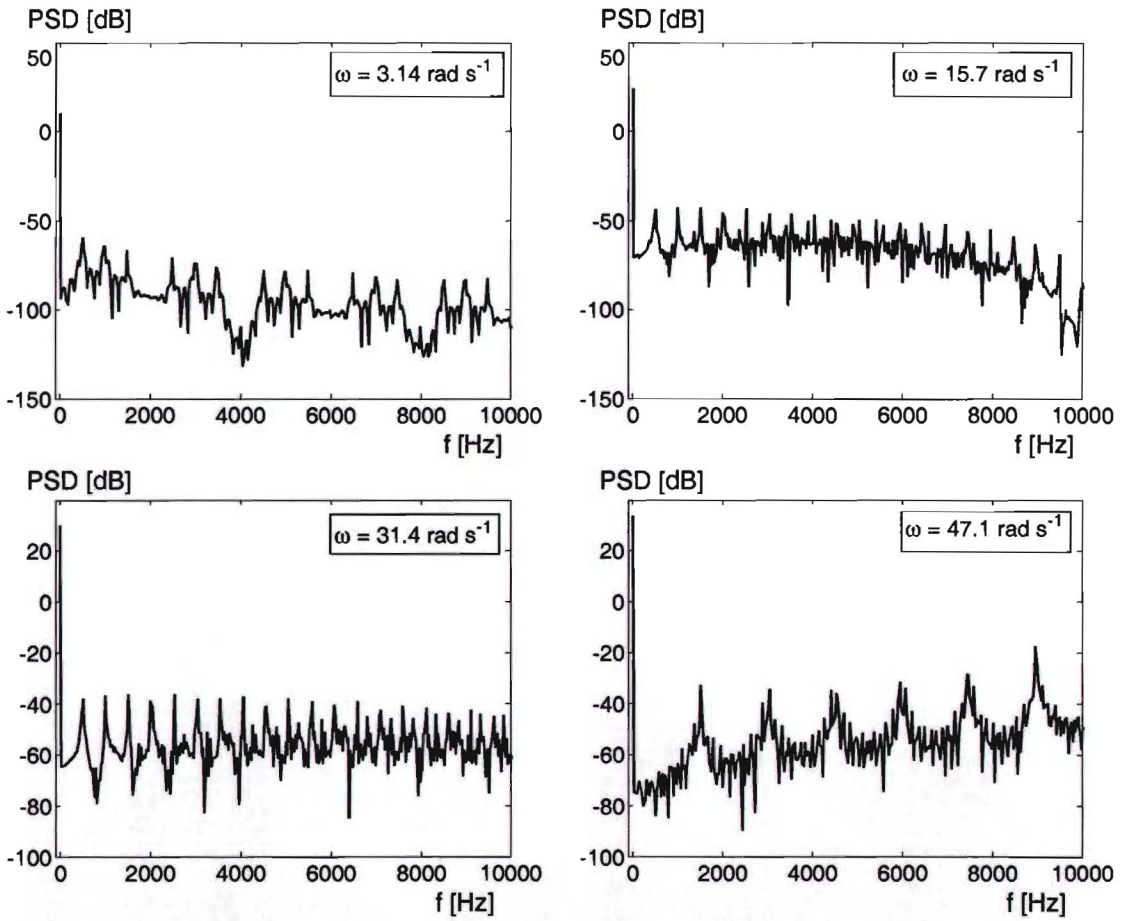

Figure 12-1: Spectral noise introduced by encoder at different constant speeds

The resulting plots show the non-linear behaviour of the encoder. The input spectrum should be only a peak at frequency zero, but when the speed is recorded by an encoder, several new frequency peaks emerge. Also within the region of the stepping frequency and the natural frequency of the rotor, making it difficult to predict if a peak in the spectrum really is measured, or is a measurement attribute.

To be able to distinguish between measured signals and encoder attributes, the table below lists all the peaks encountered for each simulation of the encoded angular speeds from figure 12.1.

ω [rad s^{-1}]	Peaks in spectrum [Hz]
3.14	500, 1000, 1500, 2500, 300, 3500, ..
15.7	130, 260, 390, ..
31.4	500, 1000, 1500, ..
47.1	145, 290, 435, ..

Angular speed measurements with encoders will also show new peaks when recording oscillations. Figure 12.2 shows these attributes for a angular speed oscillations with a frequency of 250 Hz. This frequency is also the natural resonance frequency of the 17PM-K404.

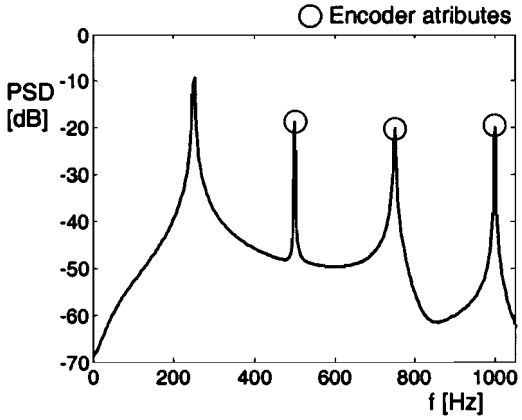

Figure 12-2: encoder attributes for 250 Hz oscillation

12.2 *Encoder measurements with the 23KM-K308*

The four plots below show the spectral analysis of measured and simulated angular speeds of the 23KM-K308 at different stepping rates.

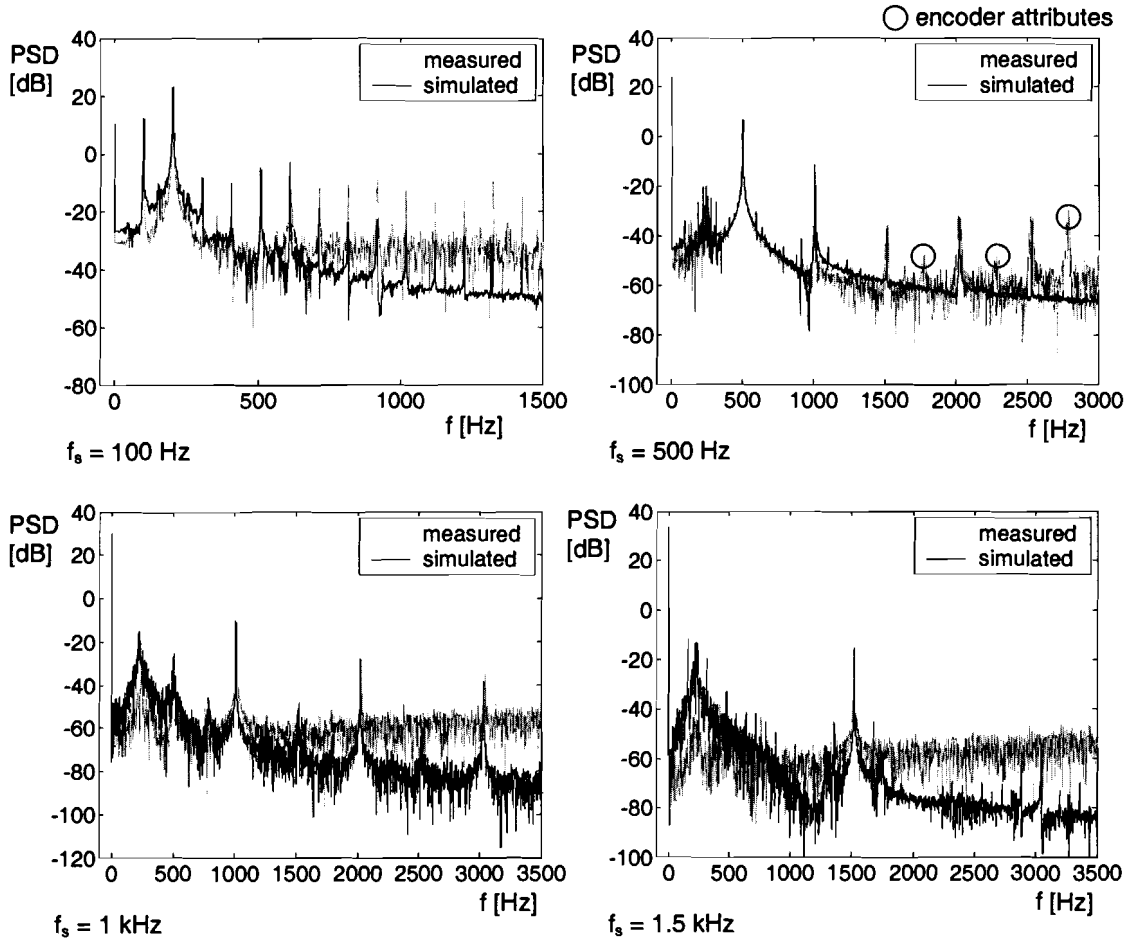

13 Appendix C: Measured currents versus simulated currents

Winding currents of the 17PM-K404 at different loads. T_x is the brake torque applied to the stepper motor.

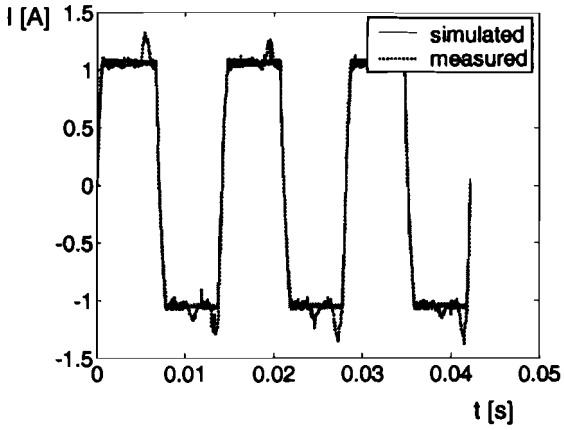

f_s = 284 Hz, T_x = 50mNm

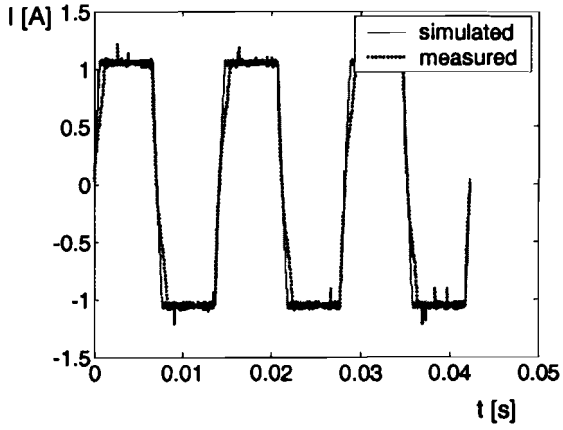

f_s = 284 Hz, T_x = 100mNm

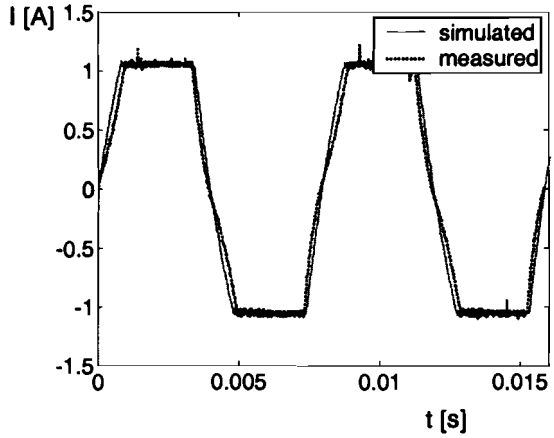

f_s = 505 Hz, T_x = 50mNm

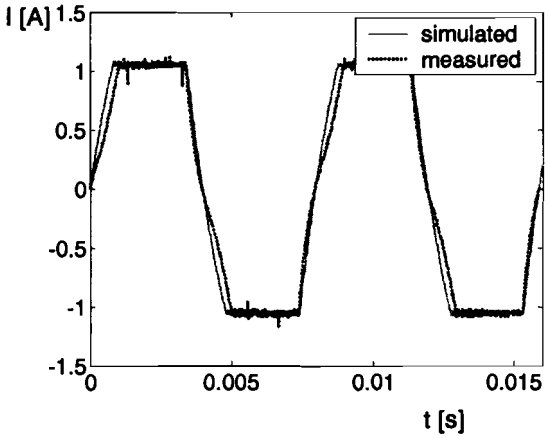

f_s = 505 Hz, T_x = 100mNm

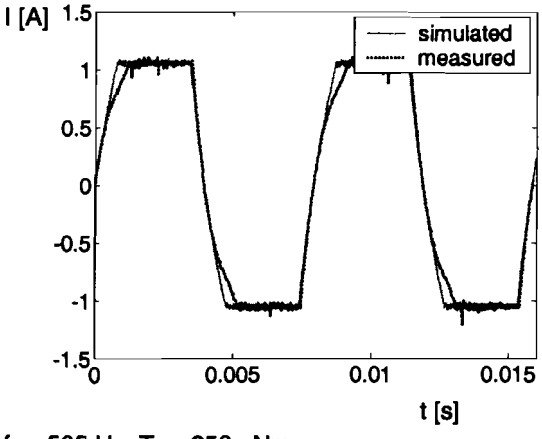

f_s = 505 Hz, T_x = 250mNm

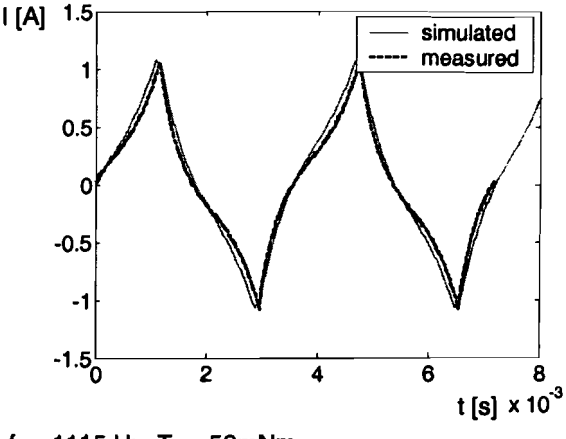

f_s = 1115 Hz, T_x = 50mNm

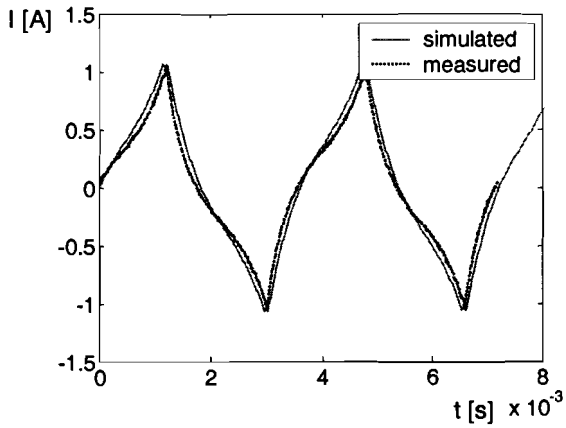

f_s = 1115 Hz, T_x = 100mNm

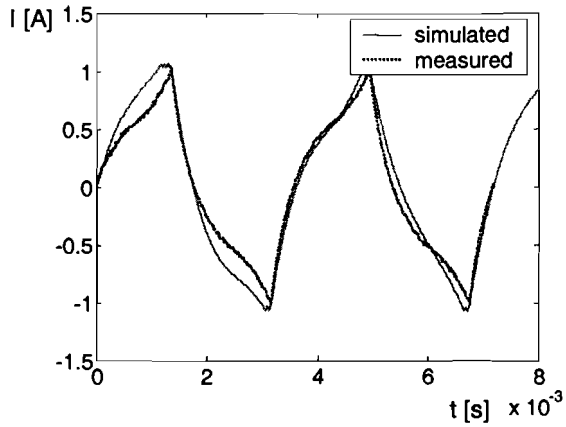

f_s = 1115 Hz, T_x = 250mNm

Measurement situation:
V_{bridge} = 24 V
R_{bridge} = 0.81 Ω/phase
R_{sense} = 0.25 Ω/phase
I_{ref} = 1.05 A
J_x = 2·10-5 kg m^2

14 Appendix D: StepperGUI a user friendly stepper motor design tool

To make the stepper motor simulation model more accessible, a simulation environment with graphic user interface has been created: StepperGUI. Instead of having to use one function with at least 23 input parameters, the simulation environment give the user an organised and understandable way to supply the necessary input parameters for performing simulation.

The simulation environment currently supports three kinds of simulations:
- Pull out simulations
- Single step response simulations
- Reference run simulations

The structure of the simulation environment is showed by figure 14.1. The environment has been developed for matlab, and can be considered as a separate toolbox. This appendix is an user manual for the StepperGUI toolbox.

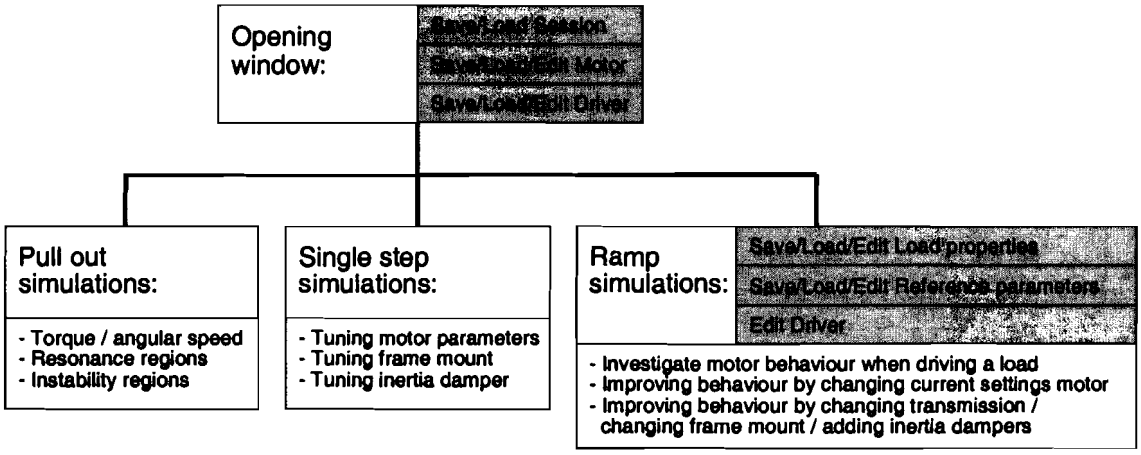

Figure 14-1: Simulation environment structure of StepperGUI

The program has been designed with the assumption that the user has a known mechanical system, which he or she wants to drive with a stepper motor.

The recommended design path with StepperGUI is:
1. Choose a motor from the manufacturer datasheets
2. Use the pull out simulations to get a better idea of the constant speed behaviour of the motor (motor torque, resonance's, instabilities). If the motor seems to satisfy the mechanical load demands, proceed to next step, if not go back to the first step
3. Check the single step response of the stepper motor with the single step simulation option. If a measured single step response of the stepper motor is available, tune the simulation response by changing the viscous and coulomb friction parameters of the stepper motor. If no additional information is available, change the viscous damping so the settling time of the step response is less then 100 ms
4. Perform the ramp simulations:
   - The load properties editor enables the user to model the actual load to be driven
   - With the speed ramp or displacement ramp editor the user can define the reference speed or displacement ramps for the motor or load
   - Additional forces can be added by the special load torque or force editors, enabling the user to add additional disturbances to the behaviour of the load
   - When all settings are complete, the simulation can be performed and the stepper motor behaviour can be analyse with a series of plots
5. Motor behaviour can be improved by:
   - Changing the current settings with the current settings editor
   - Changing the transmission ratio between motor and load
   - Changing the step mode (low speeds only)
   - Changing the motor frame mount dynamics
   - Adding an inertia damper

6. When satisfied with the motor behaviour, the simulation settings can be saved. If the stepper motor behaviour is not satisfactory, the whole process can be repeated from the first step

The frame mount and the inertia dampers discussed in chapter 7 can be optimised with the single step response simulation.

14.1 Editing motors and drivers

When executing the steppergui command in the base steppergui directory, the opening window emerges. As the openings window suggests, before any simulation can be performed, the stepper motor and driver must be either defined or loaded via the menus. The bipolar motor and driver structure is as discussed by chapter 4. Appendix E discusses the unipolar motor - driver structure, but this option is still in an experimental stage of development. Figure 14.2 shows a picture of the motor and driver properties editors.

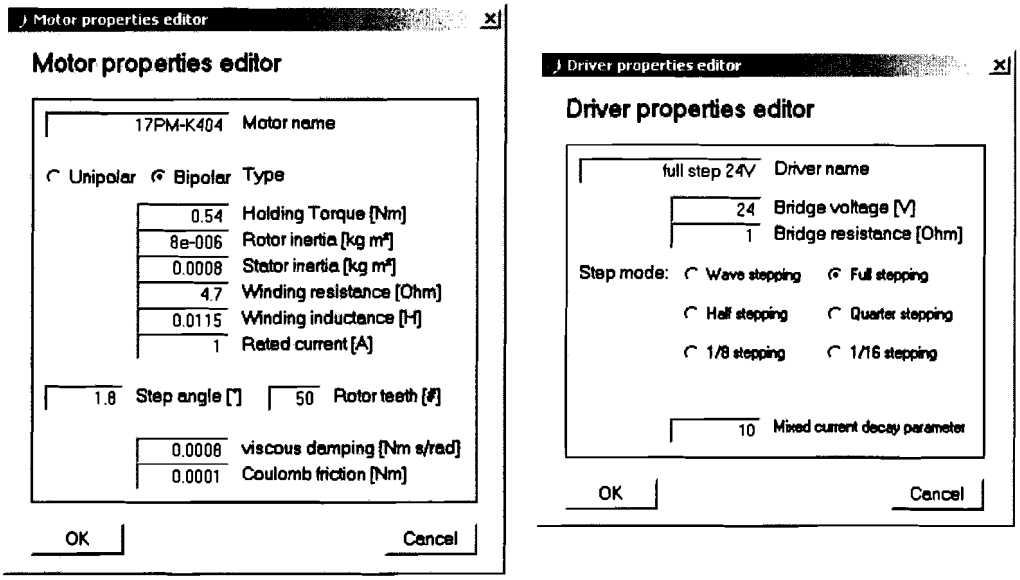

a) Stepper motor editor b) Stepper motor driver editor

Figure 14-2: Stepper motor and driver editor

When starting a session with a new motor and a new driver, the motor and driver editors enable the user to supply the necessary motor/driver variables. Most variables can be acquired from the datasheet of both motor and driver manufacturers, with exception of:

- The stator inertia, motor manufacturers do not supply information about the stator inertia. This parameter is only important when experimenting with the frame mount. StepperGUI automatically calculates a stator inertia of ten times the rotor inertia, when no stator inertia is supplied.
- The viscous and coulomb damping between the rotor and stator of the motor. These parameter actually contains several unknown power losses of the motor. When a single step response of the motor is known, the parameters can be estimated (using the single step response simulation). Otherwise, just tune the viscous damping, so the single step response is stable (a settling time of less then 100 ms should be the aim).
- The mixed current decay parameter (bipolar motor), this parameter is needed for simulating the mixed decay modes during higher step modes with a bipolar stepper motor. The parameter is set to 10, which should be an acceptable choice. If not satisfied with the higher step modes current waveforms, changing this parameter might improve the waveforms (this is the R_{md} parameter of Chapter 4.3).
- The current decay parameter (unipolar motor), this parameter simulates the current decay in the disabled windings.

14.2 *Performing pull out simulations*

The pull out simulation uses a binary search for determining the pull out curve of a stepper motor. Figure 14.3 shows the layout of the pull out simulation window.

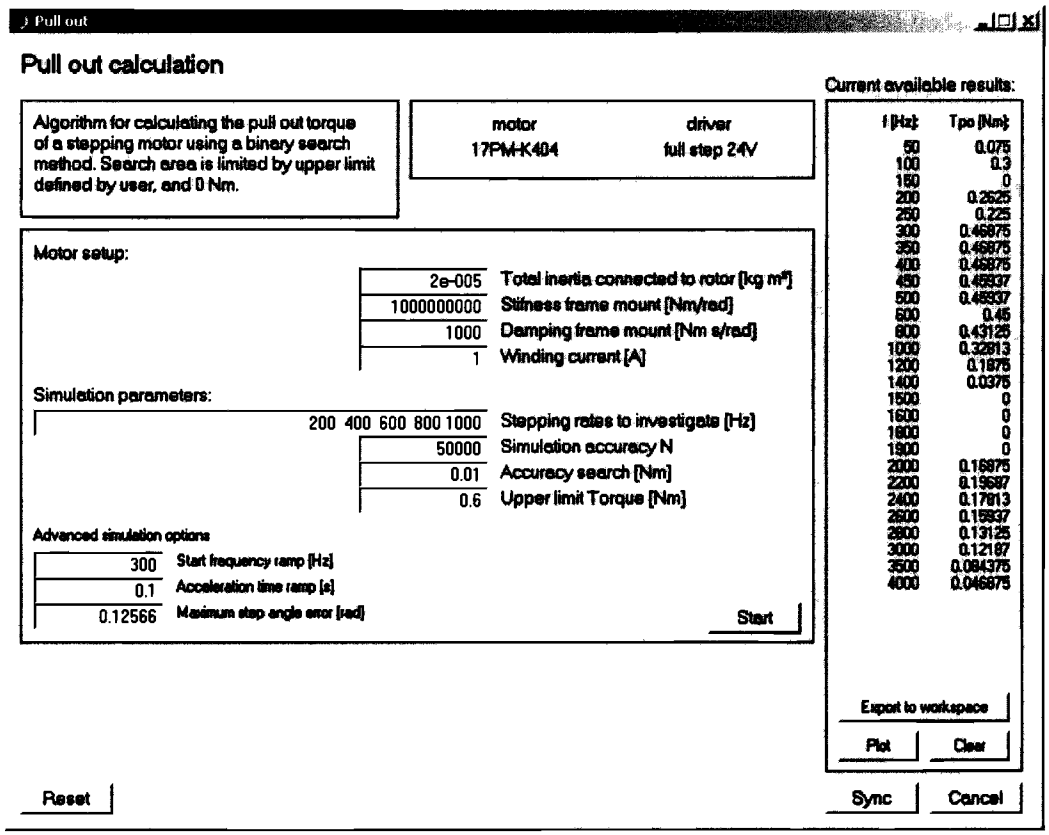

Figure 14-3: The pull out simulation window

Figure 14.4 shows the used motor set-up for determining the pull out torque. The simulation procedure is as follows: Ramp the stepping motor to the step rate to be investigated. Increase the external torque (T_x [Nm]) on the rotor, and search for the highest torque, with which the stepping motor does not lose its synchronisation. The search is a binary search between 0 and an user supplied maximum torque.

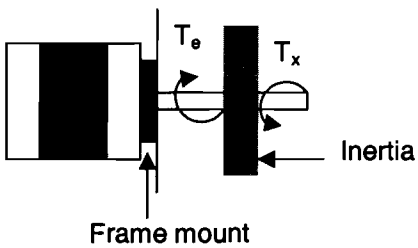

Figure 14-4: Pull out motor set-up

In order to perform the pull out calculations, a series of parameters is required to be supplied:

- The motor set-up parameters: The frame mount, the total inertia attached to the rotor and chopper reference current (see chapters 4 and 6)
- The simulation parameters: A list with the stepping rates to investigate, the simulation accuracy of the stepper motor model, the search accuracy for the binary search algorithm and the upper torque limit

The advanced simulation parameters are initialised with reliable data, so these parameters should not have to be changed.

When ready for simulating, press the start button, and a new window will appear. This window will show the stepping rates to be investigated by a graph with blue bars. If something seems to be wrong, the simulation can be aborted before starting. When pushing the go button, the algorithm will search for the pull out torque for each supplied stepping rate. The bar plot will show the current simulation status. After the simulation the new results can be added to the current results by pressing the OK button in the keep results frame.

The results of the pull out simulations can be analysed by plotting the pull out curve in a separate window, or by exporting the results to the workspace. When using the sync button, the results will be added to the session data.

14.3 Performing single step simulation

The single step response simulation has three purposes:
- Tuning the viscous and coulomb frictions between the stator and rotor
- Tuning the frame mount
- Tuning the viscously / elastically coupled inertia damper

By changing these parameters, the single step response will give an indication of the damping of the rotor movement. Figure 14.5 shows the window lay out of the single step response.

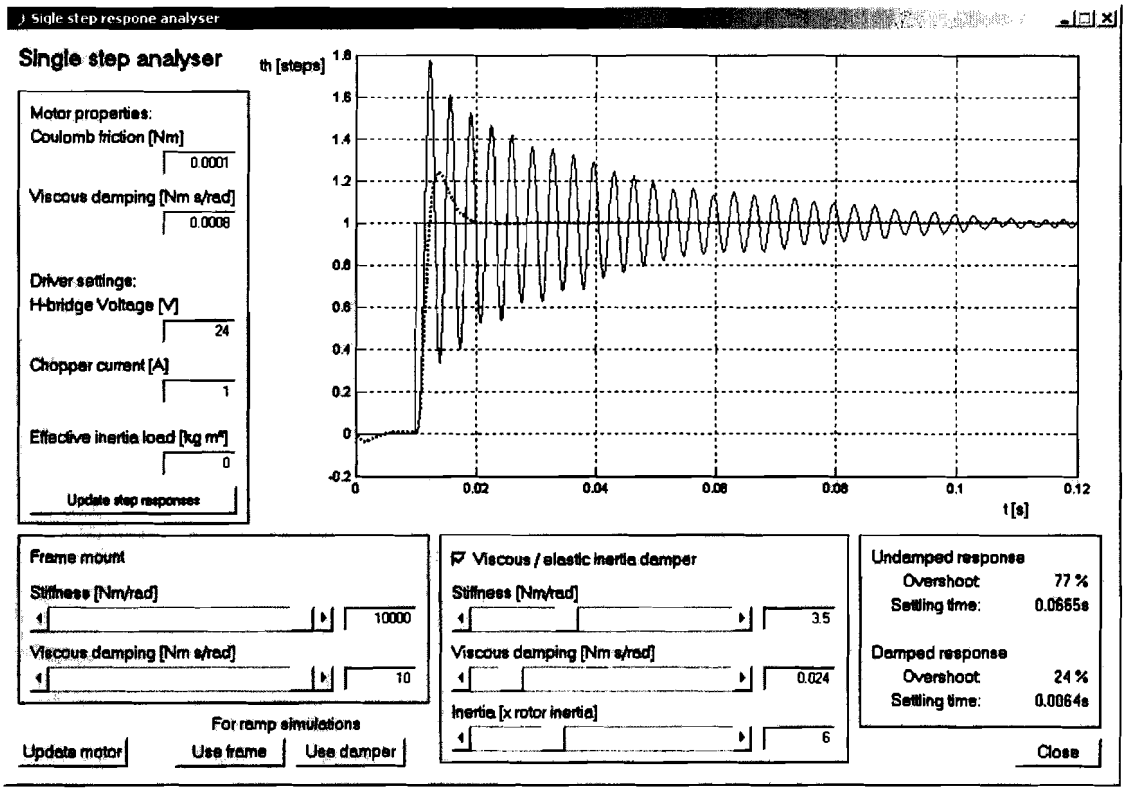

Figure 14-5: The single step simulation window

The single step plot at the upper right of the window shows both the step response without any additional damping (blue) and with the frame and/or inertia damper (dotted black).

When the single step response of a stepper is known, the viscous friction and coulomb friction between the rotor and stator can be estimated. Chapter 5.3 shows the technique with the 17PM-K404 and the 23KM-K308. If no single step information is available, the best choice is to tune the viscous damping so the settling time is below the 100 ms, and leave the coulomb friction zero.

When considering to use a damper, the single step response can help optimising the damper, or just analyse the effect of a chosen damper. Chapter 7 deals with mechanical

dampers, their principle of operation, and optimising them. Using the sliders gives a more or less real time update of the single step response, so playing with different parameters should give an indication of their influence on the damping of the rotor movement.

Because the damper choice depends on the stepper motor stiffness, the stepper motor stiffness can be decreased by lowering the winding current (simulating the fact that the stepper motor can not maintain the reference current levels at higher stepping frequencies). The damper choice also depends on the effective inertia attached to the stepper motor, so this parameter can be supplied too.

When tuning the coulomb and viscous damping parameters of the motor, the actual motor parameters can be updated with the tuned parameters by pressing the "Update motor" button at the bottom left part of the screen. The damper and frame mount can be used for ramp simulations, when pressing the "Use frame" or "Use damper" buttons.

14.4 Performing ramp simulations

The last simulation option is the ramp simulations. With this simulation the stepper motor can be simulated, driving a known load with a known reference speed or displacement trajectory. Figure 14.6 shows the ramp simulation window.

Before any ramp simulation can be performed, the following steps have to be followed:
- The load dynamics must be supplied via the load editor
- The reference must be chosen (speed or displacement)
- The location and unit of the reference signal must be chosen
- The reference ramp must be supplied with the speed or displacement editor
- The reference settings for the current must be supplied
- When special force or torque dynamics take place at the load during operation, these dynamics can be supplied via the force / torque editor (e.g. a piece of paper passing through the system)

This is quite a to do list, that is why all simulation data can be saved separately, or together as a complete application. The simulation can not be started when no speed or displacement ramp is supplied (the motor behaviour can be predicted without any simulation). The small pictures of the load, speed or displacement ramp, current settings and special torque / force dynamics at load give an impression of simulation settings.

Mechanical load editor:
The mechanical load to be driven by the stepper motor will play a big role in the total system behaviour. The StepperGUI toolbox has an editor to facilitate the implementation of a mechanical load. Figure 14.7 shows the mechanical load editor. At the left part of the window is a figure showing the motor load configuration, and at the right part are the parameters of the chosen mechanical system.

The configuration options for the load are:
- Rotational: without or with transmission, without or with inertia damper
- Linear: without or with inertia damper

When a choice has been made, the relevant load properties will automatically by enabled or disabled. The internal lay-out of the load is described by chapter 6.

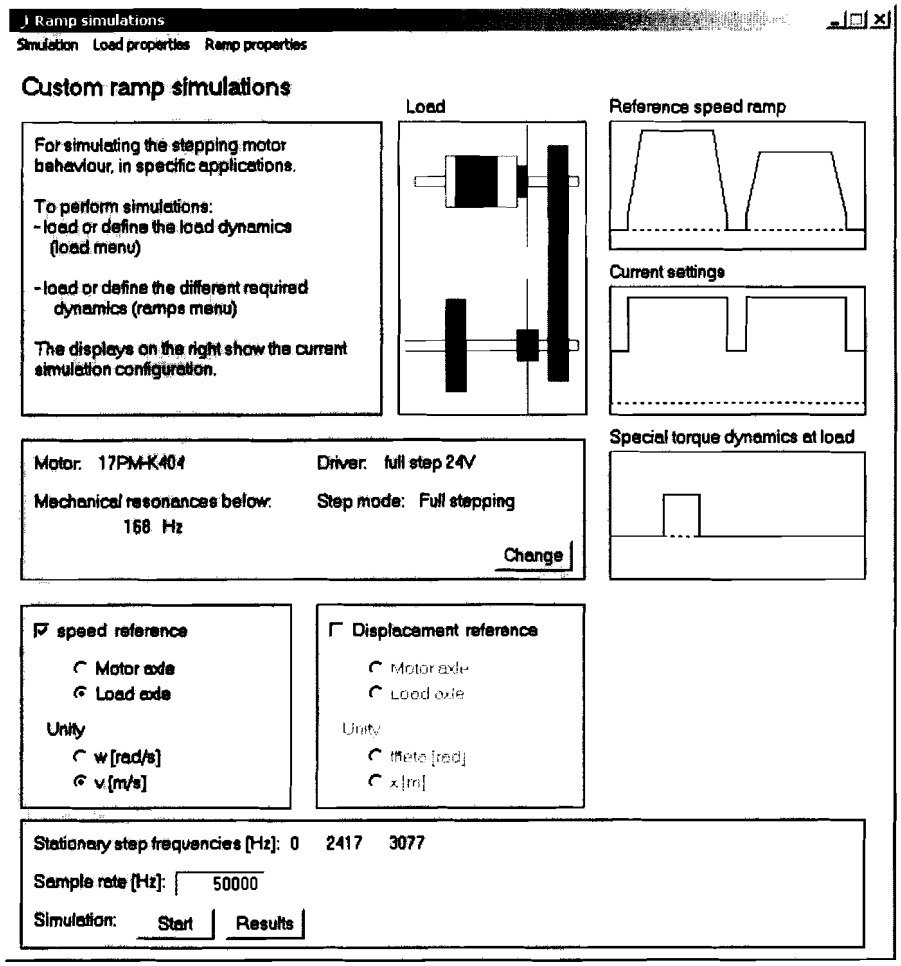

Figure 14-6: The ramp simulation window

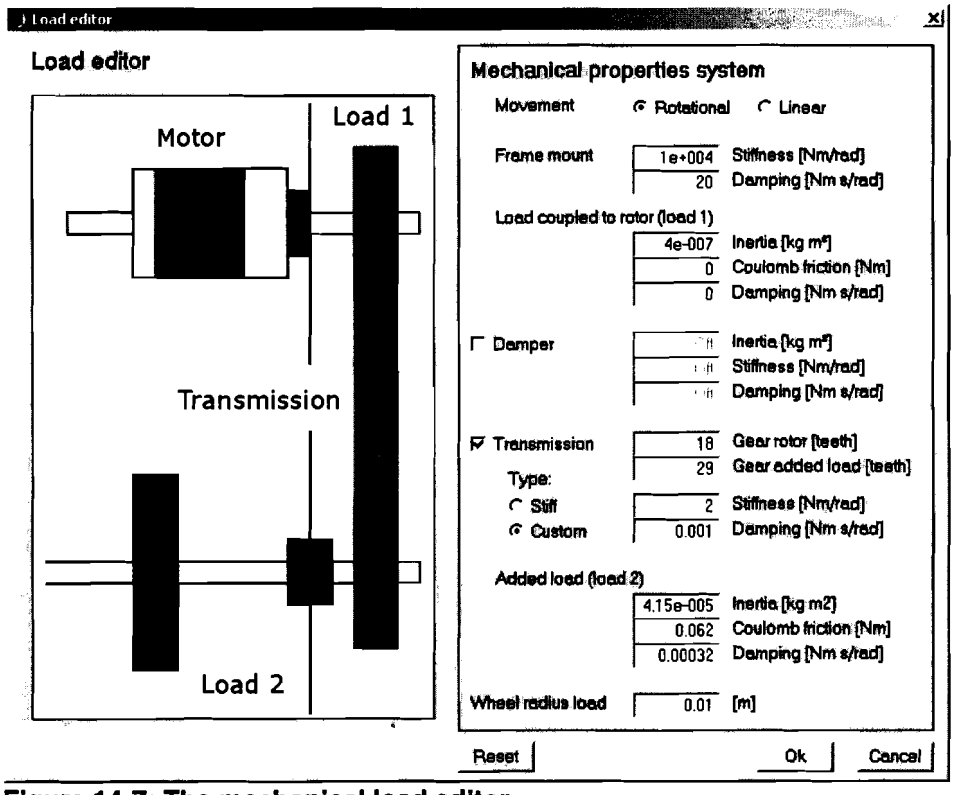

Figure 14-7: The mechanical load editor

The speed ramp editor:
Speed ramps can be supplied by this editor. When a ramp has been constructed, this ramp will be seen as the reference speed for your application. Making any changes to the load or stepping motor will affect the stepping rates of the stepping motor, but not the reference ramp! Only the speed editor can change the reference speed ramp.

Figure 14.8 shows the window layout of the speed ramp editor. A small plot shows the complete ramp, and the selected segment of the ramp. Each segment of the ramp can be selected by the list besides the speed ramp plot. A selected segment of the speed ramp can be edited, moved up or down the list, and deleted.

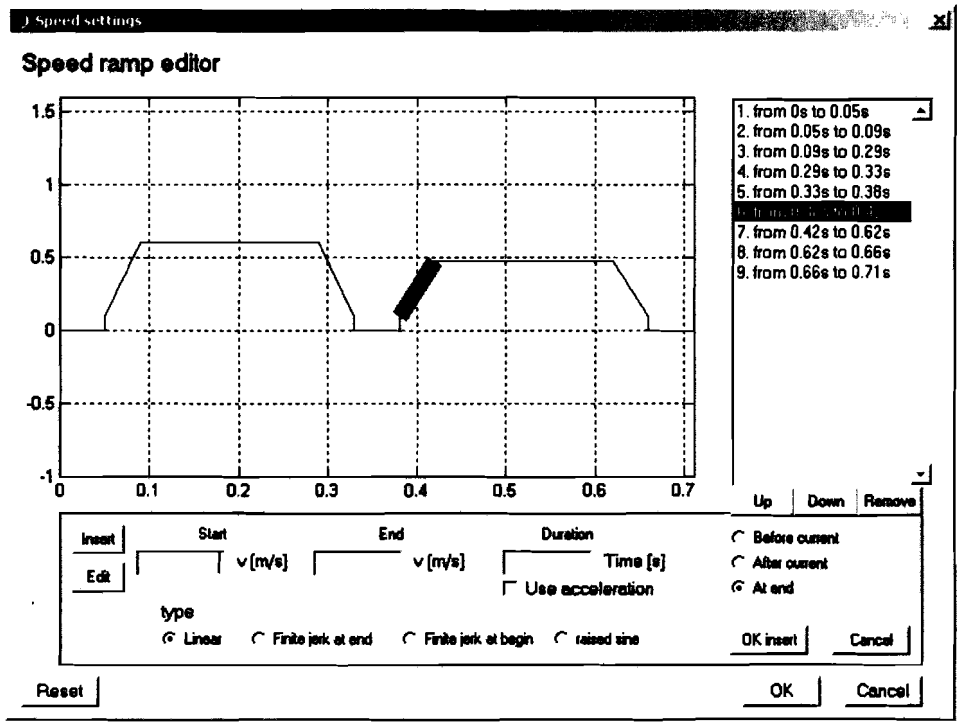

Figure 14-8: The speed ramp editor

New segments can be added to the speed ramp by pushing the insert button. Each segment of the speed ramp consist out of a initial speed, a final speed and the duration of a segment. When the initial speed is not equal to the final speed, also an acceleration may be chosen.

When inserting a new part also the location of the placement and the acceleration type can be chosen. The placement choices are before the selected segment, after the selected segment or at the end of the ramp. The acceleration types are displayed by figure 14.9. Because the stepper motor needs some time to initialise, the first 50 ms segment of the ramp cannot be changed nor removed. The place before current button will be ignored when the first segment is chosen.

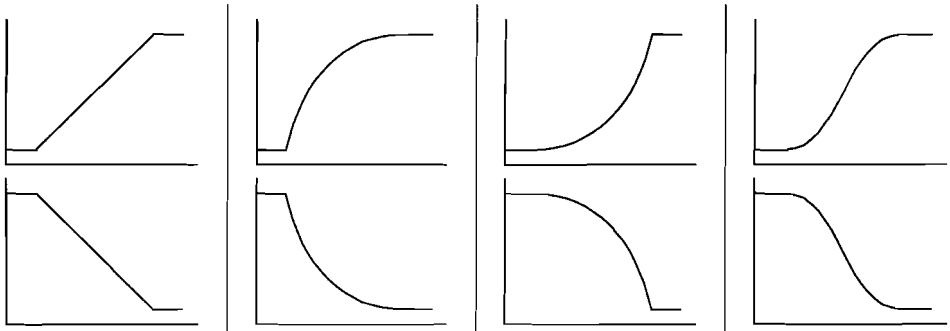

Figure 14-9: Acceleration choices for the speed ramp

The displacement ramp editor:
When the stepper motor reference is a displacement ramp, the displacement ramp editor must be used to supply the ramp. Unlike the speed ramp, which consist out of a series of segments, the displacement ramp consist out of a series of displacement versus time points. Figure 14.10 shows the displacement editor. Again a small plot at the left shows the displacement ramp, and the list at the right shows the displacement data of the ramp. A selected displacement data point can be edited or removed.

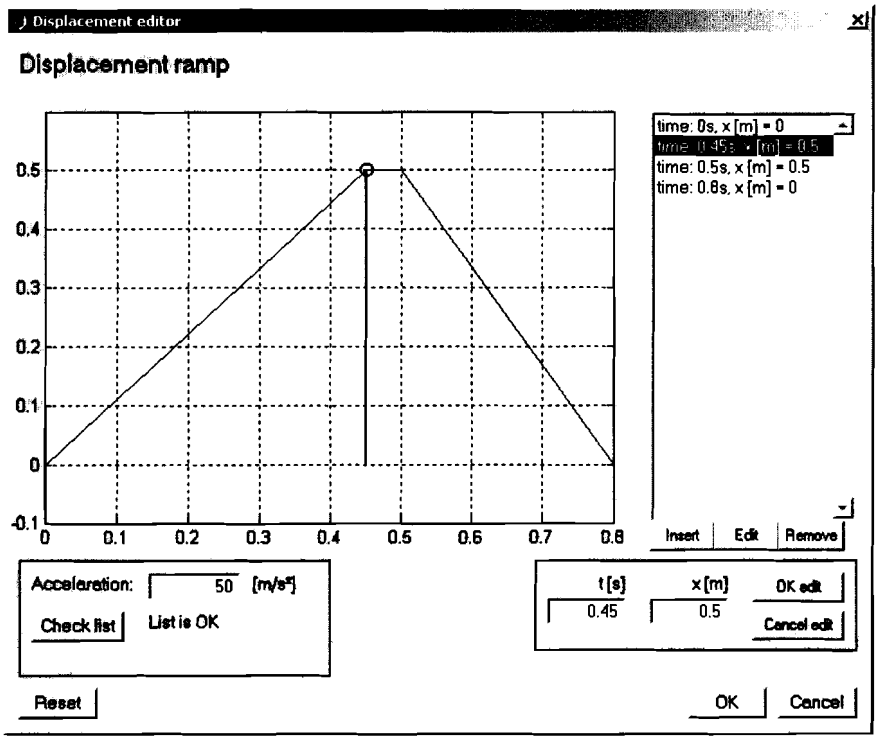

Figure 14-10: The displacement ramp editor

New data points can be supplied with the insert button. The time and desired displacement can then be supplied. If an new entry or an edited entry is placed at the same time instance as existing entries, the entry will be ignored. The first entry can not be changed nor removed, as the motor cannot instantaneously change from position, and the start position is always at displacement zero.

The final displacement list will be calculated with one acceleration constant. This constant must be supplied at the bottom left frame of the screen. To check if the displacement ramp is executable with the chosen acceleration, a check list button will calculate the list, and return a positive or negative conclusion. The displacement ramp can not be used for simulations when the list is not valid (the user must either chose a different acceleration or change the list).

The current settings editor:
The current settings editor gives the user two options:
- Using the stepper motor with one constant current
- Using a series of current segments

When the current settings are set to constant current operation, the window will only ask for a constant current level for the chopper. When the current settings are set to dynamic operation, the window will change to a speed ramp editor like layout. Figure 14.11 shows the window layout for the current settings editor when choosing the dynamic current operation.

At the left part of the screen is a plot of the current dynamics, and at the right part is a list with the current settings segments. The segments in the list can be edited, moved up or down the list or be removed from the list. Also new segments can be inserted. A segment consists out an initial current, a final current and a duration. The construction of the current editor is almost the same as the speed ramp editor, when inserting a new segment also the placement can be supplied.

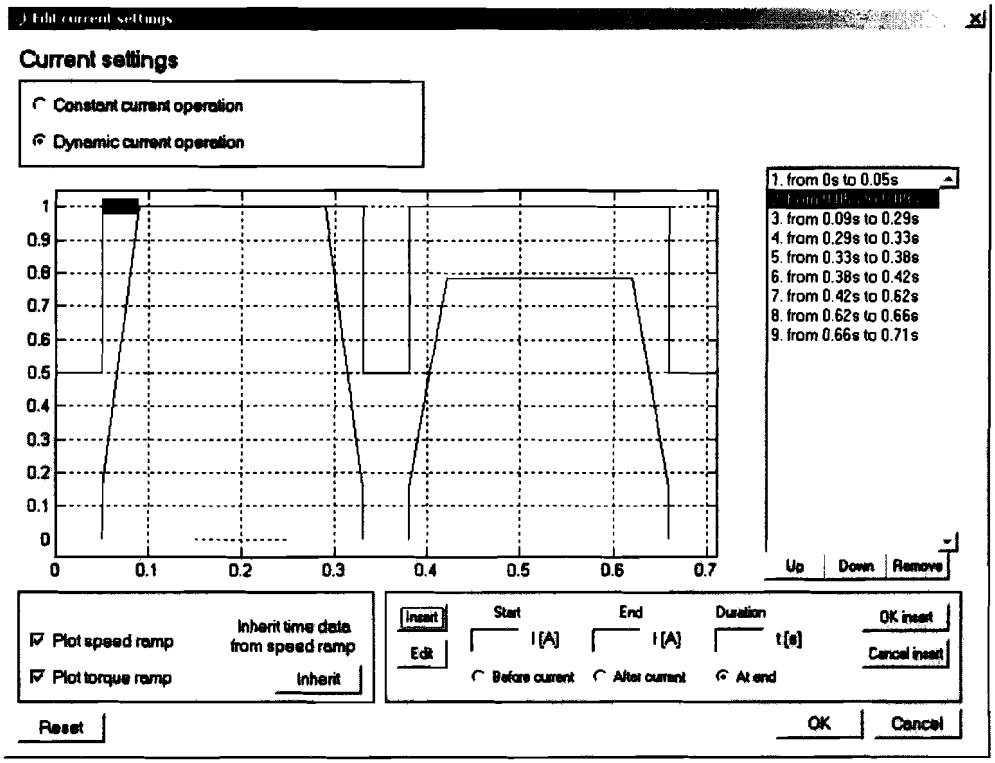

Figure 14-11: The current setting editor

Besides the speed ramp like properties of the current settings editor, some extra options have been included to facilitate the creation of a current setting list. Both the normalised speed ramp and torque ramp can be plotted together with the current setting ramp, by activating the checkboxes at the bottom left part of the editor window. When the speed ramp has been displayed, the time data from the speed ramp list can be used for the current ramp, by pressing the inherit button besides the check boxes.

Simulating with the ramp simulation:
When all load and reference signals have been set, the ramps can be simulated by pressing the start button in the ramp simulation window. When the simulation has been calculated a small preview plot at the bottom right part of the screen emerges. The results can be further inspected by pressing the results button. A whole series of plots can be shown, to analyse the motor performance. Besides the plots, the results can also be exported, or some basic statistics about the results can be displayed.

When not satisfied with the results, some improvement can be acquired by:
- Experimenting with the current settings
- Experimenting with the transmission
- Experimenting with the step modes (low stepping rates only)
- Experimenting with the frame mount and inertia dampers
- Choosing a different stepper motor

15 Appendix E: Unipolar (hybrid) PM stepper motor model

Chapter four and six described the construction of the bipolar stepping motor simulation model. A model for the unipolar stepping motor has also be constructed, but has not yet been validated. The structure of the unipolar simulation model, which is very similar to the bipolar version, is described by this appendix.

Figure 15.1 shows the winding configurations for both the unipolar and bipolar PM stepper motors. The unipolar winding configuration can still be described with the electrical circuit from figure 4.2, but now with four phases (A^+, A^-, B^+, B^-). The mechanical part of the stepper motor, as described by chapters 4 and 6 also remain valid.

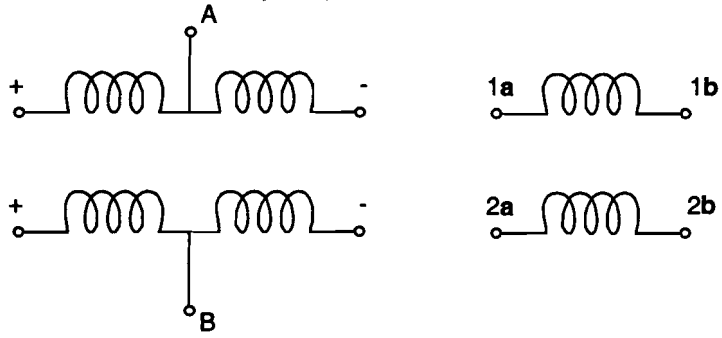

a) Unipolar b) Bipolar

Figure 15-1: Winding configurations

Of course not all dynamics remain the same. The torque is now a function of the four winding currents:

$$T_e = -k \cdot \{(I_{A+} - I_{A-})\sin(p \cdot (\theta_r - \theta_s)) - (I_{B+} - I_{B-})\cos(p \cdot (\theta_r - \theta_s))\} \qquad \textbf{Equation 15-1}$$

With T_e [Nm] the torque produced by the motor, k [Nm/A] the motor constant, I_{A+} [A] and I_{B+} [A] the currents through the positive winding of the phases, I_{A-} [A] and I_{B-} [A] the currents through the negative windings of the phases, p the number of rotor teeth, θ_r [rad] and θ_s [rad] the rotor and stator angles, and ω_r [rad/s] and ω_s [rad/s] the rotor and stator angular speeds

Also the emf equations have to be changed, as each positive and negative phase has its own emf voltage source:

$$\begin{cases} V_{emf,A+} = -k \cdot \sin(p(\theta_r - \theta_s))(\omega_r - \omega_s) \\ V_{emf,A-} = -V_{emf,A+} \\ V_{emf,B+} = k \cdot \cos(p(\theta_r - \theta_s))(\omega_r - \omega_s) \\ V_{emf,B-} = -V_{emf,B+} \end{cases} \qquad \textbf{Equation 15-2}$$

With again k the motor constant.

Figure 15.2a shows a driver circuit for a unipolar motor (only for the A phase). Compared with the H bridge used for bipolar motors (figure 4.5), this driver circuit is less complicated (only two transistors per phase, instead of the four transistors used for the H bridge). Besides the reduced circuit complexity, also the timing of the transistors signals is not critical (Bad signal timing when using a H-bridge can destroy the circuitry).

Theoretically, when the inputs of both the transistors T_1 and T_2 would be low, no current can flow through the winding. Unfortunately, when using a voltage chopper this is not true. As the phase layout of figure 15.2 suggests, the positive and negative windings are magnetically coupled. So for example, when breaking the current through the positive phase, the winding current can discharge via the negative phase and diode D_2.

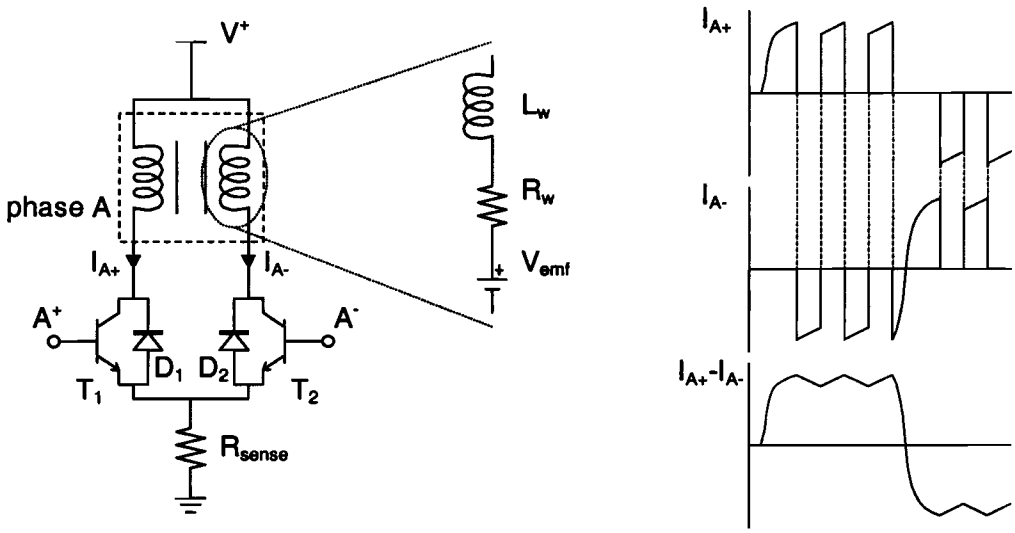

a) Unipolar driver circuit b) Current waveforms

Figure 15-2: Unipolar driver circuit and winding current waveforms for phase A

Figure 15.2 shows the winding currents of phase A, when using a voltage chopper to maintain a constant current through the winding. Notice as when phase A^+ is switch off, the current in phase A^- discharges the winding current built in phase A^+ and vice versa. Although this effect seems to be nuisance, actually the current that is used to build the magnetic field of the phase, I_{A+} - I_{A-} (see figure 15.2b), has a very similar wave form to the H-bridge chopped currents of the bipolar motor (see figure 4.6).

For the simulation model, this principle of winding current flow has been formalised with the use of a virtual current $I_A = I_{A+} - I_{A-}$. Because both positive and negative phases are never excited simultaneously:

- if A^+ is enabled, $I_{A+} = I_A$, when disabling A^+, $I_{A+} = 0$, $I_{A-} = -I_A$
- if A^- is enabled, $I_{A-} = -I_A$, when disabling A^-, $I_{A-} = 0$, $I_{A+} = I_A$

The control strategy for maintaining a constant virtual current I_A is now exactly the same as chopper the strategy of the H-bridge:

- **If I_{A+} must be equal to I_{ref} then**
  - **If $I_A < I_{ref} - \gamma$ then $V_{A+} = V^+$**
  - **If $I_A > I_{ref} + \gamma$ then $V_{A+} = 0$**

- **If I_{A-} must be equal to I_{ref} then**
  - **If $I_A > I_{ref} + \gamma$ then $V_{A-} = V^+$**
  - **If $I_A < I_{ref} - \gamma$ then $V_{A-} = 0$**

With I_{ref} [A] the reference current for the chopper, and γ a constant to prevent the circuit from continuously chopping. The same procedure is used for the B phase.

Because the current dynamics now rely on the feedback of the virtual current I_{phase} ($I_{phase} = I_{phase,+} - I_{phase,-}$), the current equation for the positive and negative windings must also be changed:

$$\begin{cases} \dot{I}_{phase,+} = \dfrac{1}{L_w}\left(-R_w \cdot I_{phase} + V_{phase,+} - V_{emf,phase,+}\right) \\ \dot{I}_{phase,-} = \dfrac{1}{L_w}\left(R_w \cdot I_{phase} + V_{phase,+} + V_{emf,phase,+}\right) \end{cases}$$

Equation 15-3

This model has not been validated, but a few comments can be made:

- Just as the bipolar model the magnetic losses, iron losses and eddy currents have not been implemented

16 Appendix F: Hypothesis on electrical instability

As stated in chapter 3 section 2.2 the pull out torque curve of a stepping motor show dips at the mechanical resonance stepping rates and the electrical instability regions. While the mechanical resonance of stepping motors is well documented, literature shows different theories about electrical instability. Most instability theories seem to be flawed, and have not been further studied.

The main investigations concerning electrical instability assume the phenomena to be purely electrical. This seems to be improbable as the instability can be suppressed by damping the stepper motor with each of the mechanical dampers discussed by chapter 7. The instability problem seems to be more about the way a stepping motor is used, rather then being a motor impairment, although motor parameters such as the winding induction and winding resistance do play a role in the location of these electrically instable regions.

When using a stepping motor the traditional way, both the rotor speed and the motor torque are forced electrically. The speed is forced by the winding commutation, while the torque is forced by the winding currents. This means that a "constant" amount of power is introduced at the electrical side, without considering the power demand of the mechanical load. If the power demand of the mechanical load is higher then the power input at the electrical system the stepper motor will not be able to drive the mechanical load. But when the input power is higher then the mechanical power demand, the mechanical part of the system has to somehow dump the excessive electrical power.

This power dump can be achieved by angular speed oscillations as described by chapter 5 section 3. The continuing acceleration and deceleration of the rotor / mechanical load combination results into a loss of power, as the stepper motor driver is not able to convert mechanical energy to electrical energy. This explanation does not consider the exact way these angular speed oscillations result from the power dump, but it does explain the improvement of the motor behaviour when using mechanical dampers, as these dampers are a mean to dissipate angular speed oscillation energy.

The exact way these oscillations are build and maintained during motor operation is difficult to analyse, as the phenomena is of a non linear origin. The angular speed oscillation frequency f_{osc} is equal to the natural frequency of the stepper motor, while input step frequency f_{step} is not equal to the f_{osc}. One of the definitions of linearity is that the output spectrum of a linear system cannot contain other frequencies as the frequencies introduced at the input.

But with simulations it can be shown that the instability of a single stepping motor can occur at any stepping rate, when using a constant voltage stepper motor driver. This appendix just shows a possible explanation for the instability, further investigation should be performed to get a better understanding of this phenomena

17 Appendix G: NMB stepper motors used during investigation

Table 17-1: Motor data 17PM-K404

Holding Torque (2 phases on)	0.54 Nm
Rotor Inertia	$8 \cdot 10^{-6}$ kg m^2
Winding Resistance	4.7 Ω
Winding inductance	11.5 mH
Rated current	1 A
Step size	1.8º

Table 17-2: Motor data 23KM-K308

Holding Torque (2 phases on)	0.85 Nm
Rotor Inertia	$23 \cdot 10^{-6}$ kg m^2
Winding Resistance	1.6 Ω
Winding inductance	3.4 mH
Rated current	2 A
Step size	1.8º

Motor data from NMB, 2005